SRI International

Final Report • 31 December 1997

PROCESS MODELS FOR INFRARED FOCAL PLANE ARRAY FLEXIBLE MANUFACTURING

Prepared by:

M. A. Berding, Senior Research Physicist
Applied Physical Sciences Laboratory

SRI Project 6452

Prepared for:

Air Force Office of Scientific Research — AFOSR/NE
Directorate of Physics and Electronics
110 Duncan Avenue, Suite B115
Bolling Air Force Base, DC 20332-0001

Attn: Major Michael W. Prairie

Contract F49620-95-C-0004

Approved:

Elizabeth J. Brackmann, Co-Director
Applied Physical Sciences Laboratory

333 Ravenswood Avenue • Menlo Park, CA 94025-3493 • (415) 326-6200 • FAX: (415) 326-5512 • Telex: 334486

REPORT DOCUMENTATION PAGE

Form Approved
OMB No. 0704-0188

1. AGENCY USE ONLY *(Leave Blank)*	2. REPORT DATE	3. REPORT TYPE AND DATES COVERED
	31 December 1997	Final Technical Report

4. TITLE AND SUBTITLE
PROCESS MODELS FOR INFRARED FOCAL PLANE ARRAY FLEXIBLE MANUFACTURING

5. FUNDING NUMBERS
Darpa
63739E
B718/04

6. AUTHOR(S)
M. A. Berding

7. PERFORMING ORGANIZATION NAME(S) AND ADDRESS(ES)
SRI International
333 Ravenswood Avenue
Menlo Park, CA 94025

8. PERFORMING ORGANIZATION REPORT NUMBER
6452FR

9. SPONSORING/MONITORING AGENCY NAME(S) AND ADDRESS(ES)
Air Force Office of Scientific Research—AFOSR/NE
Directorate of Physics and Electronics
110 Duncan Avenue, Suite B115
Bolling Air Force Base, DC 20332-0001

10. SPONSORING/MONITORING AGENCY REPORT NUMBER
F49620-95-C-0004

11. SUPPLEMENTARY NOTES

12a. DISTRIBUTION/AVAILABILITY STATEMENT
Approval for public released;
Distribution unlimited

12b. DISTRIBUTION CODE

13. ABSTRACT *(Maximum 200 words)*

The objective of this work is to assist industry in its efforts to devise a flexible manufacturing means for production of high performance Hg(1-x)Cd(x)Te-based focal plane arrays at reduced costs. The program has focused on the properties of impurities and native defects in the material, and how they subsequently impact the device performance. We find that the cation vacancy is a single acceptor in x = 0.2 material, contrary to previous findings. We have explained the inactive incorporation of the group VII elements under mercury-deficient conditions. We have shown that the group I elements have a large fraction of interstitial incorporation, thereby explaining their fast diffusion. We have predicted a model for the amphoteric behavior of arsenic, and have explained its behavior in liquid phase epitaxy from both the tellurium-melts and the mercury-melts. Annealing strategies for activation arsenic as a p-type dopant following growth by molecular beam epitaxy have also been suggested. Our modeling of the MBE growth surface indicates that growth rates are fastest on the {211}B surface, but that there will be fewer grown-in defects on the {211}A surface.

14. SUBJECT TERMS	15. NUMBER OF PAGES
HgCdTe, Focal Plane Arrays, semiconductors, impurities, defects, MBE growth modeling, infrared devices	16. PRICE CODE

17. SECURITY CLASSIFICATION OF REPORT	18. SECURITY CLASSIFICATION OF THIS PAGE	19. SECURITY CLASSIFICATION OF ABSTRACT	20. LIMITATION OF ABSTRACT
UNCLASSIFIED	UNCLASSIFIED	UNCLASSIFIED	UNLIMITED

CONTENTS

1 EXECUTIVE SUMMARY 1

2 APPROACH 2

3 NATIVE DEFECTS IN LPE MATERIAL, MBE MATERIAL, AND DURING PROCESSING 3

4 IMPURITIES IN HgCdTe AND CdTe SUBSTRATES 4
- 4.1 *n*-Type Dopants in HgCdTe 4
- 4.2 *p*-Type Dopants in HgCdTe 5
- 4.3 Activation of Arsenic in HgCdTe 5
- 4.4 "Bothersome Impurities": Lithium and Sodium in HgCdTe 7
- 4.5 Impurity Interaction for HgCdTe and CdTe 8

5 MBE GROWTH SURFACE CALCULATIONS 10

6 PUBLICATIONS 11

REFERENCES 12

APPENDICES

1 EXECUTIVE SUMMARY

The objective of this work is to assist industry in its efforts to devise a flexible manufacturing means for production of high-performance $Hg_{1-x}Cd_xTe$-based focal plane arrays at reduced costs. The program has focused on the properties of impurities and native defects in the material, and how they subsequently impact the device performance. Because impurities and native defects are introduced, annihilated, gettered, and in other ways modified during growth and subsequent processing, careful attention has been paid to the relevant thermodynamical conditions coupling in all of the relevant phase diagram information. Our *ab initio* calculations predict the properties of native point defects in HgCdTe in general agreement with experiment, however, there are notable differences with prior data interpretation that impact device design and processing strategies. We find that the cation vacancy is a single acceptor in $x = 0.2$ material, contrary to previous findings. Close collaboration with the Stanford group under this program has led us to believe that our predictions of interstitial densities are too low, and that the mercury interstitialcy (two mercury atoms sharing a lattice site) may be the actual defect involved. Our calculations have explained the experimental finding on the behavior of impurities in HgCdTe in general. We have explained the inactive incorporation of the group VII elements under mercury-deficient conditions. We have shown that the group I elements have a large fraction of interstitial incorporation, thereby explaining their fast diffusion. We have predicted a model for the amphoteric behavior of arsenic, and have explained its behavior in liquid phase epitaxy (LPE) from both the tellurium melts and the mercury melts. Annealing strategies for arsenic activation as a *p*-type dopant following growth by molecular beam epitaxy (MBE) have also been suggested. We discuss the trends found among the compounds in terms of the underlying bond strengths to understand why the various elements behave the way they do. Our modeling of the MBE growth surface indicates that growth rates are fastest on the {211}B surface, but that there will be fewer grown-in defects on the {211}A surface. We have interacted expectively with Lockheed Martin (LMIRIS), Texas Instruments (now Ratheon TI Systems), Rockwell Science Center, and Santa Barbara Research Center (SBRC). The predictions we have made have influenced their focal plane array processing strategies, and we believe, have improved performance.

2 APPROACH

The approach we use in this work is described in our technical papers written under this program and included as Appendices A–H. Here we provide a brief overview; the reader is referred to the more extensive write-ups provided in the appendices for further details and for literature references.

The calculations of thermodynamic behavior of impurities and native defects in HgCdTe and CdTe can be divided into two major parts: The first consists of the statistical theory from which the concentrations of the defects in various positions in the lattice are predicted; the second consists of all of the parameters that enter into the statistical theory.

The statistical theory we use is based on an extended quasichemical formalism which includes an arbitrary cluster size and overlap, and which also includes the equilibration of the electronic subsystem simultaneously with the atomic system. In the theory, the real space lattice is divided into clusters. Here we choose clusters consisting of four lattice sites (two cation and two anion) and four tetrahedral interstitial sites. This is the minimum size cluster for calculating the defect complexes considered in this paper. An energy, a set of ionization states, a set of ionization-dependent degeneracies, and a chemical identity is associated with each cluster. The free energy of the system can be expressed in terms of the cluster-specific free energies, the configurational entropy, and the free energy of the electronic excitations. The equilibrium set of clusters is determined by minimizing the free energy, subject to a set of constraint equations.

One of the inputs to the statistical theory is the set of neutral cluster energies; these energies are calculated using the full-potential linear muffin-tin orbital method (FP-LMTO) within the local density approximation (LDA). Gradient corrections to the LDA were added so that the vapor phase of mercury could be used in the calculations to establish the state of the material within the existence region. Defect energies were calculated in the FP-LMTO using 32-lattice-site supercells; and 4-lattice-site cluster energies for the statistical theory were extracted by subtracting off the energy of a 28-lattice-site cell with no defect. Ionization energies were also calculated in the LDA and are cast in terms of one-electron excitations. No negative-U states were found. Vibrational excitations were also calculated [1]. Electronic excitations are calculated using Fermi-Dirac statistics. The temperature- and x-dependent band gap were taken from experiment. The density of states hole effective mass of 0.43 was used, and the conduction band density of states was fit to the intrinsic carrier concentrations using a linear dispersion for the band shape.

3 NATIVE DEFECTS IN LPE MATERIAL, MBE MATERIAL, AND DURING PROCESSING

We have refined our calculations of native point defects in HgCdTe and have modified our previous findings [1] only slightly. First we have found that the mercury vacancy is only a singly ionized acceptor in $x = 0.2$ material, contrary to the findings of Vydyanath [2] who deduced that the mercury vacancy was a doubly ionized acceptor based on mobility measurements. This finding has been coupled into the simulators developed at Stanford University under this program. SRI International has investigated the mercury interstitial and find that it is likely to be an interstitialcy (two mercury atoms sharing a common cation lattice site); this is important to understanding the diffusion of mercury in low-temperature mercury-saturated anneals. The interstitial densities we predict are still much lower than those used in the Stanford University simulators. The Frenkel pair energy (related to the generation rate of mercury–interstitial mercury vacancy pairs) has been calculated and it is found to be unbound by approximately 1 eV. A diagram showing the deviation from stoichiometry as a function of temperature has been developed [3].

Our calculations can be applied to both mercury- and tellurium-rich materials at all temperatures, and thus are applicable to both LPE and MBE growth conditions as well as to subsequent processing steps. Native point defects have also been included in all of our calculations of the properties of the impurities. Pairing of impurities with native point defects has been found to be very important — for example, all of the *n*-type dopants (indium, iodine, and arsenic incorporation on the cation sublattice) have been found to pair with cation vacancies. These vacancies bound into impurity complexes are an additional source of vacancies and important to include — for example, when developing a model of arsenic activation [4-5].

4 IMPURITIES IN HgCdTe AND CdTe SUBSTRATES

In this work, a wide array of impurities were studied under a variety of growth and processing conditions [3–8].

4.1 *n*-TYPE DOPANTS IN HgCdTe

Indium is the element most often used for *n*-type doping in both LPE and MBE growth, and is generally considered to be "well behaved." Our calculations reflect these findings. We predict that the indium incorporates nearly 100% on the cation sublattice where it behaves as a shallow donor. There is a significant binding of an indium substituting on the cation sublattice to a cation vacancy, and while these complexes are present in the material, they account for less than 1% of the indium incorporation for all temperatures. The indium interstitial fraction is extremely small, and therefore the indium-vacancy complexes are probably the means by which indium diffuses. In material doped with 10^{15} cm^{-3} indium and subjected to a typical 250 °C, mercury-saturated anneal, the indium-vacancy complex density is only ~10^{7} cm^{-3}, accounting for the observed stability of indium-doped devices [3-6] (Appendices H and C).

Although indium has been a satisfactory dopant in materials grown by LPE and MBE, gas-phase reactions with indium have made it a less desirable dopant for growth by metal organic vapor phase epitaxy (MOVPE). Iodine is the species most often used in MOVPE growth. Like indium, iodine has a low interstitial fraction and low incorporation fraction on the "wrong" sublattice, and in this sense iodine is a well-behaved *n*-type donor. Iodine substituting on the anion sublattice behaves as a donor and binds to the cation acceptor vacancy, resulting in a neutral complex. For high iodine densities and mercury-deficient conditions, this complex accounts for the majority of the iodine incorporation. In Figure 3 of Appendix H, we have plotted the iodine incorporation and native point defects for a fixed iodine concentration of 3×10^{19} cm^{-3}, as a function of the mercury partial pressure at 500 °C. We have also calculated the carrier concentrations at 77 K assuming the high-temperature defect structure is quenched into the crystal, and we compare this to some experimental results on bulk grown and annealed samples. The theory is in very good agreement with experiment, showing a *p*-to-*n*-type conversion as the mercury partial pressure is increased, with the *p*-type behavior at low pressures due to cation vacancies and the *n*-type behavior at higher mercury partial pressure due to the iodine. The discrepancy with experiment can be accounted for by a small shift in our predicted position in the existence region.

4.2 *p*-TYPE DOPANTS IN HgCdTe

Copper, silver, and gold are found to be incorporated nearly exclusively on the metal sublattice and to be 100% active for all near-equilibrium growth and processing conditions. The density of interstitial copper is high enough to impact copper diffusion. Solubility of these dopants is found to decrease as the mercury partial pressure increases, although the interstitial fraction increases with increasing mercury partial pressure. These findings are important in understanding how these dopants behave under interstitial injection — for example, during the anneals following implantation, as in the Texas Instruments process. As mercury interstitials are injected into a material, the material moves to mercury-rich conditions, lowering the dopant solubility, and mobilizing them by increasing their interstitial fraction. The dopants are kicked out of the annealed region, and move ahead of the interstitial diffusion front. Further discussion of our work on copper, silver, and gold can be found in References 3 and 6–8, or in Appendices C, D, F, and H.

The behavior of the group V impurities, phosphorus, arsenic, and antimony are much more complex than the group I dopants. We will discuss arsenic as the prototypical group V dopant; qualitatively similar behavior for phosphorus and antimony was found in our previous work [Reference 6]. Arsenic has been known to behave amphoterically in HgCdTe, with the desired *p*-type behavior under mercury-rich conditions, and *n*-type behavior under tellurium-rich conditions. Our calculations predict this amphoteric behavior. We find negligible incorporation of arsenic at interstitial sites, but do find incorporation on the cation sublattice that dominates the arsenic incorporation at low mercury partial pressures. The arsenic on the cation sublattice behaves as a donor, thus explaining the observed *n*-type behavior of arsenic-doping in mercury-deficient materials. Some of the arsenic on the cation sublattice are bound to cation vacancies, creating neutral complexes. These complexes are most likely the means by which arsenic diffuses in this material. Our findings have been correlated with literature on the behavior of the group V elements in bulk grown material, LPE material from the tellurium and mercury melts, and MBE material both as-grown and subjected to subsequent anneals. Further discussion of our work on the group V dopants can be found in References 3–6, or in Appendices C, E, G, and H.

4.3 ACTIVATION OF ARSENIC IN HgCdTe

In Section 4.2 we discussed the equilibrium behavior of the group V dopants in HgCdTe. In this section we discuss the activation process, once again focusing on arsenic, the most commonly used *p*-type dopant; similar results are expected for phosphorus and antimony.

From our equilibrium calculations we concluded that the amphoteric behavior of the group V dopants is due to incorporation on the cation sublattice under tellurium-saturated conditions. This is in agreement with findings on growth by LPE from the tellurium melt, and also with results on MBE growth which is believed to occur under mercury-deficient conditions. Thus to render inactive arsenic active, it must transfer from the cation to the anion sublattice.

We propose a mechanism for transfer of an arsenic from the cation to anion sublattice (the essential step in the activation process) as follows, and as shown schematically in Figure 3 in Appendix G. The starting defect for the transfer is the arsenic on a cation site bound to a mercury vacancy. Our calculations show that this defect complex will be present in large densities in as-grown material. In the first step of the activation process, the intervening tellurium will transfer into the cation vacancy site, creating a tellurium antisite, with the arsenic following and transferring to the vacated tellurium site and leaving behind a cation vacancy. In the final step, the cation vacancy–tellurium antisite pair, which was previously shown to form a bound pair, will diffuse away from the arsenic now residing on the tellurium sublattice. As a result of the transfer process, the density of the vacancy–antisite pairs will be supersaturated, and they must diffuse to a surface where they can be annihilated.

The model of the activation has a number of attractive features. The activation model involves only a short-range bulk process. It does not require the creation or destruction of a unit cell, other than through the eventual equilibration of the neutral vacancy–antisite pair which is generated in the site transfer process. The model also involves only the major defects in the lattice. Unfortunately, as a result of the arsenic site transfer, the system is supersaturated with tellurium; the vacancy–antisite pairs can annihilate either at a free surface, or they can form tellurium precipitates in the bulk. Because the vacancy–antisite pair is neutral, even if it is not fully equilibrated and nonequilibrium concentrations remain in the material following the activation, it will not be electrically active and will not affect the carrier concentrations. Due to its strain (the tellurium antisite results in a compressive strain in the surrounding lattice) and charge dipole, the vacancy–antisite pair will provide an additional scattering center, and if present, may adversely affect mobilities.

We consider the mechanisms occurring when MBE-grown material is subjected to a low-temperature mercury-saturated anneal directly following growth. As the temperature is raised to ~ 220 °C under mercury-saturated conditions, two processes occur simultaneously: (1) cation vacancies are filled, establishing new equilibrium concentrations; and (2) arsenic is transferred from the cation to the anion sublattice, approaching a new equilibrium with arsenic on the two sublattices. According to our proposed model, for the second process to proceed, cation vacancies must be present, so that for optimum transfer one wants the second process to occur more rapidly than the first. We predict that if the phase field is traversed too rapidly—which can occur by going directly to mercury-saturated conditions following MBE growth—the mobile mercury interstitials fill the cation vacancies more quickly than the site transfer can occur. Because vacancies are necessary for the site transfer to proceed, the arsenic becomes locked onto the cation sublattice, where it behaves as a donor. This is consistent with the finding that MBE material subjected to a mercury-saturated anneal directly following growth is *n*-type. We have calculated the 77 K carrier concentration for material that has been equilibrated under MBE growth conditions, and then subjected to a mercury-saturated anneal at 220 °C, but suppressed the transfer of arsenic to the anion sublattice to mimic this phenomenon. We find that the

material is *n*-type with a carrier concentration equal to the total arsenic concentration. The experiments find that an *n*-type carrier concentration is closer to 10% of the total arsenic concentration. The discrepancy between theory and experiment can be attributed to uncertainties in the theory—for example, the exact location of the donor level associated with As_{Hg} and its temperature dependence, or our prediction of the pressure at which the crossover between arsenic occupying the cation and anion sublattice occurs—or the partial activation of the arsenic, with some of it transferring to the anion sublattice under the annealing conditions.

Our model for the activation process involves only the primary defects in the lattice. The net product of the activation process is the generation of a tellurium antisite in the form of a tellurium antisite–vacancy pair; and as a consequence of the activation process, the density of this defect pair is initially supersaturated. Although the pair is neutral, if the vacancy–antisite pairs do not all equilibrate in post-growth processing, it may serve as a scattering and/or recombination center and thereby degrade the device properties. This is because the antisite produces strain in the lattice (the antisite is too big, producing tensile stress about it) and additionally will have a charge dipole associated with it. This supersaturated density of vacancy–antisite pairs may also condense to form micro-precipitates.

Effective activation anneals will involve elevated temperatures so that sufficient thermal energy is available to surmount the activation barrier for site transfer, and also so that sufficient vacancies are available to catalyze the reaction. More important is the need to traverse the phase field from tellurium- to mercury-saturated conditions slowly, particularly in the pressure regime where the dominant arsenic incorporation changes from the cation to the anion sublattice, so that the transfer process outlined above can take place before the mercury vacancies are depleted.

4.4 "BOTHERSOME IMPURITIES": LITHIUM AND SODIUM HgCdTe

Lithium and sodium are both impurities which in most HgCdTe-based device structures are considered undesirable, but that are often observed to be present. Not much work has been done on the properties of lithium, and less still on the properties of sodium in HgCdTe, but both are typically characterized as fast diffusers, and lithium gettering to regions of damage and high vacancy concentration has also been observed. The behavior of lithium and sodium are similar to the behavior of copper, silver, and gold. Both lithium and sodium are acceptors when incorporated on the cation sublattice, and neither shows any substitution on the anion sublattice. Both lithium and sodium repel cation acceptor vacancies, and therefore have a negligible pairing with vacancies. The interstitial fractions for lithium and sodium are much higher than for the Column IB dopants, and are the highest for sodium. This accounts in large part for the high mobility of these impurities, given that the interstitials are faster diffusers than substitutionals. Furthermore, we find that the interstitial fraction increases as the temperature is lowered and as the mercury partial pressure is increased. Thus we expect these impurities to be very mobile under conditions of low-temperature, cation-rich anneals. Our conclusion is that lithium and

sodium may account for some of the variability seen in devices since these impurities will be very mobile and may be gettered to and released from sites under low-temperature processing . Further discussion of our work on copper, silver, and gold can be found in References 3, 7, and 8, or in Appendices D, F, and H.

4.5 IMPURITY INTERACTION FOR HgCdTe AND CdTe

The properties of the impurities in CdTe-based substrate have also been calculated. The basic properties of the impurities in CdTe are similar to those found in HgCdTe: (1) incorporation on the cation sublattice dominates for most temperatures and pressures; (2) on the cation sublattice they all produce acceptor levels near to the valence band edge; (3) interstitials represent the second most important incorporation site; and (4) incorporation on the anion sublattice is negligible.

Strategies for substrate cleaning have been proposed. If the CdTe material is subjected to a cadmium-rich anneal prior to the epilayer growth, the cation vacancy concentration will be reduced and the impurity chemical potential increased. Consider a preanneal at 470 °C under cadmium-saturated conditions ($P_{Cd} = 10^{-2}$ atm). If this material is subjected to LPE growth of HgCdTe with comparable impurity density, there will be a strong driving force for the impurity to leave the region of high chemical potential (in the CdTe) and enter a region of low chemical potential (the HgCdTe). The lower the temperature for the cadmium-saturated preannealing of the CdTe, the larger the driving force for the gettering. Optimal impurity gettering will also occur if the HgCdTe is grown tellurium rich. This sacrificial HgCdTe layer could then be removed. A version of this strategy has been reported previously by II-VI Incorporated.

Following substrate cleaning, a strategy for minimizing impurity gettering from the substrates into the epilayer has also suggested. If the CdTe material is subjected to a tellurium-saturated anneal prior to epilayer growth, the vacancy density will be maximized and the impurity chemical potential in the substrate will be driven down, reducing the driving force for out-diffusion into the HgCdTe. The more cation vacancies introduced into the CdTe during the preanneal, the lower the impurity chemical potential in the substrate will be during epilayer growth, and the larger the gettering into the substrate (or the smaller the gettering into the epilayer) will be.

We have also examined the response of the impurities to strain in the lattice, in part to see if the occasionally observed pileup of these impurities at interfaces can be explained by a strain release mechanism. Our calculations show that the strain associated with lithium, sodium, and copper impurities substituting both on the cation sublattice and interstitially is small, and could result in no more than a 10% concentration enhancement of the impurity at an otherwise ideal interface. As we showed above, though, lithium and sodium will be mobilized during the low-temperature, mercury-saturated anneal, and will be pushed ahead of the in-diffusing flux of mercury interstitials. Thus, these impurities will be swept out of the HgCdTe toward the epilayer-substrate interface, where they might be pinned by dislocations (both by decorating the core and by forming a Cotrell atmosphere), and other extended defects.

Further discussion of our work on impurity interaction between the epilayer and the substrate can be found in References 7 and 8, or in Appendices D and F.

5 MBE GROWTH SURFACE CALCULATIONS

We calculated energies required to remove atoms from various configurations on (111), (110), (100), and (211) HgTe surfaces. The excess pair energies for various species are then calculated and are used in a thermodynamic model to study the growth. All energies are obtained using a Green's function method. The pair distributions are calculated from these energies in a generalized quasichemical approximation. The calculated critical temperatures for surface roughness transition are found to be considerably higher than the usual growth temperature of 185 °C, so the growth on these surfaces is expected to be layer-by-layer with formation of two-dimensional islands. However, among the surfaces studied, only the (211) surfaces have an attractive binding energy for Hg, making those surfaces suited for better growth. The critical temperature for growth on (211) Hg is slightly higher than that for (211) Te, but we also find that the Hg sticking coefficient on a (211) Hg surface is considerably lower than that on a (211) Te surface. These calculations are consistent with the observed higher growth rate of the (211) Te surface. Our calculations suggest that there will be fewer grown-in vacancies and Te antisites, at the expense of growth rate and sticking coefficient, for crystals grown on a (211) Hg surface. We further calculated the Hg and Te vacancy formation energies as functions of surface orientations and layer depth. The cation vacancy formation energies from completed surface regions (islands) are higher than bulk values near anion terminated surfaces and smaller than bulk values near cation terminated surfaces.

6 PUBLICATIONS

All publications have been included as appendices to this document. Publications are listed chronologically here.

A. Sher, M. A. Berding, S. Krishnamurthy, M. van Schilfgaarde, and A.-B. Chen, "Alloys for infrared applications," *Anales de la Asociacion Quimica Argentina*, **85**, 23 (1996)

S. Krishnamurthy, A.-B. Chen, and A. Sher, "Comparison of HgTe materials growth in (100), (110), (111) , and (211) orientations," (PLEASE CHECK THIS TITLE FOR ME) *J. Electron. Mater.* **25**, 1254 (1996).

M. A. Berding, A. Sher, and M. van Schilfgaarde, "Behavior of *p*-type dopants in HgCdTe," *J. Electron. Mater.* **26**, 625 (1997).

M. A. Berding, A. Sher, and M. van Schilfgaarde, "Bothersome impurities in LWIR HgCdTe," *Proceedings of the 1997 IRIS Materials Meeting.*

M. A. Berding, A. Sher, and M. van Schilfgaarde, "Arsenic activation in MBE-grown HgCdTe," *Proceedings of the 1997 IRIS Materials Meeting.*

M. A. Berding and A. Sher, "Dopants in HgCdTe," *Proceedings of the 1997 IRIS Materials Meeting.*

REFERENCES

1. M. A. Berding, A. Sher, and M. van Schilfgaarde, *Phys. Rev. B*,. **50**, 1519 (1994).
2. H. R. Vydyanath, *J. Electrochem. Soc.* **128**, p. 2609 (1981).
3. M. A. Berding and A. Sher, submitted to *Proceedings of the 1997 Fall Meeting of the Materials Research Society*, and included as Appendix H.
4. M. A. Berding and M. van Schilfgaarde, *Proceedings of the 1997 IRIS Materials Meeting,* and included as Appendix E.
5. M. A. Berding, A. Sher, M. van Schilfgaarde, A. C. Chen, and J. Arias, submitted to *J. Electron, Mater.,* and included as Appendix G.
6. M. A. Berding, A. Sher, and M. van Schilfgaarde, *J. Electron, Mater.,* **26,** 625 (1997) and included as Appendix C.
7. M. A. Berding, A. Sher, and M. van Schilfgaarde, *Proceedings of the IRIS Meeting*, and included as Appendix D.
8. M. A. Berding, A. Sher, and M. van Schilfgaarde, *J. Electron, Mater.,* and included as Appendix F.
9. S. Krishnamurthy, A.-B Chen, and A. Sher, *J. Electron, Mater.,* **25,** 1254 (1996) and included as Appendix B.

APPENDIX A

A. Sher, M. A. Berding, S. Krishnamurthy, M. van Schilfgaarde, and A.-B. Chen, "Alloys for infrared applications," *Anales de al Asociacion Quimica Argentina*, **85**, 23 (1996)

ALLOYS FOR INFRARED APPLICATIONS

A. Sher, M.A. Berding, M. van Schilfgaarde

SRI International, Menlo Park, CA 94025

ABSTRACT

This review focuses initially on the workhorse of materials for infrared focal plane arrays (IRFPAs), $Hg_{1-x}Cd_xTe$. In the past ten years, the technology has progressed from a situation where, with poor yield, 64 x 64 photoconducting arrays could be built, to one where it is becoming routine to make 256 x 256 photodiode arrays, and 512 x 512 or 940 x 4 arrays are often made as well. We will review, in generic terms, the major modifications in materials growth and processing that have been responsible for these impressive steps. This will, as a matter of course, take us into aspects of modern computational methods. These methods now permit us to appreciate the idiosyncrasies of $Hg_{1-x}Cd_xTe$ that give it its special character, but more importantly to devise ways to circumvent its worst faults. Often, these improvements were in fact discovered experimentally, but the theory provides a means to frame the important results in a coherent picture.

We will touch on issues involving substrates, liquid phase epitaxy (LPE), molecular beam epitaxy (MBE), native point defects, dislocations, dopants, and passivation. Then, we will briefly introduce new classes of alloys, $In_{1-x}Tl_xP$ and $In_{1-x}Tl_xAs$, that are predicted to be superior materials for IRFPAs. The existence of these materials was first suggested theoretically and they have now been grown. Preliminary experiments indicate that they exhibit the predicted properties.

INTRODUCTION

The subject of materials to support various infrared (IR) applications is a rich one, ranging over many natural and engineered materials. This review focuses on $Hg_{1-x}Cd_xTe$, the workhorse alloy for mid- and long-wave IR (MWIR and LWIR) applications. Then, properties of prospective alternatives, $In_{1-x}Tl_xP$ and $In_{1-x}Tl_xAs$, are discussed. This leaves out, for example, $Pb_{1-x}Sn_xTe$, Pt:S, InSb, strained-layer superlattices, and quantum-well materials. Some of these materials have advantages relative to $Hg_{1-x}Cd_xTe$ alloys, but they also have drawbacks. Some are already materials of the past, and others, analogous to the relation between GaAs and Si, may perpetually be materials of the future.

To appreciate the demands made on materials suitable for IR focal plane arrays (IRFPAs), we must understand a few system issues.[1] An ideal active material would be grown on large-area, dislocation-free, lattice-matched semi-insulating substrates. The active material would be made into arrays of high-quantum-efficiency, passivated diodes. These diodes must be uniform over the array, so the corrections that must be programmed in the read-out integrated

circuit (ROIC) fall within realizable bounds. The IR sensitive array must be coupled into the ROIC in a way that will survive many temperature cycles. The IRFPA should function at near background-noise-limited performance levels for each pixel, at as high an operating temperature as possible. The response time of the array should be as fast as possible. The product ($NE\Delta T \cdot \Delta A \cdot \tau$) of the noise equivalent temperature difference ($NE\Delta T$) that an array can distinguish between resolution elements, the resolution area ΔA, and the response time τ is a measure of the system capabilities. This product should be made as small as possible. Generally, this product is materials-property limited, and for a given spectral interval, device design and operating temperature trades can be made among the three features, depending on application needs.

With these concepts in mind, we can discuss how a set of materials properties set the most important materials-dominated characteristics of $Hg_{1-x}Cd_xTe$ alloys. We will present an overview of substrates, native point defects, dislocations, and passivation. These are not the only important materials-related issues, but they illustrate how far control of these materials has advanced, and where improvements would be helpful.

This sets the stage for the introduction of two new alloys, $In_{1-x}Tl_xP$ and $In_{1-x}Tl_xAs$, that we have predicted[2] will serve as superior materials for IRFPA applications. The materials had never been prepared when we used our first-principles methods, based on Schrödinger-equation solutions, to predict their properties. They have now been grown, and preliminary experiments indicate that they exhibit the predicted properties.[3]

SUBSTRATES FOR $Hg_{1-x}Cd_xTe$-BASED IRFPA

A number of issues dictate substrate choices.[1,4] They should be

- Lattice matched to the active material to minimize dislocations in the epitaxially grown active material
- Uniform over large areas to enable high $NE\Delta T$ values and to allow effective manufacturing of several IRFPAs on each substrate
- Free of precipitates, dislocations, and other extended defects
- Free of Cu and other impurities that can diffuse into devices and degrade performance

While alternative substrates are under development, $Zn_{1-x}Cd_xTe$ lattice matched to $Hg_{0.88}Cd_{0.22}Te$ for LWIR or to $Hg_{0.70}Cd_{0.30}Te$ for MWIR applications continues to be the favored substrate material. The bond lengths d of HgTe, CdTe, and ZnTe are, respectively, 2.797 Å, 2.805 Å, and 2.643 Å. The bond lengths of alloys closely follow Vegard's Law. For a $A_{1-x}B_xC$ pseudobinary alloy, it states that the lattice constant is $\bar{d} = (1 - x)d_{AC} + xd_{BC}$. Thus, a ~4% ZnTe in CdTe lattice matches to LWIR-MCT. Several groups[4,5] have now succeeded in making uniform, large-area, single crystals ($\lesssim$5 cm^2) of $Zn_{0.04}Cd_{0.96}Te$. Annealing at high temperatures in a high Cd vapor pressure eliminates most Te inclusions.[6] The Cu content is reduced to acceptable levels by growing sacrificial layers of HgCdTe on them.[7] The Cu preferentially segregates into the MCT layers, leaving the substrate free of Cu. This sacrificial MCT layer is then etched off before the devices are grown.

Candidate alternative substrates under development consist of either Si, GaAs, or Al_2O_3 wafers[8] with buffer layers of $Zn_{1-x}Cd_xTe$. While these substrate materials can be prepared in large areas, and are rugged, they tend to have dislocation densities high enough to significantly reduce the performance of devices grown on them.

NATIVE POINT DEFECTS AND IMPURITIES

The properties of nearly all devices on any materials are determined by a few fundamental bulk crystalline parameters, and by imperfections.[9–11] Some imperfections, like donors or acceptors, are introduced by intent. However, imperfections are often harmful and a great deal of engineering effort is devoted to their elimination. The native point defects (NPDs) in MCT are more prevalent than in almost any other semiconductor alloy.[12,13] Berding et al.,[13] based on first-principles calculations (see Fig. 1), have shown that Hg-vacancies (V_{Hg}), Te-antisites (Te_{Hg}), and Hg-interstitials (Hg_I) are free energy permitted for many processing conditions in high enough concentrations to affect devices. The other NPDs' Hg-antisites (Hg_{Te}), Te-vacancies (V_{Te}), and Te-interstitials (Te_I) have such small densities for most processing conditions that they can be neglected.

It was well known from experiments that V_{Hg} were present in these materials in high concentration, and this center, even at low temperatures, is a double acceptor.[12] However, the densities and characters of the other defects were unknown.

Theory now predicts that the Te_{Hg} and Hg_I are both donors[13] and the Te_{Hg} may be present in high enough concentrations for typical growth and processing conditions to affect IRFPA performance. The Hg_I densities are generally too low to directly impact devices, but because this NPD has a high diffusion constant, it does influence some important processes.[14]

While the equilibrium concentration [Te_{Hg}] of Te_{Hg} sites in one typical processing step designed to fill V_{Hg} sites (~250 °C anneal in a high Hg partial pressure) is quite low (see Fig. 1), equilibrium is rarely reached, because Te_{Hg} diffuses via a slow V_{Hg} exchange mechanism. The diffusion rate is further slowed if the V_{Hg} are filled. Therefore, the [Te_{Hg}] concentration often is frozen-in at nonequilibrium values and thus depends on the growth and processing history. We have argued[13] that Te_{Hg} have three major means through which they may influence devices. First, Te_{Hg} may be the "residual donor" in normally undoped material that is nearly always present following low-temperature Hg-saturated anneals, and does not freeze out even at 2 K. No experiments have ever identified an impurity responsible for this behavior. Second, Te_{Hg} are most likely a principal Shockley-Read nonradiative recombination center, and limit lifetimes. Finally, Te_{Hg} are feedstock for Te precipitates. (These second-phase extended defects are associated with dislocation clusters, strain fields, and other device degradation mechanisms. The presence of a Te-precipitate near the p-n junction of a pixel will often cause it to fail.)

The [Te_{Hg}] concentration can be minimized in a liquid-phase epitaxially (LPE) grown layer if it is accomplished from a Hg-rich melt.[15] The reasons are evident upon examination of Fig. 2 on the Hg side of the existence curve where [Te_{Hg}] is low at the typical growth temperature (500 °C). On the other hand, materials grown from Te-rich melts on the Te edge of the existence curve have a high [Te_{Hg}]. It would therefore seem logical to always grow from a Hg-rich melt. However, while one can get In (a donor) into this melt and into the epitaxial layer, this is not true for As (the preferred acceptor). To *p*-dope with As, LPE growth is done from Te-rich melts.

Many manufacturers dope *p*-type with V_{Hg}; however, these materials have shorter lifetimes than those that are As doped. This difference has been ascribed to the possibility that V_{Hg}, in addition to serving as an acceptor, also have mid-gap states acting as recombination centers. This view was reinforced by studies that show lifetimes roughly tracking [V_{Hg}] concentrations.[16] However, there is no theoretical support for V_{Hg} mid-gap states. It is more

likely that Te_{Hg} sites are the recombination centers, and the $[Te_{Hg}]$ concentrations correlate with those of $[V_{Hg}]$, as indicated, for example, in Fig. 2.

DISLOCATIONS

Numerous dislocation types exist, but the discussion here will treat them as if they can be classed into one or another of only two species. The first arises from misfits between the lattice constant of the substrate and epitaxially grown active layers.[9–11] A very small misfit can cause dislocation densities in the 10^9 cm^{-2} range. This density is sufficient to kill any device whose p-n junction falls into the thin (<1 μm) layer adjacent to an interface where these high misfit dislocation densities reside. The second class is threading—edge dislocations often originating in the substrate and continuing up through the active layers grown on it.[17] The minimum threading dislocation densities attainable are normally set by the substrate, which is one reason why it is important to have good substrates. Edge dislocations have strain fields associated with them, and because MCT is piezoelectric these strain fields generate spatial varying potentials.[17] These potentials are generally screened in the bulk material, but in the depletion layers associated with p-n junctions they will add to the built-in junction potentials. Their net effect is to increase the tunneling currents responsible for leakage and noise. A single dislocation in a pixel degrades performance slightly, but several conspire to degrade performance in a nonlinear manner.

Theory indicates the reasons why the long-range strain fields should affect tunneling currents in a nonlinear fashion,[16] but the observed quadratic dependence of leakage currents in a pixel on dislocations number has not been predicted.[9,10] Achieving uniform performance from pixels in an array requires not only low dislocation densities ($<10^5$ cm^{-2}), but also the avoidance of dislocation clusters.

An as yet unidentified mechanism is responsible for variability of the pixel response distribution, even among pixels in which no threading dislocations are observed.[9–11] Studies are continuing to identify the cause of these variations.

PASSIVATION

To avoid crosstalk among pixels, the pixels are usually built as individual mesas with the p-n junctions parallel to the mesa tops, and located somewhere within them. Leakage currents at mesa surfaces, particularly across the p-n junction, will degrade device performance. To avoid this leakage, coatings are grown on these surfaces to "passivate" them.[18,19] Many reasons exist for excess current leakage at surfaces. Most are related to effects of dangling bond states, dopant surface segregation, or alloy surface segregation. A good passivant will tie up the dangling bond states, and ensure that there is no important segregation occurring in processing steps that follow the passivant deposition.[20]

A key problem in $Hg_{1-x}Cd_xTe$ is related to alloy segregation. In general, two mechanisms drive surface segregation of the constituents in alloys.[20] The first is related to the bond energies of the constituents. The alloy surface enthalpy is minimized if the constituent making the weaker bond is on the surface where it makes fewer bonds. However, if all of one species is on the surface this leads to a low entropy. Thus, the surface free energy is minimized by some finite concentration of both constituents on the surface, but one that may differ from their bulk concentrations. In $Hg_{1-x}Cd_xTe$, it is the Hg that this mechanism tends to drive to the surface. The second general mechanism, strain release, is inactive in $Hg_{1-x}Cd_xTe$. The minority alloy constituent tends to be driven to the surface because these atoms experience less strain

energy on the surface than in the bulk. Because the lattice constants of HgTe and CdTe are so close, strain release plays a small role in the $Hg_{1-x}Cd_xTe$ alloys.

The net effect of alloy surface segregation in $Hg_{1-x}Cd_xTe$ is to produce a thin Hg-rich layer at the surface. For a bulk $x < 0.4$, the equilibrium surface concentration x_s is small enough that four surface layers are semimetal-like in the transverse plane and therefore will contribute greatly to leakage currents.

If a passivant is used that causes both cations to have the same binding energy at the interface, the driving force for segregation vanishes. A semi-insulating CdTe layer on $Hg_{1-x}Cd_xTe$ has this character. On the other hand, if the passivant is such that Cd makes a stronger bond to it than Hg, the interface tends to be Cd rich. A CdS or SiO_2 passivant has this character. The most successful passivant has proven to be CdTe. It is a near lattice match and minimizes dangling bonds. It also minimizes alloy segregation, and produces relatively small driving forces for dopant segregation.

$In_{1-x}Tl_xP$ AND $In_{1-x}Tl_xAs$ ALLOYS

We have evaluated three III-V semiconductor alloys[2,21,22]—$In_{1-x}Tl_xP$ (ITP), $In_{1-x}Tl_xAs$ (ITA), and $In_{1-x}Tl_xSb$ (ITS)—as possible candidates for future LWIR detector materials. The cohesive energies, elastic constants, band structures, electron mobilities, and phase diagrams were calculated and compared to those of $Hg_{1-x}Cd_xTe$ (MCT) alloys. The band gaps of all three III-V alloys change from negative to positive values as the alloy composition x decreases from 1 to 0. The x values for the 0.1-eV gap are estimated to be 0.67, 0.15, and 0.08, respectively, for ITP, ITA, and ITS. While both ITP and ITA form stable zincblende solid solutions for all alloy compositions, zincblende ITS is stable only for a range of x less than 0.15. The complication of the phase diagram in ITS is caused by the existence of a stable CsCl phase for pure TlSb. The alloy mixing enthalpies for ITP and ITA are comparable to those in MCT, and their phase diagrams should be qualitatively similar, characterized by simple lens-shape liquidus and solidus curves. Both ITP and ITA have considerably larger cohesive energies and elastic constants than those of MCT, indicating that they are structurally robust. At a 0.1-eV gap, the band structures near the gap and the electron mobilities in ITP, ITA, and ITS are also found to be comparable to those of MCT. Since the lattice constants of TlP and TlAs are less than 2% larger than the respective values in InP and InAs, the latter should provide natural substrates for the growth of active LWIR alloys, and offer a potential to integrate the detector array and read-out circuit.

Detector-Related Results

As stated earlier, the alloys $In_{1-x}Tl_xP$ and $In_{1-x}Tl_xAs$ have properties that distinguish them as outstanding candidates for IR electro-optic receiver and emitter devices. Here, we concentrate on the properties of $In_{1-x}Tl_xP$ in the LWIR because this alloy nearly lattice-matches to InP substrates and, therefore, offers the prospect of integrated laser emitters, focal-plane-array (FPA) detectors, and ROICs on the same chip. This capability could enable use of device architectures formerly deemed impractical because currently used LWIR materials are incapable of supporting them.

According to our first-principles theory, the following properties of TlP make it an attractive IR material candidate:

- It forms in the zincblende structure.
- Its lattice constant (5.96 Å) closely matches that of InP (5.83 Å) (so the pseudo-binary $In_{1-x}Tl_xP$ liquidus and solidus phase diagrams have simple lens shapes).
- Its cohesive energy (2.56 eV/atom) is 58% greater than that of HgTe (1.62 eV/atom).
- It is a semimetal with a negative gap of -0.27 eV, about the same as that of HgTe (-0.3 eV).

The accompanying table presents the properties of the alloy with a 0.1-eV band gap that are related to LWIR-FPA performance and processing. The salient features are the following:

- The alloy concentration is x = 0.67, and the concentration variation of the gap |dEg/dx| is 1.42 eV, 16% smaller than that of $Hg_{0.78}Cd_{0.22}Te$ (1.69 eV).
- The elastic constants are ~33% larger than those of the LWIR HgCdTe alloy.
- The transverse optical phonon energy is 34.6 meV, 139% larger than that of HgCdTe (14.5), thereby limiting very-long-wave infrared (VLWIR) utility to $\lambda_c < 36$ μm (this is the only negative feature relative to HgCdTe).
- The temperature variation of the band gap[23] dE_g/dT near 77 K is small (~-0.05 meV/K), about one-seventh as large as that of HgCdTe (0.36 meV/K). (dE_g/dT for $Hg_{1-x}Cd_xTe$ vanishes near x = 0.5, while that of $In_{1-x}Tl_xP$ vanishes close to x = 0.67, the LWIR concentration, greatly simplifying designs for variable temperature operation and eliminating spatial variation in pixel performance caused by temperature gradients over array areas.)
- The electron effective mass is 0.008, almost identical to that of HgCdTe (~0.008).
- The hole effective mass is 0.37, 43% smaller than that of HgCdTe (0.65) (which implies higher hole mobilities and substantially longer electron Auger recombination lifetimes for InTlP).
- The electron mobility at 80 K (6×10^4 $cm^2/V\text{-}s$) is 44% smaller than that of HgCdTe, but it does not die off as rapidly as temperature increases; consequently, electron mobility at 200 K is 4.5×10^4 $cm^2/V\text{-}s$, while the same for HgCdTe is 2.24×10^4 $cm^2/V\text{-}s$, only half as large. (This means that the high temperature responsivity should not degrade as rapidly in InTlP.)

ITA also has some virtues as an LWIR detector. While InAs is not as attractive a substrate as InP (bond energy per atom 3.10 eV) it is still better bound than CdTe (2.20 eV). The gap of TlAs is predicted to be -1.34 eV, so the LWIR concentration of $In_{1-x}Tl_xAs$ is x = 0.15. The predicted cohesive energy per atom of this alloy is 2.80 eV, far better than that of LWIR MCT (1.66 eV). Perhaps the most useful property of ITA is that its electron mobility falls very slowly as temperature increases, so at 200 °C LWIR ITA has $\mu_e = 0.5 \times 10^4$ $cm^2/V\text{-}s$ compared to MCT with $\mu_e = 2.24 \times 10^4$ $cm^2/V\text{-}s$. At still higher temperatures, the ratio of electron mobilities exceeds a factor of 10. Thus, minority carrier responsivities of *p*-type material may remain reasonably high at high temperature.

This collection of properties—plus the extra ease of processing, the lower defect densities expected as a consequence of the high cohesive energy, and the superior InP and InAs substrates (for InP there are 3-inch-diameter wafers available with average dislocation densities of

~10^4 cm^{-2})[3]—lends support to the contention that $In_{1-x}Tl_xP$ will prove to be a striking LWIR-FPA material, and there may be niches for $In_{1-x}Tl_xAs$.

CONCLUDING REMARKS

The narrow-gap alloys discussed in this review all share the problem of being relatively poorly bound. The major consequence of this characteristic is that the materials are fragile, prone to contain high densities of native point defects, and subject to high dislocation densities. Despite these materials difficulties, thirty years of concerted effort have resulted in sufficient control of $Hg_{1-x}Cd_xTe$ so that high-quality images can be made from it with yields that bring costs into a region where commercial as well as military products may soon be affordable.

The Tl-based III-V compound alloys are in their infancy. These materials have been grown, but are certainly not developed. They have the potential to be more robust than their II-VI counterparts. We will have to wait a few months to see if they live up to their promise.

ACKNOWLEDGMENTS

We are indebted to many colleagues who contributed to the work behind this paper: C. Abernathy, S. Krishnamurthy, M.W. Muller, A.T. Paxton, and M. van Schilfgaarde. The work was supported in part by contracts from ARPA, AFOSR, and ONR.

REFERENCES

1. R. Balcerak, *Semicon. Sci. Technol.*, **6**, 1 (1991).
2. M. van Schilfgaarde, A.-B. Chen, S. Krishnamurthy, and A. Sher, *Appl. Phys. Lett.*, **65**, 2714 (1994).
3. C. Abernathy (private communication, 1995).
4. J.P. Tower, S.P. Tobin, M. Kestigian, P.W. Norton, A.B. Bollong, H.F. Schaake, and C.K. Ard, *J. Elect. Mater.*, **24**, 497 (1995).
5. W.J. Everson, C.K. Ard, J.L. Sepich, B.E. Dean, G.T. Neugenbauer, and H.F. Schoake, *J. Elect. Mater.*, **24**, 505 (1995).
6. H.R. Vydyanath, J.A. Ellsworth, J.B. Parkenson, J.J. Kennedy, B. Dean, C.J. Johnson, G.T. Neugenbauer, J. Sepich, and P-R. Liao, *J. Elect. Mater.*, **22**, 1073 (1993).
7. R. Triboulet, A. Fromson-Carli, D. Lorans, and T.N. Duy, *J. Elect. Mater.*, **22**, 827 (1993).
8. S.M. Johnson, T.J. deLyon, C.A. Cockrum, W.J. Hamilton, T. Fung, F.I. Gesswein, B.A. Baumgratz, L.M. Ruzicki, O.K. Wu, and J.A. Roth, *J. Elect. Mater.*, **24**, 467 (1995).
9. S.M. Johnson, A. Righer, J.P. Rosbech, J.M. Petersen, S.M. Tailor, and M.E. Boyd, *J. Vac. Soc. Technol. B*, **10**, 1499 (1992).
10. S.H. Shin, J.M. Arias, D.D. Edwall, M. Zandian, J.G. Pasko, and R.E. deWames, *J. Vac. Soc. Technol. B*, **10**, 1492 (1992).
11. R.S. List, *J. Elect. Mater.*, **24**, 1017 (1995).

12. H.R. Vydyanath, *J. Electrochem. Soc.*, **128**, 2609 (1981).

13. M.A. Berding, M. van Schilfgaarde, and A. Sher, *Phys. Rev. B*, **50**, 1519 (1994).

14. C.R. Helms, J.L. Melendez, H.G. Robinson, S. Holander, J. Hasan, and S. Halepete, *J. Elect. Mater.*, **24**, 1137 (1995).

15. H.R. Vydyanath, *J. Elect. Mater.*, **24**, 1275 (1995).

16. M.C. Chen, L. Colombo, J.A. Dodge, and J.H. Tregilgas, *J. Elect. Mater.*, **24**, 539 (1995).

17. T.A. Paxton, A. Sher, M.A. Berding, M. van Schilfgaarde, and M.W. Muller, *J. Elect. Mater.*, **24**, 525 (1995).

18. Y. Nemirovsky, N. Amir, D. Goren, G. Asa, N. Murnzer, and E. Weiss, *J. Elect. Mater.*, **24**, 1161 (1995).

19. L.O. Bubulac, W.E. Tennant, J. Bajaj, J. Sheng, R. Brigham, A.H.B. Vanderwyck, M. Zandian, and M.V. McLevige, *J. Elect. Mater.*, **24**, 1175 (1995).

20. A. Sher, M.A. Berding, S.R. Patrick, and A-B. Chen, *Proc. IRIS Mater.*, 323 (1990).

21. M. van Schilfgaarde, A. Sher, and A-B. Chen, *Appl. Phys. Lett.*, **62**, 1857 (1993).

22. A. Sher, M. van Schilfgaarde, S. Krishnamurthy, M.A. Berding, and A-B. Chen, *J. Elect. Mater.*, **24**, 1119 (1995).

23. S. Krishnamurthy, A.-B. Chen, A. Sher, and M. van Schilfgaarde, *J. Elect. Mater.*, **24**, 1121 (1995).

FIGURE CAPTIONS

FIG. 1. Total mercury vacancy (solid line) and tellurium antisite (dashed line) densities as a function of mercury partial pressures (atm). Full equilibration of all defects is assumed at all temperatures.

FIG. 2. The concentration of native points as a function of mercury pressure within the phase stability region at (a) 500 °C, corresponding to the LPE growth temperature, (b) 185 °C, the growth temperature for MBE, and (c) 220 °C, a typical temperature for mercury-saturated anneals. A range of concentrations for the mercury vacancy tellurium antisite pair is shown, based on our preliminary results.

LWIR MCT ITP AND ITA PROPERTIES COMPARISONS

	Property	$Hg_{0.78}Cd_{0.22}Te$		$In_{0.33}Tl_{0.67}P$	$In_{0.85}Tl_{0.15}As$
		Theory	Experiment	Theory	Theory
1	$\overline{E}_g$ [eV]	0.1	0.1	0.1	0.1
2	$\overline{E}_b$ [eV/atom]	1.66	1.75	2.75	
3	$\overline{a}$ [Å]	6.45	6.46	5.92	6.08
4	$\hbar\omega_{To}$ [meV]	14.5	14.12	34.6	25.8
5	B[10^{12}erg/cm^3]	0.46	0.42	0.61	0.58
6a	dE_g/dx [eV] @ E_g (77 K) = 0.1 [eV]	1.71	1.69 @ 0 K	1.42	1.80
6b	dE_g/dT [meV/K]	0.36	0.3	—0.05	—
7	m_e^* @ 0 K	0.008	~0.009	0.008	0.007
8	m_h^* @ 0 K	0.65	0.38–0.71	0.37	0.375
9	μe[cm^2/V-s]				
9a	@ 80 K	1.07×10^5	0.986×10^5	6×10^4	1.16×10^5
9b	@ 200 K	2.24×10^4	2.0×10^4	4.5×10^4	6.72×10^4
10	μ_h[cm^2/V-s]				
10a	@ 77 K	—	600–1400	—	—
10b	@ 200 K	—	300–600	—	
11a	teA[ns] @ 1016 [cm^{-3}]	—	10	t(MCT) < t(ITP)	—
11b	t_{hA}[ns]	—	40	—	—

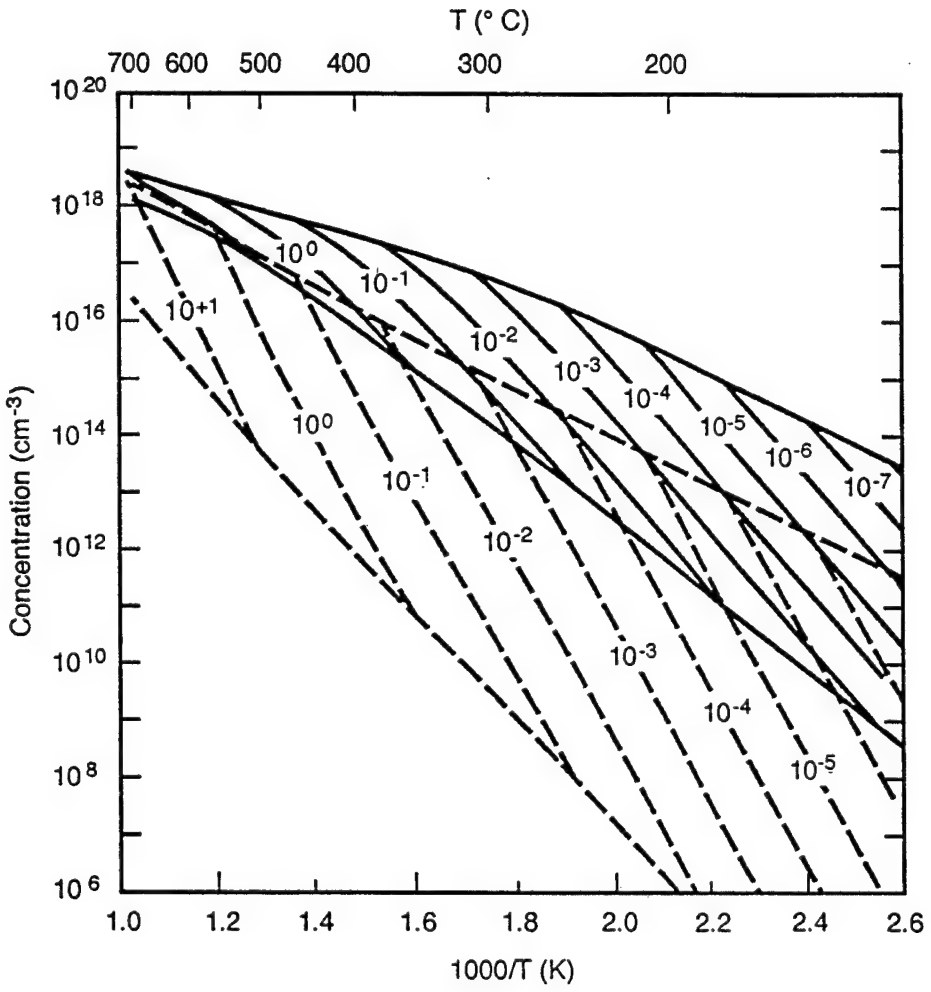
T (° C)
700 600 500 400 300 200
10^{20}
10^{18}
10^{16}
10^{14}
10^{12}
10^{10}
10^{8}
10^{6}
Concentration (cm^{-3})
10^{0}
10^{-1}
10^{-2}
10^{-3}
10^{-4}
10^{-5}
10^{-6}
10^{-7}
10^{+1}
10^{0}
10^{-1}
10^{-2}
10^{-3}
10^{-4}
10^{-5}
1.0 1.2 1.4 1.6 1.8 2.0 2.2 2.4 2.6
1000/T (K)

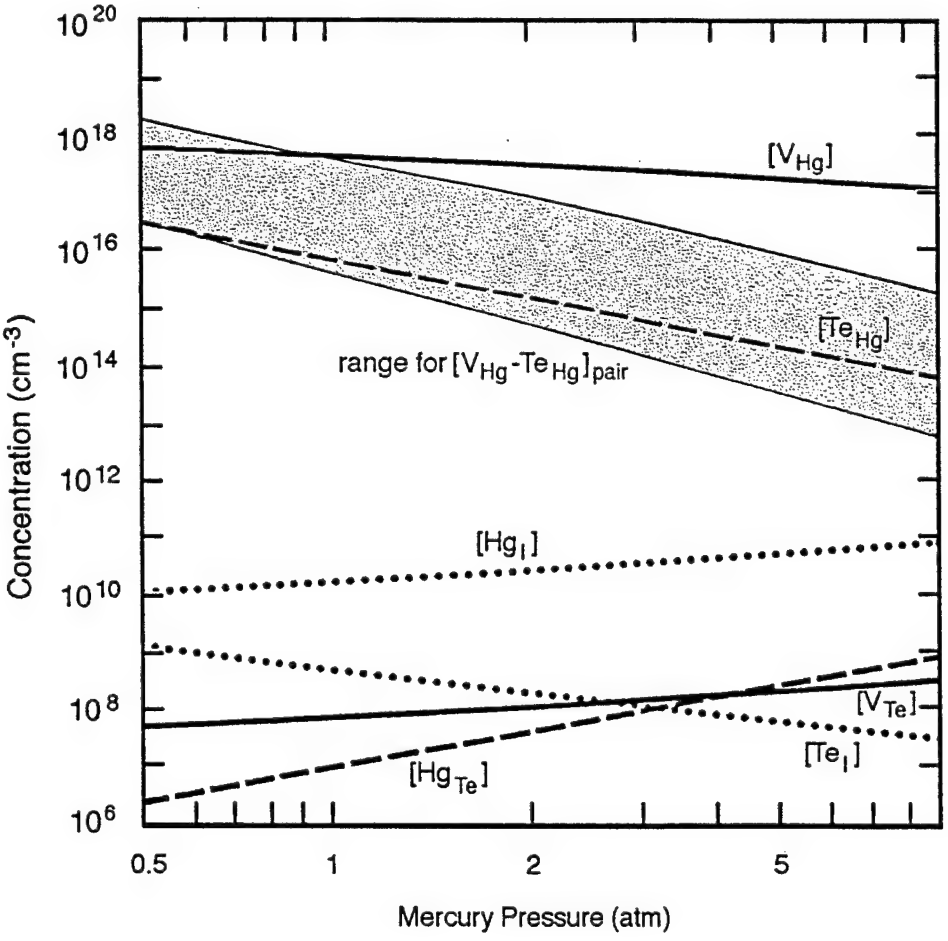
10^{20}
10^{18}
10^{16}
10^{14}
10^{12}
10^{10}
10^{8}
10^{6}
Concentration (cm^{-3})
$[V_{Hg}]$
$[Te_{Hg}]$
range for $[V_{Hg}\text{-}Te_{Hg}]_{pair}$
$[Hg_I]$
$[V_{Te}]$
$[Te_I]$
$[Hg_{Te}]$
0.5
1
2
5
Mercury Pressure (atm)

APPENDIX B

S. Krishnamurthy, A.-B. Chen, and A. Sher, "Comparison of HgTe materials growth in (100), (110), and (211) orientations," *J. Electron. Mater.*, **25**, 1254 (1996)

Comparison of HgTe materials grown in (100), (110), (111), and (211) Orientations

Srinivasan Krishnamurthy[a], A.-B. Chen[b], and A. Sher[a]
[a] SRI International, Menlo Park, CA 94025
[b] Physics Department, Auburn University, Auburn, AL 36349

Abstract

We calculated energies required to remove atoms from various configurations on (111), (110), (100), and (211) HgTe surfaces. The excess pair energies for various species are then calculated and are used in a thermodynamic model to study the growth. All energies are obtained using a Green's function method. The pair distributions are calculated from these energies in a generalized quasi-chemical approximation. The calculated critical temperatures for surface roughness transition are found to be considerably higher than the usual growth temperature of 185°c, so the growth on these surfaces is expected to be layer-by-layer with formation of two-dimensional islands. However, among the surfaces studied, only the (211) surfaces have an attractive binding energy for Hg, making those surfaces suited for better growth. The critical temperature for growth on (211)Hg is slightly higher than that for (211)Te, but we also find that Hg sticking coefficient on (211)Hg surface is considerably lower than that on (211)Te surface. These calculations are consistent with the observed higher growth rate of the (211)Te surface. Our calculations suggest that there will be fewer grown-in vacancies and Te antisites, at the expense of growth rate and sticking coefficient, for crystals grown on (211)Hg surface. We further calculated the Hg and Te vacancy formation energies as functions of surface orientations and layer depth. The cation vacancy formation energies from completed surface regions (islands) are higher than bulk values near anion terminated surfaces and smaller than bulk values near cation terminated surfaces.

Key words: growth modeling, critical temperature, vacancy formation, defect density, growth rate, HgTe

1. INTRODUCTION

The growth rate, quality of growth, ratio of constitutional vapor pressures required to achieve stoichiometric growth, and defect densities depend sensitively on the choice of growth orientation of the substrate. The growth of HgTe in (100), (111)Hg, (111)Te, (211)Hg, and (211)Te orientations have been tried. It has been demonstrated[1] that high quality growth, without formation of twin faults, can be obtained in the (211)Te orientation.

Previously,[2] we had calculated various energies required in a reliable modeling of growth of HgTe in (111), (110), and (100) directions. Those energies were then used in a thermodynamic growth model to successfully explain the apparent anomaly in the required vapor pressure ratios for the growth in (111)Hg and (111)Te directions.

We have carried out similar energetic calculations for the (211)Hg and (211)Te directions. The excess pair energies, which can be used in quasi-equilibrium thermodynamic or non-equilibrium Monte-Carlo growth models, are obtained using a Green's function method with full band structures. We develop a thermodynamic model to describe multilayer growth using effective excess pair energies and a generalized quasi-chemical approximation (GQCA). We use our calculated excess pair energies in a three bilayer model to study the critical temperature and island formation on (100), (111), (110), and (211) orientations. In order to get insight into vacancy segregation, we calculate the vacancy formation energy as functions of layer depth and surface orientations.

2. METHOD

Each layer-unit, in our multilayer growth model, consists of atomic species 1 and 2. On non-polar surfaces such as (110) and (211), the layer unit is an atomic layer that contains both anions and cations. However, on polar orientations, the layer-unit is a bilayer with the convention that species 1 be on the top layer of that unit. For example, index 1 will represent an anion on the (111)B surface, but a cation on the (111)A surface. We assume surface energies can simply be written as a sum of pair energies. There are intraunit 1-1, 2-2, and 1-2 bonds, and 1-2, 2-1 interunit bonds with coordination, α_1, α_2, η_1, η_2, and η_3 respectively. Note that 1-1, 2-2 are second

neighbor bonds. The interunit pair 1-2 connect species 1 of layer-unit i and species 2 of layer-unit i_1, and the pair 2-1 connects the layer i and i_2. For example, anions and cations on the ith layer of (211) surface connect to cation of (i-1)th layer and anion of (i-2)nd layer as shown in Figure 1. In such a case, i_1 and i_2 are (i-1) and (i-2) respectively. i_1 is undefined for polar surfaces. The total number of intralayer pairs $M_j^i = \frac{\alpha_i}{2} N$ (j=1, 2) and inter-layer pairs $L_j^i = \eta_j N$ (j=1,2,3). N is the total number of sites per layer per species. For each bond j, four pairs denoted respectively by index k are possible– namely, atom-atom, atom-vacancy, vacancy-atom, vacancy-vacancy. The corresponding interlayer and intralayer pairs are denoted as M_{jk}^i and L_{jk}^i. The free energy F is

$$F = \sum_{ijk} (E_{jk} M_{jk}^i + \epsilon_{jk} L_{jk}^i) - k_B T \sum_i ln(W_i) \tag{1}$$

where $E_{jk}(\epsilon_{jk})$ is the intra(inter)layer kth pair energy of jth bond, $k_B \ln(W_i)$ is the entropy, and k_B is the Boltzmann's constant. Dividing Eq.(1) by N and defining $y_{jk}^i = M_{jk}^i / M_j^i$, $z_{jk}^i = L_{jk}^i / L_j^i$, we get

$$f = \sum_{ijk} (\frac{1}{2} \alpha_j E_{jk} y_{jk}^i + \eta_j \epsilon_{jk} z_{jk}^i) - \frac{k_B T}{N} \sum_i ln(W_i) \tag{2}$$

The equilibrium distribution of pairs and surface coverage for a given surface concentration X_1 and X_2 by minimizing the free energy given in Eq.(2) subject to the following constraints.

$$\begin{aligned}
y_{j1}^i + y_{j2}^i &= x_j \\
y_{j4}^i + y_{j2}^i &= 1 - x_j \\
y_{j3}^i &= y_{j2}^i \\
z_{11}^i + z_{12}^i &= x_1^i \\
z_{13}^i + z_{14}^i &= 1 - x_1^i \\
z_{11}^i + z_{13}^i &= x_2^i \\
z_{14}^i + z_{12}^i &= 1 - x_2^i \\
z_{21}^i + z_{22}^i &= x_1^i
\end{aligned}$$

$$
\begin{aligned}
z^i_{23} + z^i_{24} &= 1 - x^i_1 \\
z^i_{21} + z^i_{23} &= x^{i_1}_2 \\
z^i_{24} + z^i_{22} &= 1 - x^{i_1}_2 \\
z^i_{31} + z^i_{32} &= x^i_2 \\
z^i_{33} + z^i_{34} &= 1 - x^i_2 \\
z^i_{31} + z^i_{33} &= x^{i_2}_1 \\
z^i_{34} + z^i_{32} &= 1 - x^{i_2}_1 \\
\sum_i x^i_1 &= X_1 \\
\sum_i x^i_2 &= X_2
\end{aligned}
\tag{3, 4}
$$

The entropy term is obtained from W_i given by GQCA for pairs,

$$
\begin{aligned}
W_i = \; & \frac{N!}{(Nx^i_1)!(N-Nx^i_1)!}\frac{N!}{(Nx^i_2)!(N-Nx^i_2)!} \\
& \Pi^2_{j=1}[M^i_j!\,\Pi^4_{k=1}\frac{[y^i_{jk}(0)]^{M^i_{jk}}}{M^i_{jk}!}] \\
& \Pi^3_{j=1}[L^i_j!\,\Pi^4_{k=1}\frac{[z^i_{jk}(0)]^{L^i_{jk}}}{L^i_{jk}!}]
\end{aligned}
\tag{5}
$$

where $y^i_{jk}(0)$ and $z^i_{jk}(0)$ are the random value of respective pairs. They are,

$$
\begin{aligned}
y^i_{j1}(0) = (x^i_j)^2, y^i_{j2}(0) = x^i_j(1-x^i_j) = y^i_{j3}(0), y^i_{j4}(0) = (1-x^i_j)^2 \\
z^i_{11} = x^i_1 x^i_2, z^i_{12} = x^i_1(1-x^i_2), z^i_{13} = (1-x^i_1)x^i_2, z^i_{14} = (1-x^i_1)(1-x^i_2) \\
z^i_{21} = x^i_1 x^{i_1}_2, z^i_{22} = x^i_1(1-x^{i_1}_2), z^i_{23} = (1-x^i_1)x^{i_1}_2, z^i_{24} = (1-x^i_1)(1-x^{i_1}_2) \\
z^i_{31} = x^{i_2}_1 x^i_2, z^i_{32} = x^{i_2}_1(1-x^i_2), z^i_{33} = (1-x^{i_2}_1)x^i_2, z^i_{34} = (1-x^{i_2}_1)(1-x^i_2)
\end{aligned}
\tag{6}
$$

Although there are four variables per bond, only one of them is a free variable owing to three constraints of Eq.(4). Hence, by substituting Eq.(4) into Eq.(2), we can rewrite the excess free energy, Δf in terms of y^i_{12}, y^i_{22}, z^i_{12}, z^i_{22}, z^i_{32}, x^i_1, and x^i_2.

$$
\frac{\Delta f}{Nk_BT} = \quad \frac{1}{2}\alpha_j \sum_{j=1}^{2}[-y^i_{j2}e_j + g(x^i_j - y^i_{j2}) + 2g(y^i_{j2}) + g(1-x^i_j - y^i_{j2})]
$$

$$
\begin{aligned}
&+\eta_1[-z^i_{12}\epsilon_1 + g(x^i_1 - z^i_{12}) + g(z^i_{12}) + g(x^i_2 - x^i_1 + z^i_{12}) + g(1 - x^i_2 - z^i_{12})] \\
&+\eta_2[-z^i_{22}\epsilon_2 + g(x^i_1 - z^i_{22}) + g(z^i_{22}) + g(x^{i_1}_2 - x^i_1 + z^i_{22}) + g(1 - x^{i_1}_2 - z^i_{22})] \\
&+\eta_3[-z^i_{32}\epsilon_3 + g(x^i_2 - z^i_{32}) + g(z^i_{32}) + g(x^{i_2}_1 - x^i_2 + z^i_{32}) + g(1 - x^{i_2}_1 - z^i_{32})] \\
&-(\alpha_1 + \eta_1 + \eta_2 - 1)(g(x^i_1) + g(1 - x^i_1)) - \eta_3(g(x^{i_2}_1) + g(1 - x^{i_2}_1)) \\
&-(\alpha_2 + \eta_1 + \eta_3 - 1)(g(x^i_2) + g(1 - x^i_2)) - \eta_2(g(x^{i_1}_2) + g(1 - x^{i_1}_2)) \qquad (7)
\end{aligned}
$$

where g(x), e_j, and ϵ_j are defined respectively to be x ln(x) ,(E_{j1}+E_{j4}-E_{j2}-E_{j3})/k_BT, and $(\epsilon_{j1} + \epsilon_{j4} - \epsilon_{j2} - \epsilon_{j3})/k_B T$. The minimum in the above excess free energy is obtained by setting first derivative (w.r.t. each variable) to zero. Thus, obtained analytical expressions for y^i_{j2} and z^i_{j2} in terms of x^i_1 and x^i_2 are

$$
\begin{aligned}
y^i_{j2} &= \frac{1}{2(1-a_j)}[-a_j + [(a_j)^2 + 4a_j(1-a_j)x^i_j(1-x^i_j)]^{\frac{1}{2}}] \\
z^i_{12} &= \frac{[-\{b_1 + (x^i_2 - x^i_1)(1-b_1)\} + [\{b_1 + (x^i_2 - x^i_1)(1-b_1)\}^2 + 4b_1(1-b_1)x^i_1(1-x^i_2)]^{\frac{1}{2}}]}{2(1-b_1)} \\
z^i_{22} &= \frac{[-\{b_2 + (x^{i_1}_2 - x^i_1)(1-b_2)\} + [\{b_2 + (x^{i_1}_2 - x^i_1)(1-b_2)\}^2 + 4b_2(1-b_2)x^i_1(1-x^{i_1}_2)]^{\frac{1}{2}}]}{2(1-b_2)} \\
z^i_{32} &= \frac{[-\{b_3 + (x^{i_2}_1 - x^i_2)(1-b_3)\} + [\{b_3 + (x^{i_2}_1 - x^i_2)(1-b_3)\}^2 + 4b_3(1-b_3)x^i_2(1-x^{i_2}_1)]^{\frac{1}{2}}]}{2(1-b_3)} \\
a_j &= exp(-e_j) \\
b_j &= exp(-\epsilon_j) \qquad (8)
\end{aligned}
$$

As all pair probabilities are expressed in terms of x^i_1 and x^i_2, there are only 2n-2 independent variables, in an n-layer growth model, with which the excess free energy has to be minimized. The results obtained by numerical minimization of free energy in HgTe are discussed in the following section.

3. RESULTS

The enthalpy component of the free energy is written as a sum of intralayer and interlayer pair energies. The Green's function approach (described in detail in a previous publication[2]) is used to calculate the extraction energies of constituent species from a fully completed surface and from an almost empty surface. Appropriate correction is applied when the final state is a molecular state instead of an atomic state.

A binding energy of 2.8 eV for Te_2 molecules is used. The excess pair energies e_j and ϵ_j are calculated from these extraction (or sublimation) energies. In addition to the previously studied (100), (110), and (111) surfaces, we study growth on the (211) oriented surface. (211) is a nonpolar surface. The planar unit should contain at least three atomic layers in order to be treated without modifying our previous Green's function method.[2]

Table 1 lists the coordinations (α and η) of atoms and the plane index that anion and cation of i-th layer connect (i_1 and i_2) respectively on various surfaces. Although (211) is a nonpolar surface, anions and cations have different numbers of bonds with the layers below. On the (211)A(B) surface, cations (anions) make one bond within the layer and two bonds with the layer below. For a (211) surface, calculation of the pair sublimation energy of anions and cations, in addition to their individual sublimation energies, for both concentrated and dilute[4] surfaces is required to compute the excess pair energies.

Table 2 lists the calculated pair energies on various surfaces. When the excess pair energy is positive, atom-atom bonds are preferred to atom-vacancy bonds. For positive excess energies at growth temperature T_g well below the critical temperature for the surface roughness transition T_c, the growth tends to take place with the segregation of atoms and vacancies resulting in island growth. However, the T_c is determined not just by any one single excess pair energy, but rather by the collective variations of the enthalpy and the entropy.

We use the values given in Tables 1 and 2 in a three-layer model. In this model, the cations (anions) that arrive at the surface will be allowed to occupy any cation (anion) sites in any of the three layers, as dictated by the total free energy of the surface. The anti-sites are not allowed. The three-layer surface state is designated in terms of its temperature and site occupancy. A connection between source flow rates and surface occupancy must still be made. These limitations will be removed in our future work. The present work is expected to offer an understanding of the observed trends and to set directions for future improvements.

When the concentration x is equal to 3, all three layers are fully grown. T_c is defined to be the temperature at which the second derivative of the excess free energy (Eq.(7)) with respect to x evaluated at x=1.5 vanishes. T_c thus calculated is given in

Table 2. We find that T_c is considerably higher than the usual growth temperature T_g of 185°C. For such cases where T_g is much smaller than T_c, and for slow growth rates so the surface has time to equilibrate, the growth is expected to be smooth and layer-by-layer with formation of two-dimensional islands. The concentration in the islands can be obtained from the minima in free energy versus concentration curve. In Figure 2 the free energy is plotted as a function of concentration for the (211)Te surface at a typical growth temperature of 185°C. We see that minima occur at x ($=x_c$) very near to zero and 1 meaning the growing surface will have islands nearly full and the rest of surface is nearly empty. The quantity ($1-x_c$) on an island depends on the ratio T_g to T_c. Consequently, the vacancy density can be related to the ratio of T_g to T_c. While this has not been done, it is clear that surfaces with large T_c are preferred for higher-quality growth.

In Figure 3, surface coverage as a function of concentration is shown for growth on the (211)Te surface at 185°C. We see that growth takes place layer-by-layer; that is, the next layer starts to grow only after the previous layer is complete. However, the finer details– such as how many vacancies are frozen in the first layer– are beyond the numerical accuracy of this calculation. A separate thermodynamic calculation or Monte-Carlo simulations using our excess energies and sublimation energies are required.

Although T_c is a good indicator of ideal growth quality, it alone does not completely characterize the growth. Also, our calculations of T_c and equilibrium configurations assume that the atoms are already on the surface and they rearrange to minimize the free energy. Hence, the correct interpretation of our results on T_c is that the surfaces will grow layer-by-layer *if* they can stick to the surface. The information on sticking coefficients is not included in this modeling. However, our calculation of sublimation energies of the constituent species from various surfaces offers some insight into the strength of the sticking coefficients. The calculated values for Hg are provided in Table 2. A positive energy indicates that the atom would like to bind to that surface. We found that Te has positive sublimation energies on all the surfaces (not shown in Table 2), suggesting a finite and large positive sticking coefficient. However, as seen from Table 2, Hg has positive sublimation energy only on (211) surfaces. On all other surfaces, it has a repulsive interaction and consequently possesses

extremely low sticking coefficients. This sublimation energy could be increased only by increasing the vapor pressure. Such an increase in vapor pressure is known to increase the sticking coefficient. In fact, growth on these surfaces can only occur in a Te-stabilized mode in which each Hg atom sticking to the surface is rapidly covered by a Te; i.e., the pair is bound. Our calculation of sublimation energies in Table 2 suggests that Hg has finite positive sticking coefficients on both (211) surfaces, even for relatively low Hg over-pressures. The combination of high T_c and finite positive sublimation energy make the (211) surfaces more favorable for high quality growth than the other surfaces, in agreement with experiments.[1] It also suggests it should be possible to grow $Hg_{1-x}Cd_xTe$ alloys away from the Te edge of existence curve.[4] This is yet another way to reach the conclusion that there could be fewer grown-in Hg vacancies and Te anti-sites, for materials grown on (211) surfaces.

The (211)Hg and (211)Te are the only two surfaces in which all sublimation energies are positive and the roughness transition temperature is much higher than T_g. Although the potential material quality is predicted to be very high on both these surfaces, our calculations suggest that the (211)Hg surface is preferred for its slightly higher T_c. Consequently, vacancy population frozen in lower layers is expected to be smaller when grown on the (211)Hg surface. However, this surface is weaker attraction between Hg and the layer below (yielding a smaller sticking coefficient) may induce faceted growth because of slower growth rate. We recommend careful growth experiments on the (211)Hg surface, with reduced Te-to-Hg flow rates to see if these predicted advantages can be realized.

4. VACANCY FORMATION ENERGIES

The energies required to remove an atom from the bulk HgTe, leaving behind a vacancy, had been calculated and successfully used in predicting the bulk defect densities by Berding et al.[5] However, near a completed surface (or an island), the vacancy formation energy depends on the depth of the layer from which the atom is removed and on the orientation of the surface. Based on bond-breaking arguments, one would to expect the surface vacancy formation energy to be lower than the bulk vacancy formation energy. However, our calculations suggest that this rule is not uniformly obeyed. In addition, we calculated energies required to extract atoms

from a number of sub-surface layers. These calculated Hg and Te vacancy formation energies (in excess of their respective bulk values) are given in Table 3 as functions of surface orientation and layer depth. The surfaces being treated here are *concentrated* not *dilute*. It means that the vacancies are in a nearly completed surface. A positive energy indicates that the vacancy in that sub-surface layer has a higher formation energy (and is less preferred) than in bulk.

First let us consider polar surfaces such as (100) and (111). We find that the surface vacancy formation energy monotonically reaches the bulk value typically in four bilayers. Notice that in many cases the vacancy formation near the surface is *more* expensive than that in the bulk. The bulk value of Te vacancy formation energy is very high (3.5eV as compared to 1.9 eV for Hg) and hence the anion vacancy density can be safely neglected. We note that Hg-vacancy formation is easier on Hg-terminated (100) and (111) surfaces. However, Hg-vacancy formation is considerably hindered on Te-terminated (100) and (111) surfaces.

The values obtained for (211) surfaces do not change monotonically because these surfaces have several steps. Our calculations suggest that vacancy formation is easier on both A and B surfaces than in the bulk. A detailed surface segregation calculation based on these calculated energies should predict the cation vacancy density to be high in samples grown in (211) orientations and in samples grown in (111)B orientation. However, for growth rates slow compared to Hg diffusion rate, these excess surface vacancy concentrations may not be trapped to form excess bulk vacancy concentration in MBE-grown material.

5. CONCLUSIONS

We have used a Green's function method combined with full band structures to calculate the excess pair energies. Our model calculations of the free energy with GQCA and pair energies provide considerable insight into the epitaxial growth of HgTe. When excess pair energies are positive, the growth takes place with formation of islands at temperatures lower than the critical temperature. The growth in this mode is slow but of high quality and is preferred. Native point defect densities are functionals of the ratio of critical temperatures to the growth temperatures. To have uniformly good growth, all surface atom-atom interactions have to be attractive

(positive excess and sublimation energies). Based on this criteria, our calculations suggest the growth in (211)Hg and (211)Te directions will be considerably better than that on (100), (111), or (110) surfaces. In addition, owing to weak Hg sticking coefficient, growth in (211)Te orientation is faster than that in the (211)Hg orientation for the same source materials flow rates. These calculations are consistent with the observed superiority of (211)Te surface growth. However, our calculations suggest that there will be fewer vacancies and Te anti-sites, at the expense of growth rate and sticking coefficient, for crystals grown on (211)Hg surface.

We thank Dr. Marcy Berding for many valuable discussions and Dr. M. Methfessal for plotting codes used to obtain Figure 1. Funding from ARPA / AFOSR (Contract F49620-95-C-0004) is gratefully acknowledged.

6. References

1. R. J. Koestner and H.F. Schaake, *J. Vac. Sci. Tech.* **A6** 2834(1987)

2. S. Krishnamurthy, A.-B. Chen, A. Sher, *J. Appl. Phys.* **68**, 4020 (1990)

3. S. Krishnamurthy, A.-B. Chen, A. Sher, *J. Crys. Growth* **109**, 88 (1991)

4. In references (2) and (3), the term *concentrated* is used to denote one in which all sites in the surface layer are occupied. A *dilute* surface is one with a few surface layer sites occupied.

5. M. A. Berding, A. Sher, and M. van Schilfgaarde, *J. Elec. Matr.* **24** 1127 (1995)

TABLES

TABLE 1. Coordinations (α, η) of atoms on various HgTe surfaces. Labels 1 and 2 indicate the atoms in the top and bottom layer of layer-unit. i_1 and i_2 are the layers connected to atoms 1 and 2 of i-th layer respectively.

surface	α_1	α_2	η_1	η_2	η_3	i_1	i_2
(211)Hg	2	2	1	2	1	i-1	i-2
(211)Te	2	2	1	2	1	i-1	i-2
(111)Hg	6	6	3	0	1	-	i-1
(111)Te	6	6	3	0	1	-	i-1
(100)Hg	4	4	2	0	2	-	i-1
(100)Te	4	4	2	0	2	-	i-1
(110)Te	2	2	2	1	1	i-1	i-1

TABLE 2. Excess pair energies (in eV), roughness transition temperature (in °C), and Hg sublimation energies (in eV).

surface	e_1	e_2	ϵ_1	ϵ_2	ϵ_3	T_c	E_{sub}
(211)Hg	0.89	0.89	0.36	0.41	0.69	3920	0.06
(211)Te	0.60	0.53	0.40	0.04	0.96	3320	0.26
(111)Hg	0.23	0.06	0.27	-	0.19	4140	-0.30
(111)Te	0.10	0.08	0.11	-	0.61	1320	-0.20
(100)Hg	0.20	0.12	0.20	-	0.20	2500	-0.20
(100)Te	0.12	0.20	0.20	-	0.20	2505	-0.20
(110)Te	0.22	0.00	0.20	0.30	0.30	1040	-0.30

TABLE 3. Hg (Te) excess vacancy formation energy(in eV) as functions of orientation and layer depth from the surface.

Layer	(111)Hg	(111)Te	(100)Hg	(100)Te	(211)Hg	(211)Te
1	-0.29(0.69)	1.19(-0.39)	-0.94(1.09)	1.08(-0.97)	-0.76(-0.07)	-0.91(-0.56)
2	-0.26(0.16)	0.15(-0.33)	-0.48(0.26)	0.86(-0.44)	-0.86(+0.43)	-0.53(-0.73)
3	-0.06(0.05)	0.05(-0.07)	-0.12(0.09)	0.04(-0.08)	+0.11(+0.18)	-0.53(+0.21)
4	0.00(0.00)	0.00(0.00)	0.00(0.00)	0.00(0.00)	-0.07(+0.01)	-0.35(+0.05)
5	0.00(0.00)	0.00(0.00)	0.00(0.00)	0.00(0.00)	-0.01(+0.00)	-0.15(+0.00)
6	0.00(0.00)	0.00(0.00)	0.00(0.00)	0.00(0.00)	0.00(+0.00)	0.00(+0.00)

FIGURES

FIG. 1. (211)Te surface. Layers i, i-1, and i-2 are labeled. Te of layer i connect Hg of layer (i-1) and Hg of layer i connect Te of layer (i-2). Hence i_1 and i_2 for this surface are respectively are (i-1) and (i-2). For coordination numbers see Table 1. e_j and ϵ_j are the excess energies for the shown pairs.

FIG. 2. Change in excess free energy with concentration at 185°C on (211)Te surface

FIG. 3. Surface coverage of Hg (dotted) and Te (solid) with concentration at 185°C on (211)Te surface

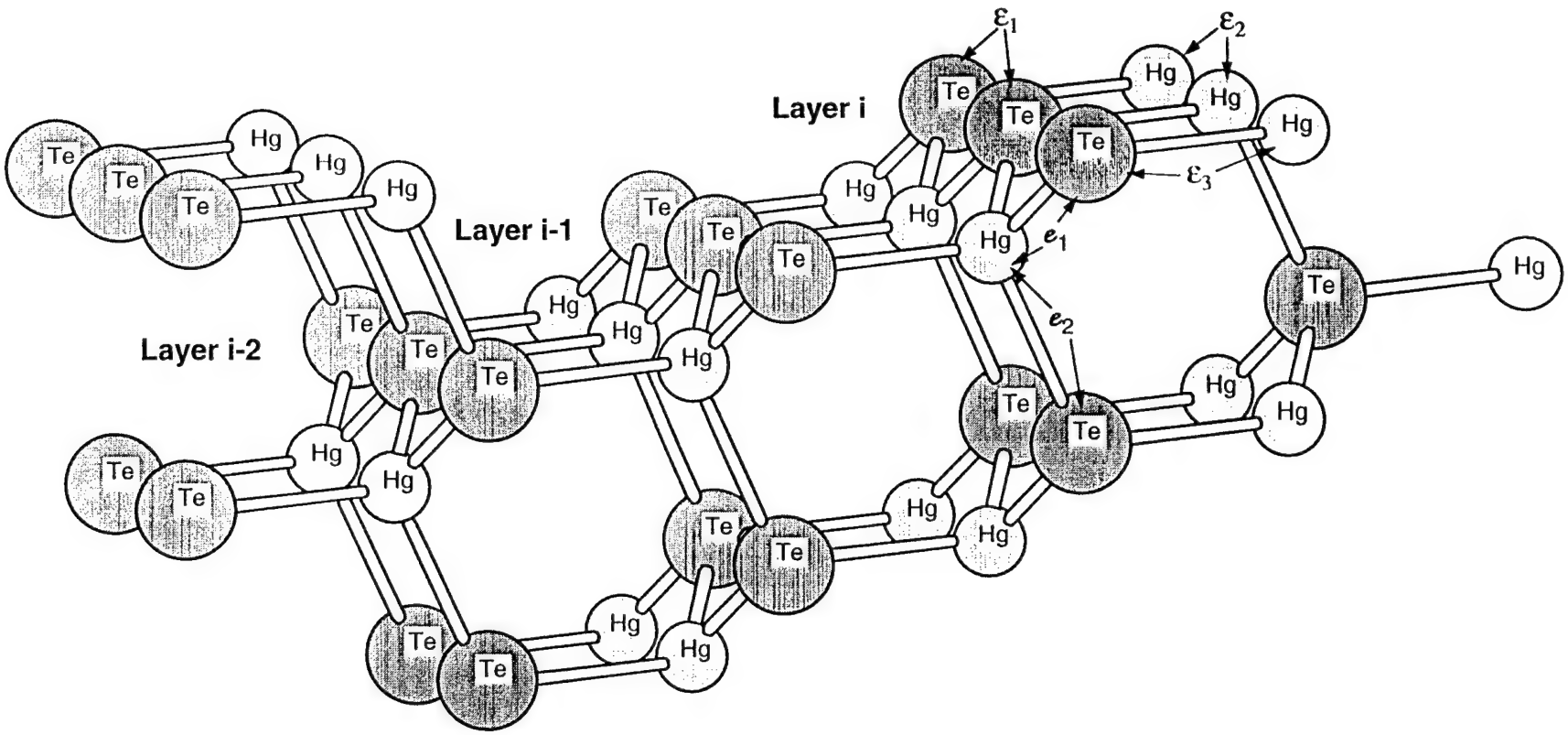
Layer i
Layer i-1
Layer i-2
ε_1
ε_2
ε_3
e_1
e_2
Te
Hg

sh-183195-sd

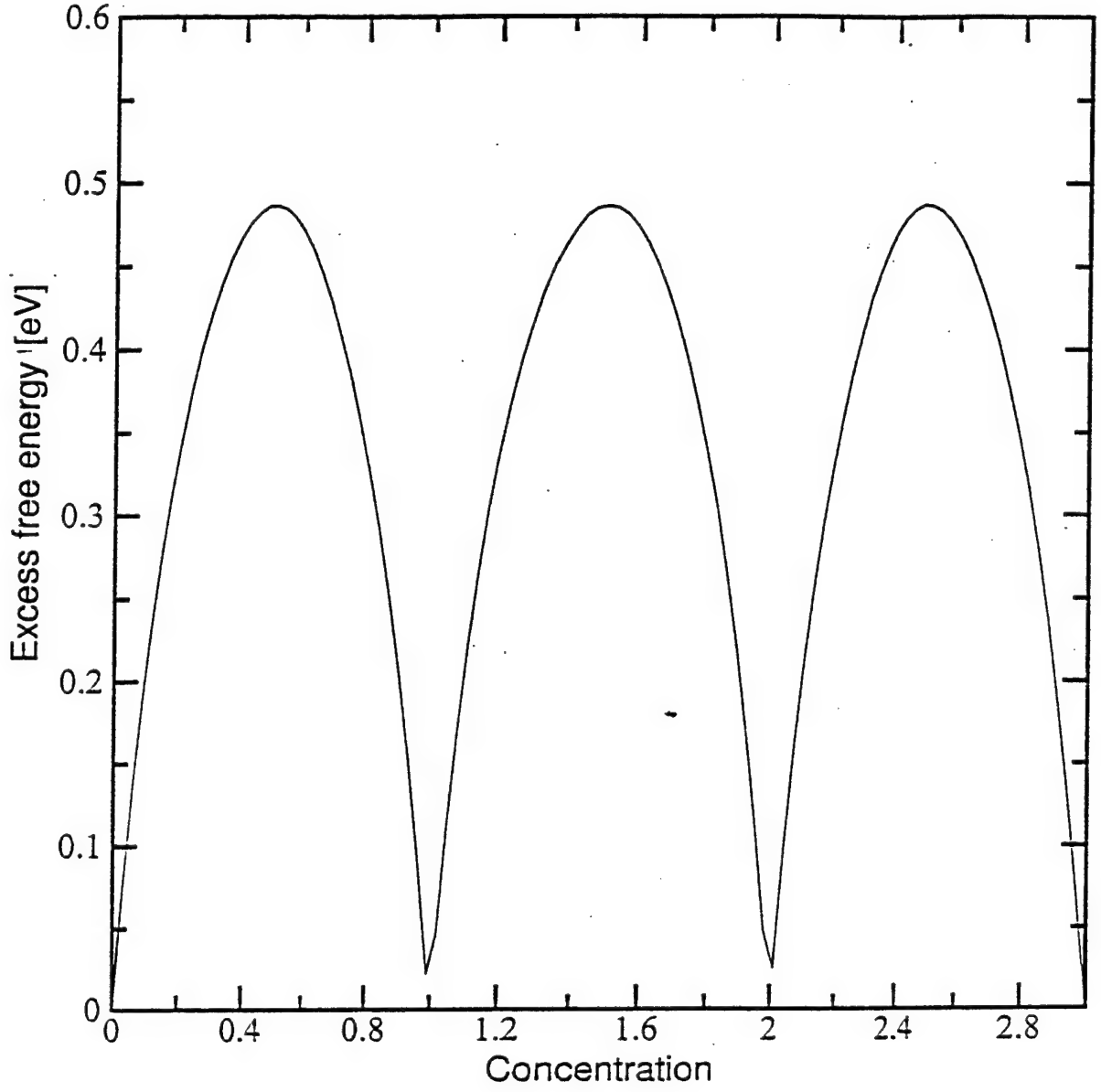

FIG. 2. Change in excess free energy with concentration at 185°C on (211)Te surface

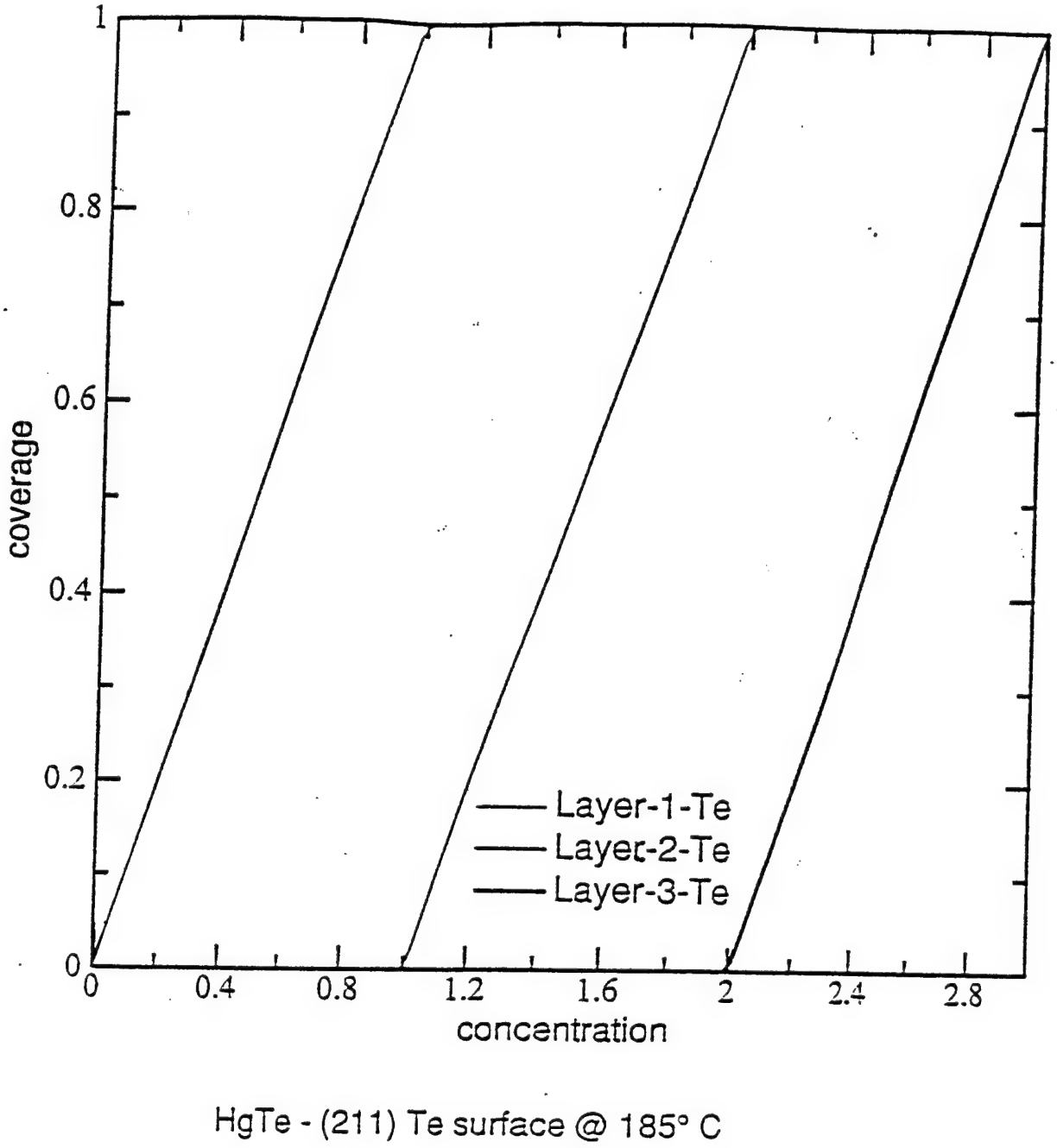

Figure 3. Surface coverage of Hg and Te (bilayers) with concentration at 185°C on (211) Te surface

APPENDIX C

M. A. Berding, A. Sher, and M. van Schilfgaarde, "Behavior of *p*-type dopants in HgCdTe," *J. Electron. Mater.*, **26**, 625, 1997

Journal of Electronic Materials, Vol. 26, No. 6, 1997

Behavior of p-Type Dopants in HgCdTe

M.A. BERDING, A. SHER, and M. VAN SCHILFGAARDE

SRI International, Menlo Park, CA 94025

Obtaining high concentrations of active p-type dopants in HgCdTe is an issue of much current interest. We discuss the results of our calculations on column IB and VA dopants. The full-potential linear muffin-tin orbital method, based on the local density approximation is used to calculate electronic total energies and localized levels in the band gap. Free energies are predicted and incorporated into a thermodynamical model to calculate impurity and native defect concentrations as a function of temperature, stoichiometry, and total impurity density. Copper, silver, and gold are found to be incorporated nearly exclusively on the metal sublattice and to be 100% active for all near-equilibrium growth and processing conditions. The density of interstitial copper is high enough to impact copper diffusion. In contrast, significant concentrations of phosphorus, arsenic, and antimony are found on the metal sublattice where they behave as n-type dopants, accounting for highly compensated, or even n-type material, depending on the equilibration temperature and equivalent mercury partial pressure.

Key words: Amphoteric dopants, doping, HgCdTe

INTRODUCTION

Obtaining high concentrations of p-type dopants in $Hg_{0.78}Cd_{0.22}Te$ is a topic of much interest in the development of the next generation of high-performance long-wave infrared (LWIR) detectors.[1,2] Although doping p-type with the native mercury vacancy is possible, the transport properties and stability of vacancy-doped material are inferior to those of extrinsically doped material. The two choices for p-type dopants are column I impurities substituting on the cation sublattice site and column V impurities substituting on the tellurium sublattice. The column I impurities copper, silver, and gold, although active in the lattice, are relatively fast diffusers and therefore may be less desirable for certain applications. In contrast, the column V impurities are slow diffusers, although it is experimentally observed[2] that they are not always incorporated as p-type dopants, and in some cases even n-type behavior is observed.

We report on our investigation of the properties of the Group I impurities copper, silver, and gold and the Group V impurities phosphorus, arsenic, and antimony. First-principles calculations are used to calculate the electronic energies of the impurities at various positions in the lattice and also their ionization states. Defect free energies are then calculated, based on these *ab initio* energies and are incorporated into a thermoydyamical formalism to predict the equilibrium densities of neutral and ionized defects as a function of growth and processing conditions.

(Received November 19, 1996; accepted February 27, 1997)

FREE ENERGIES

Electronic energies for the solids were calculated by using the full-potential linearized muffin-tin orbital (FP-LMTO) method within the local density approximation (LDA) of Barth and Hedin.[3] To ensure a good fit to the charge density and potential in the interstitial region of the non-closed-packed zinc-blende lattice, empty spheres have been included, and orbitals added to the basis by centering them on the empty spheres. Both the charge density inside the spheres and the tails of Hankel functions centered on a neighboring sphere were expanded to $l = 4$. For the calculation of the point defects, 32-atom supercells of defects were constructed, and defect energies extracted by

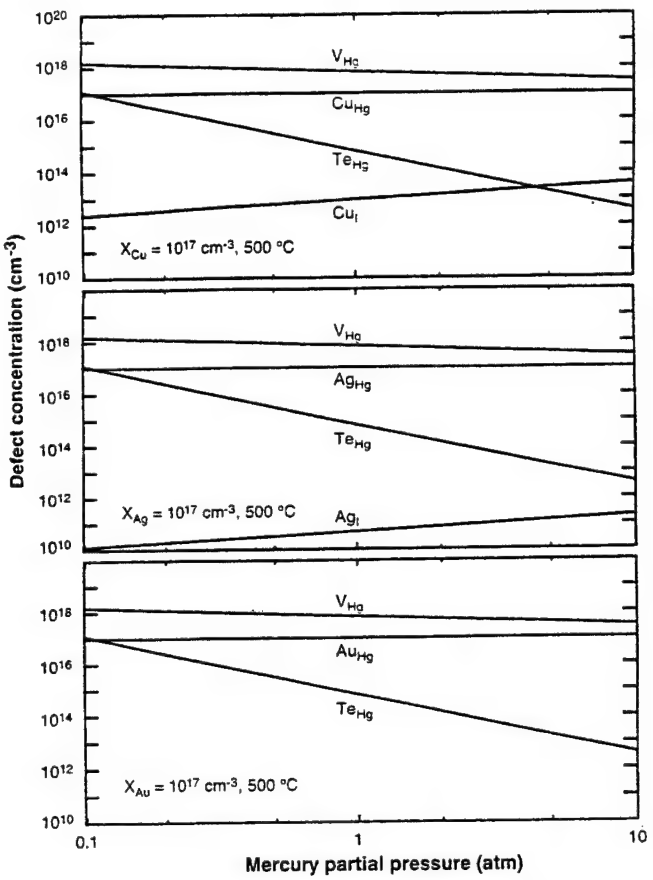

Fig. 1. Defect concentrations in $Hg_{0.78}Cd_{0.22}Te$ at 500°C as a function of mercury partial pressure and with 10^{17} cm^{-3} copper, silver, or gold impurities. In the labeling of the figures, the primary symbol refers to the defect species, where V indicates a vacancy, and the subscript refers to the lattice site occupied, where I is an interstitial site, Hg represents the predominantly mercury-occupied cation sublattice, and Te is the anion sublattice sites.

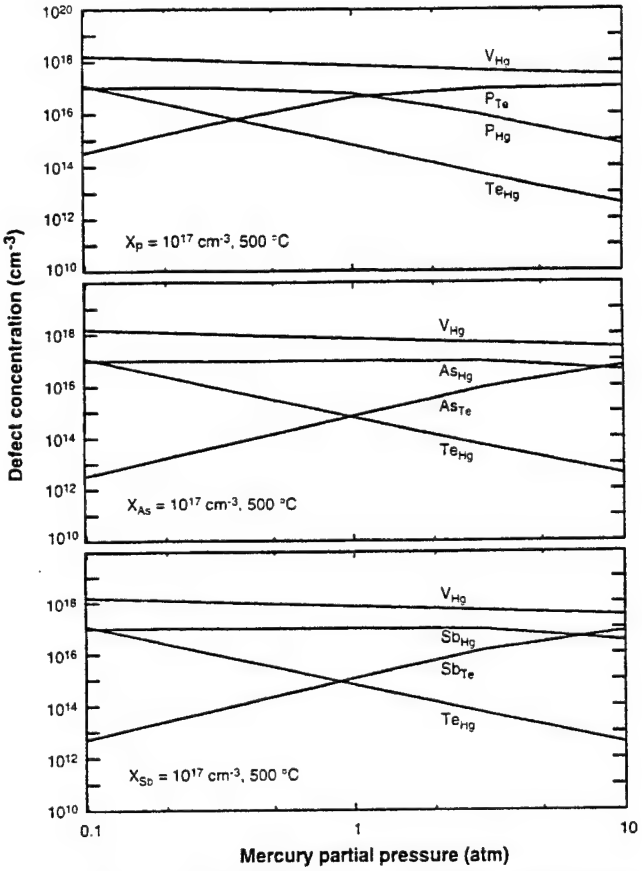

Fig. 2. Defect concentrations in $Hg_{0.78}Cd_{0.22}Te$ at 500°C as a function of mercury partial pressure and with 10^{17} cm^{-3} phosphorous, arsenic, or antimony impurities. In the labeling of the figures, the primary symbol refers to the defect species, where V indicates a vacancy, and the subscript refers to the lattice site occupied, where I is an interstitial site, Hg represents the predominantly mercury-occupied cation sublattice, and Te is the anion sublattice sites.

taking the difference of cells with and without a defect. Four special k-points were used, and the core was allowed to relax during the self-consistency cycle. The energies of the ionization states associated with a defect were calculated as discussed in Berding et al.[4] Four lattice positions of each impurity were considered: substitutional on the cation sublattice, substitutional on the anion sublattice, and interstitially at each of the two inequivalent tetrahedral interstitial sites. The supercell lattice constant and the first and second neighbor shells were allowed to relax; only radial relaxations about the defects were found.

The mercury vapor pressure was used to determine the mercury chemical potential and therefore the position of the material within the existence region. LDA is well known to predict cohesive energies for solids which are too deep, and that the gradient corrections significantly improve the agreement with experiment.[5] We have found previously[4] that the addition of gradient corrections to the LDA dramatically improves the agreement with experiment when solid energies are referenced to a free atom, and therefore are important when the vapor phase is desired as a reference phase as in the present case. Therefore, all calculations reported here were done gradient corrections, as developed by Langreth and Mehl.[6]

A lattice vibration model based on the valence force field model of the lattice[4] is used to calculate the vibrational free energies of the impurities. The vibrational free energies are included along with the electronic and ionic excitation free energies calculated from the LDA to determine the defect and impurity free energies in HgCdTe.

THERMODYNAMICS

The free energies for the impurities and native defects in $Hg_{0.8}Cd_{0.2}Te$ are incorporated into a thermodynamic formalism to calculate their populations as a function of growth and processing parameters. A generalized quasichemical formalism has been developed to calcuate absolute defect densities subject to arbitrary constraints consistent with Gibbs' phase rule. Various four-component systems will be examined (mercury, cadmium, tellurium, and one impurity), and thus for the two-phase region for the doped HgCdTe coexisting with the vapor, there are four degrees of freedom. Here, the temperature will be specified, the alloy composition will be held fixed at

78% mercury, and the mercury partial pressure will be used to determine the position of the material within the existence region, with the bounds for the existence region taken from experiment. The concentration of the impurity in the lattice is chosen as the final degree of freedom.

No attempt has been made to determine the solubility of the various impurities, where an impurity-rich phase coexists with the doped HgCdTe. Within the quasichemical formalism, the Fermi level is determined self-consistently, by using experimentally determined band parameters as discussed previously.[4]

RESULTS

The density of the group I impurities at 500°C, near to typical liquid phase epitaxy (LPE) growth temperatures, and as a function of mercury partial pressure is shown in Fig. 1. The impurity concentration was held fixed at 10^{17} cm^{-3} in all cases. For all impurities, copper, silver, and gold, the impurity prefers to reside on the cation sublattice where it serves as a p-type dopant; for the purposes of determining activation, there are negligible densities on the tellurium sublattice and interstitial sites.

For copper doping, interstitial densities exceeding 10^{13} cm^{-3} are found. Although these interstitial densities are too low to result in significant deactivation, they may be important in determining the copper diffusion constant. Impurity interstitial concentrations are reduced by more than two orders of magnitude for silver doping, and for gold are less than 10^{10} cm^{-3} throughout the existence region. Following growth by LPE, materials are often subjected to a low-temperature (200–250°C) anneal under mercury-saturated conditions to remove the as-grown mercury vacancies. For material equilibrated with these conditions, 100% activation is found for copper, silver, and gold, with interstitial densities less than 10^{10} cm^{-3} for all three. However, the annealing times alloted may not permit the slower diffusion species to reach their equilibrium, so care must be used when comparing these numbers to experiment.

In contrast to the group I dopants, the group V dopants are highly compensated at low mercury pressures. Defect populations as a function of mercury partial pressure for 10^{17} cm^{-3} phosphorous, arsenic, and antimony, at 500 and 240°C are shown in Fig. 2 and Fig. 3. Although the substitution on the anion sublattice dominates at the highest mercury pressures, the group V dopants also show large populations on the cation sublattice, with this species dominating at low mercury partial pressures. The phosphorous, arsenic, and antimony on the cation sublattice act as donors, thereby serving as compensating centers for the desired acceptors. For growth at 500°C from a mercury melt, the group V dopants are predicted to reside predominantly on the anion sublattice, while for growth from the tellurium melt the group V dopants reside predominantly on the cation sublattice. As the temperature is lowered from 500 to 240°C, the mercury pressure at which the n to p

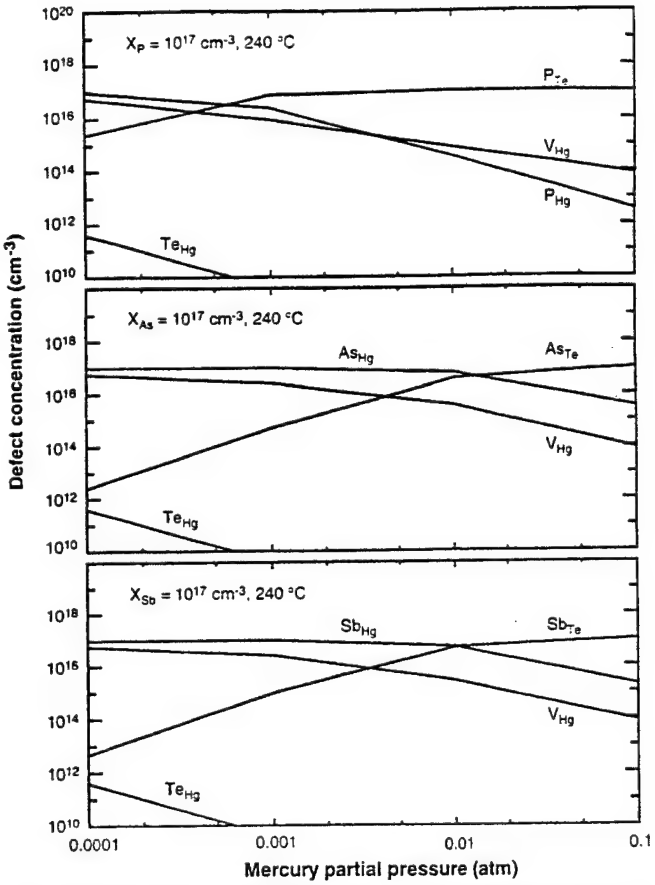

Fig. 3. Defect concentrations in $Hg_{0.78}Cd_{0.22}Te$ at 240°C as a function of mercury partial pressure and with 10^{17} cm^{-3} phosphorous, arsenic, or antimony impurities. In the labeling of the figures, the primary symbol refers to the defect species, where V indicates a vacancy, and the subscript refers to the lattice site occupied, where I is an interstitial site, Hg represents the predominantly mercury-occupied cation sublattice, and Te is the anion sublattice sites.

conversion occurs shifts away from the mercury-saturated side of the phase diagram, indicating that complete equilibration at 240°C under mercury-saturated conditions should result in nearly full activation of all three acceptors phosphorous, arsenic, and antimony. As the temperature is lowered even further to molecular beam epitaxy (MBE) growth temperatures, the cross over shifts further to the tellurium-rich side of the phase field, although n-type behavior is still predicted from tellurium-saturated growth conditions, consistent with experiment.

CONCLUSIONS

We have presented calculations of the defect concentrations as a function of mercury partial pressures for group I and V impurities in $Hg_{0.78}Cd_{0.22}Te$. The group I impurities are found to be 100% activated as donors at both 500 and 240°C, although significant copper interstitial densities are found, which must be considered in the diffusion of this species. For the group V impurities, the material is predicted to be n-type for tellurium-saturated material at 500°C, reflecting the need to grow from the mercury melt for which the group V impurities reside primarily on the

anion sublattice as acceptors. For materials subjected to annealing at 240°C under mercury-saturated conditions, we predict that the dopant should become nearly fully activated, although depending on the starting material, the time for equilibration may be quite long because of the need for atoms to switch from the cation to the anion sublattice.[7] In all cases, we find negligible densities of group V impurities at interstitial sites. The calculations predict that phosphorus offers a slight advantage over arsenic and antimony in that the onset of n-type conversion at a given temperature is at lower mercury pressures, although further refinements in our calculations are needed to establish this more firmly.

ACKNOWLEDGMENTS

This work has been supported by DARPA Contract F49620–95–C–0004.

REFERENCES

1. See for example, L.O. Bubulac, J. Bajaj, W.E. Temmant, M. Zandian, J. Pasko and W.V. McLevige, *J. Electron. Mater.* 25, 1312 (1996); P.S. Wijewarnasuriya, S.S. Yoo, J.P. Faurie and S. Sivananthan, *J. Electron. Mater.* 25, 1300 (1996); P. Mitra, Y.L. Tyan., F.C. Case, R. Starr and M.B. Reine, *J. Electron. Mater.* 25, 1328 (1996); S.H. Shin, J.M. Arias, M. Zandian, J.G. Pasko, L.O. Bubulac and R.E. De Wames, *J. Electron. Mater.* 24, 609 (1995).
2. H.R. Vydyanath, *Semicon. Sci. Technol.* 5, 213 (1990).
3. U. von Barth and L. Hedin, *J. Phys. C* 5, 1629 (1972).
4. M.A. Berding, M. van Schilfgaarde and A. Sher, *Phys. Rev. B* 50, 1519 (1994).
5. For a general discussion of the density functional formalism, upon which LDA is based, and its various modifications, see R.O. Jones and O. Gunnarsson, *Rev. Mod. Phys. 61,* 689 (1989).
6. D. Langreth and D. Mehl, *Phys. Rev. B* 28, 1809 (1983).
7. D. Chandra, M.W. Goodwin, M.C. Chen and J.A. Dodge, *J. Electron. Mater.* 22, 1033 (1993); S.H. Shin, J.M. Arias, M. Zandian, J.G. Pasko, L.O. Bubulac and R.E. De Wames, *J. Electron. Mater.* 24, 609 (1995).

APPENDIX D

M. A. Berding, A. Sher, and M. van Schilfgaarde, "Bothersome impurities in LWIR HgCdTe," *Proceedings of the 1997 IRIS Materials Meeting*

BOTHERSOME IMPURITIES IN LWIR HgCdTe[1]

July 1997

M. A. Berding and A. Sher
SRI International
333 Ravenswood Avenue
Menlo Park, CA 94025

ABSTRACT

The properties of copper, lithium, and sodium in $x = 0.22$ $Hg_{1-x}Cd_xTe$ are studied using *ab initio* calculations. In HgCdTe, all three impurities are determined to incorporate predominantly on the cation sublattice, where sodium has a shallow, and lithium and copper have deep acceptor levels. All three impurities have a negligible fraction substituting on the anion sublattice, however they have significant incorporation interstitially (where they all have donor levels resonant in the conduction band), which can in part account for the large diffusion coefficients of these impurities. A similar distribution for the impurities was found for CdTe. Strain effects on the impurity incorporation are small and do not provide a driving force for these impurities to segregate to interfaces or contacts. The driving force for the out-diffusion of copper from the CdTe-based substrates is determined to be the lower chemical potential of copper in the HgCdTe overlayer, which in turn can be attributed primarily to the relatively weak mercury-tellurium bond.

1.0 INTRODUCTION

Copper, lithium, and sodium are all impurities which in most device structures are considered undesirable. Copper is a known fast diffuser in HgCdTe, and although in some cases it is introduced intentionally for its acceptor behavior, its high diffusion coefficient is a liability in subsequent processing steps. It is known that copper present in CdZnTe substrates out-diffuses into HgCdTe epilayers during growth and can lead to undesirable effects.[2] Less work has been done on the properties of lithium and less still on the properties of sodium in HgCdTe, but both are typically characterized as fast diffusers.[3]

In previous work[4] we examined the properties of copper in x=0.22 HgCdTe and found that although copper atoms reside primarily on the cation sublattice, a significant fraction (< 0.1 %) was incorporated interstitially. In this paper we discuss our recent work on the behavior of copper, lithium, and sodium in HgCdTe. We will also discuss the relative interaction of copper with the substrate and the HgCdTe epilayer.

2.0 APPROACH

We use the full-potential linearized muffin-tin orbital (FP-LMTO) method based on the local density approximation (LDA) to calculate the ground and excited state energies of arsenic. Gradient corrections to the LDA were also included so that reference to the mercury vapor pressure could be made.[5] Several means for impurity incorporation have been considered: (1) substitution on the cation sublattice; (2) substitution on the anion sublattice; and (3) incorporation at the two different classes of tetrahedral interstitial sites.

---

1. Supported by DARPA, through AFOSR contract F49620-95-C-0004 and by Universal Technology Corporation under prime contract to U.S. Air Force F33615-94-C-5800.

2. Harris, K. A, C. K. Ard, W. J. Everson, J. L Sepich, G. L. McKinney, B. E. Dean, and D. D. Edwall, in The Proceedings of the IRIS Specialty Meeting on Infrared Materials, (1996).

3. Capper, P., *Properties of Narrow Gap Cadmium-based Compounds*, EMIS Datareviews Series No. 10, ed. P. Capper, (Inspec, 1994), p. 1630, and references therein.

4. Berding, M. A., A. Sher, and M. van Schilfgaarde, *J. Electron. Mater.* **26**, 624 (1997).

5. Berding, M. A., M. van Schilfgaarde, and A. Sher, *Phys. Rev. B* **50**, 1519 (1994).

The ground state energy of each of these defects is calculated using supercells containing thirty-two lattice sites in which the defect of interest is surrounded by HgTe. Relaxation of the first and second neighbors to the defects were permitted. As complete a basis as was computationally feasible was used and similar parameters were used in all supercell calculations.[6] Further details of the LDA calculations will be given elsewhere.[7] Contributions to the defect free energies arising from changes in the lattice vibrations were also calculated, as discussed in Ref. 5. Calculations were also repeated for the most important native point defects, the mercury vacancy and the tellurium antisite, using the same basis set, cell size, and number of k-points in the Brillouin Zone integration as was used for the arsenic defect calculations. Results using a slightly less complete basis for the behavior of copper in HgCdTe were reported earlier.[4]

Calculations were repeated for the same impurities in the CdTe lattice. The impact of the ~4% Zn typically used in substrate materials to lattice match to LWIR HgCdTe was ignored in the present calculations. Although native defects will also be present in the CdTe substrate, they have not been included in the present calculation.

For both $x = 0.22$ HgCdTe and CdTe, the energies, ionization states, and degeneracies of all of the defects are incorporated into a statistical mechanical formalism similar to that discussed in Ref. 5 and used in our previous study on arsenic.[4] Empirical expressions have been used for the temperature and x-dependent band gap.[8] For CdTe, the conduction and valence band density of states were calculated using the effective mass approximation, with m_h^*=0.8 and m_e^*=0.09. For HgCdTe, the conduction band density of states and hole effective mass were fit to empirical intrinsic carrier concentrations.[8]

3.0 RESULTS

For all calculations, the mercury pressure along the bounds of the existence region were taken from expressions given by Vydyanath and Hiner[9] for x=0.2. To improve agreement with experimental vacancy densities,[9,10] the formation energy of the vacancy was increased by 0.18 eV, similar to corrections needed in our earlier work[4] to agree with high temperature data. We cannot ascribe this correction to any particular part of our calculations; the vacancy densities that we predict depend on the accuracy of the LDA energies, the gradient corrections to the LDA, the vibrational free energies, and the valence and conduction band density of states.

3.1 PROPERTIES OF COPPER, LITHIUM, AND SODIUM IN $Hg_{0.78}Cd_{0.22}Te$

All three impurities are found to behave as acceptors when they reside on the cation sublattice, although the exact location of the levels in the gap are difficult to determine due to the LDA error in predicting the band gap and dispersion due to superlattice effects. Donor levels are found for all of the impurities when they occupy interstitial positions, with preliminary predictions indicating that the donor levels are resonant in the conduction band.

We have examined the incorporation of copper, lithium, and sodium in the lattice throughout the existence region and find that at all temperatures and pressures they are all incorporated predominantly on the cation sublattice where they all behave as acceptors. At 500°C roughly from 0.1% to 1% of the sodium is incorporated interstitially, and about an order of magnitude less interstitials are found for the lithium. As

---

6. In using similar parameters for all of the calculations one can rely on a cancellation in systematic errors. One finds that differences in energies are less sensitive to adding additional orbitals to the basis or additional k-points in the Brillouin Zone integrations that are the raw energies. The thermodynamical predictions are ultimately related to differences in energies.
7. Berding, M. A., unpublished.
8. *Properties of Mercury Cadmium Telluride* EMIS Datareviews Series No. 3, ed. J. Brice and P. Capper, (Inspec, 1987).
9. Vydyanath, H. R., and C. H. Hiner, *J. Appl. Phys.* **65**, 3080 (1989).
10. Vydyanath, H. R., *J. Electrochem. Soc.* **128**, 2609 (1981).

the temperature is lowered, proportionately few interstitials are present. The interstitial densities calculated for lithium are comparable to those we have previously reported for copper.[4]

There is negligible strain associated with impurities substituting on the cation sublattice, their dominant means of incorporation. The impurity interstitials produce a slight compressive strain in the lattice and therefore, based on strain alone, will tend to collect in regions with larger lattice constants. This effect is relatively small. For example, based on the differences in lattice constants between CdTe and HgTe, strain will result in a factor of less then ten higher impurity interstitial densities in CdTe compared to HgTe. Chemical differences in the impurity interstitials interacting with the CdTe and HgCdTe lattices will probably be as important as the strain effect. Because interstitials are minority impurity species, we do not believe there will be any observable enhancement in the total equilibrium impurity concentrations at interfaces or other regions of moderate strain based on strain alone. In the following section we will discuss chemical differences between copper in the substrate and epilayers.

3.2 IMPURITY INTERACTIONS WITH SUBSTRATE

The properties of copper in CdTe have also been calculated. The energy to form a neutral CuTe unit cell in HgCdTe and CdTe are -6.18 and -5.85 eV, respectively. Using the definition of the chemical potential $\mu = E + k_b T \ln(x)$ and equating the chemical potential of the copper in both the CdTe and HgCdTe we find that the ration of copper in the HgCdTe layer to that in the CdTe substrate in equilibrium is given by $x_{\mathrm{HgCdTe}}/x_{\mathrm{CdTe}} = \exp(0.33/k_b T)$. This corresponds to over a factor of 100 at 500°C. Thus, if substrate layers start with a copper concentration of 10^{13} cm^{-3}, the epilayers could end up with over 10^{15} cm^{-3} copper if the substrate is treated as an inexhaustible source. Because the driving force for copper out of the substrates is so high, our work supports the strategy of growing a sacrificial layer of HgCdTe on CdTe substrates to strip copper out of the substrates, as has been employed by Harris et al.[2]

4.0 CONCLUSIONS

We have examined the properties of copper, lithium and sodium in LWIR HgCdTe and find similar behavior for all of them. They all substitute primarily on the cation sublattice where they behave as acceptors, and all have donor–like interstitials populations that are small (<0.1% of the total impurity populations). We find that copper will diffuse out of CdTe substrates into HgTe driven by differences in the chemical potentials in the two materials; and because interstitial populations are relatively high, this should occur relatively rapidly.

APPENDIX E

M. A. Berding and A. Sher, "Arsenic activation in MBE-grown HgCdTe," *Proceedings of the 1997 IRIS Materials Meeting*

ARSENIC ACTIVATION IN MBE-GROWN HgCdTe[1]

July 1997

M. A. Berding and A. Sher
SRI International
333 Ravenswood Avenue
Menlo Park, CA 94025

ABSTRACT

Using *ab initio* calculations, we identify the defect complex of an arsenic substituting on the cation sublattice bound to a cation vacancy as the primary means for non-ideal incorporation of arsenic atoms into $x = 0.3$ $Hg_{1-x}Cd_xTe$ cap layers grown under MBE conditions. The switching of arsenic atoms from the cation sublattice to the anion sublattice is identified as the key step in activating arsenic atoms as acceptors. A microscopic model of the transfer process is proposed that is consistent with experimental results on arsenic diffusion and post growth annealing strategies.

1.0 INTRODUCTION

Growth of $Hg_{1-x}Cd_xTe$ by molecular beam epitaxy (MBE) is being established as an important growth technique for HgCdTe focal plane arrays, and has the advantage over competing growth methods of being a low-temperature process.[2] In the p-on-n double layer heterojunction device, a p-type cap layer with roughly x=0.3 is grown on an n-type LWIR base layer. Although doping of the base layer with indium is well in hand, the cap layer doping with arsenic is not well established and activation anneals are still used to render the cap layer p-type. If activation anneals are performed at temperatures much above the growth temperature, the advantages of the low growth temperature of MBE are reduced.

In previous work[3] we examined arsenic incorporation in x=0.22 HgCdTe and found that the inactivity of arsenic atoms as acceptors in HgCdTe grown by liquid phase epitaxy (LPE) from the tellurium melt was due to incorporation of arsenic atoms on the cation sublattice where they behave as donors. In this paper we discuss our recent work on incorporation of arsenic in x=0.3 HgCdTe, but now include several additional defects, the most important of which is a complex consisting of an arsenic on the cation sublattice bound to a cation vacancy. We examine the behavior of arsenic atoms in the as-grown MBE layers and discuss strategies for effecting the transfer of arsenic atoms from the cation to the anion sublattice under low temperature conditions.

2.0 APPROACH

We use the full-potential linearized muffin-tin orbital (FP-LMTO) method based on the local density approximation (LDA) to calculate the ground and excited state energies of arsenic. Gradient corrections to the LDA were also included so that reference to the mercury vapor pressure could be made.[4] Several means for arsenic incorporation have been considered: (1) substitution on the cation sublattice; (2) substitution on the anion sublattice with from zero to four cadmium first neighbors; (3) arsenic at the two different classes of

1. Supported by DARPA, through AFOSR contract F49620-95-C-0004 and by Universal Technology Corporation under prime contract to U.S. Air Force F33615-94-C-5800. We would also like to acknowledge many useful discussions with A. Chen and coworkers at Rockwell.

2. See for example J. M . Arias, *Properties of Narrow Gap Cadmium-based Compounds*, EMIS Datareviews Series No. 10, ed. P. Capper, (Inspec, 1994), p. 30.

3. Berding, M. A., A. Sher, and M. van Schilfgaarde, *J. Electron. Mater.* **26**, 624 (1997).

4. Berding, M. A., M. van Schilfgaarde, and A. Sher *Phys. Rev. B* **50**, 1519 (1994).

tetrahedral interstitial sites; and (4) six different defect complexes involving arsenic, to which we will restrict our discussion here to the most important complex, an arsenic atom on the cation sublattice bound to a cation vacancy. The ground state energy of each of these defects is calculated using supercells containing thirty-two lattice sites, in which the defect of interest is surrounded by HgTe (with the exception of the substitution of arsenic on the tellurium sublattice, the presence of cadmium is ignored for this part of the calculation). Relaxation of the first and second neighbors to the defects were permitted. As complete a basis as was computationally feasible was used and similar parameters were employed in all supercell calculations.[5] Further details of the LDA calculations will be given elsewhere.[6] Contributions to the defect free energies arising from changes in the lattice vibrations were also calculated, as discussed in Ref. 4. Calculations were also repeated for the most important native point defects, the mercury vacancy and the tellurium antisite, using the same basis set, cell size, and number of k-points in the Brillouin Zone integration, as were used for the arsenic defect calculations. To improve agreement with experimental vacancy densities reported by Vydyanath and Hiner at low temperatures,[7] the formation energy of the vacancy was increased by 0.18 eV, similar to the corrections discussed in our earlier work[3] to agree with high temperature data. We cannot ascribe this correction to any particular part of our calculations; the vacancy densities that we predict depend on the accuracy of the LDA energies, the gradient corrections to the LDA, the vibrational free energies, and the valence and conduction band density of states. The present results for these defects are similar to those we reported earlier.[4]

The energies, ionization states, and degeneracies of all of the defects are incorporated into a statistical mechanical formalism similar to that discussed in Ref. 4 and used in our previous study on arsenic.[3] The method has been generalized so that defects extending over several lattice sites can be incorporated. Empirical expressions have been used for the temperature-dependent band gap and intrinsic carrier concentrations.[8]

3.0 RESULTS

3.1 PROPERTIES OF ARSENIC IN AS-GROWN CAP LAYERS

The conditions of MBE growth are modeled by equilibrating all of the defects under tellurium-saturated conditions. We will assume growth at 175°C with a corresponding mercury vapor pressure of $P_{\mathrm{Hg}} = 10^{-6}$ atm.[7] Although MBE is not an equilibrium process *per se*, we shall assume that the diffusion rates on the surface and within the first few layers of the growing surface are fast enough so that near equilibrium defect distributions are obtained.

For undoped material grown at 175°C under tellurium-saturated conditions, we predict the material will be vacancy doped and p-type at 77 K, with $[p] \sim 10^{16}$ cm^{-3} and have tellurium antisite densities less than 10^{12} cm^{-3}.

First we consider the properties of material with a total concentration of arsenic of 10^{17} cm^{-3}. As grown, we predict that nearly 90% of the arsenic will be incorporated into the lattice in the form of pairs with cation vacancies ($\mathrm{As_{Hg}}$-V_{Hg}). For the present calculations we have assumed that there are no ionized states associated with this defect; calculations are in progress to determine if there are donor or acceptor levels associated with it. Because of the high density of the $\mathrm{As_{Hg}}$-V_{Hg} complex, the total vacancy density as grown is quite high. The remaining 10% of the arsenic is incorporated on the mercury sublattice as isolated defects (unbound to vacancies), where the arsenic behaves as a donor with its first donor level resonant in the

---

5. In using similar parameters for all of the calculations one can rely on a cancellation in systematic errors. One finds that differences in energies are less sensitive to adding additional orbitals to the basis or additional k-points in the Brillouin Zone integrations that are the raw energies. The thermodynamical predictions are ultimately related to differences in energies.

6. Berding, M. A., unpublished.

7. Vydyanath, H. R., and C. H. Hiner, *J. Appl. Phys.* **65**, 3080 (1989).

8. *Properties of Mercury Cadmium Telluride* EMIS Datareviews Series No. 3, ed. J. Brice and P. Capper, (Inspec, 1987).

conduction band. A negligible fraction (< 0.1%) of the arsenic occupies the tellurium sublattice as-grown. At 77 K, we predict the material will be *p*-type, dominated by free vacancies.

For higher concentrations of arsenic, the properties of as-grown material are comparable to those for 10^{17} cm^{-3}. For lower arsenic concentrations, the primary difference is that the free vacancies represent a larger fraction of the total vacancy concentration.

3.2 PROPERTIES OF ARSENIC IN ANNEALED CAP LAYERS

Under mercury saturated conditions at low temperature (nominally 220°C), we predict that *in equilibrium* the arsenic will reside predominantly on the tellurium sublattice, with over 99% activation for [As]=10^{17} cm^{-3}, reducing to closer to 90% activation for [As]=10^{19} cm^{-3}. The question now is: what is the optimal path (in time, temperature, and mercury partial pressure) to reach this state for a sample prepared by MBE?

3.3 MODEL OF ARSENIC TRANSFER FROM CATION TO ANION SUBLATTICE

Although the equilibrium calculations indicate that arsenic should transfer to the tellurium sublattice under mercury-saturated conditions, the detail mechanism by which the transfer of the arsenic from the cation sublattice (where they are incorporated during MBE growth) to the tellurium sublattice may be complex and will necessarily involve native defects. An earlier model for this transfer was suggested by Chandra et al.[9] Here we propose a mechanism for the transfer that involves the dominant defects and does not require the creation or destruction of a unit cell during the transfer process, and thus can happen in the bulk of the material.

Based on our results, we propose a mechanism for transfer of an arsenic from the cation to anion sublattice as follows, and as shown in Figure 1. The starting defect for the transfer is the arsenic on a cation site bound to a mercury vacancy, with an intervening tellurium atom bound to both. This defect is the dominant means by which arsenic is incorporated under tellurium-saturated conditions and therefore is a majority defect. In the first step of the activation process, the intervening tellurium will transfer into the cation vacancy site, creating a tellurium antisite, with the arsenic following and transfering to the vacated tellurium site in the second step, leaving behind a cation vacancy. In the final step, the cation vacancy tellurium antisite pair will diffuse away from the arsenic (which now resides on the tellurium sublattice). In earlier work[10] we showed that the tellurium antisite, which is a donor, and the cation vacancy, which is an acceptor, are bound by approximately 1 eV, and suggested that this pair is the means through which tellurium antisites diffuse. As a result of the transfer process, the density of the vacancy-antisite pairs will be super-saturated, and they will diffuse as a pair to a surface or interface where they can be annihilated.

Now we consider the mechanisms occuring when MBE-grown material is subjected to a low-temperature mercury-saturated anneal. As mercury diffuses into the mercury-deficient material, two processes will be occuring simultaneously: (1) the filling of cation vacancies to establish their new equilibrium concentrations; and (2) the transfer of arsenic from the cation to the anion sublattice and the resulting generation and subsequent equilibration of vacancy antisite pairs. For the second process to proceed, cation vacancies must be present, so that for optimum transfer one wants the second process to occur more rapidly than the first process. One way this can be accomplished is by increasing the temperature. A second way this can be accomplished is by increasing the number of cation vacancies available to assist in the transfer and for diffusing away the antisites before they can recombine with arsenic through the reverse of the process shown in Figure 1. Because increasing the temperature (for a given mercury partial pressure) will result in a reduction of As_{Hg}-V_{Hg} pairs and a net reduction in the vacancy density, these are competing mechanisms and the optimal strategy will depend on details in the rate-controlling steps of the transfer.

---

9. Chandra, D., M. W. Goodwin, M. C. Chen, and L. K. Magel, *J. Electron. Mater.* **24**, 599 (1995).
10. Berding, M. A., A. Sher, and M. van Schilfgaarde, *J. Electron. Mater.* **24**, 1127 (1995).

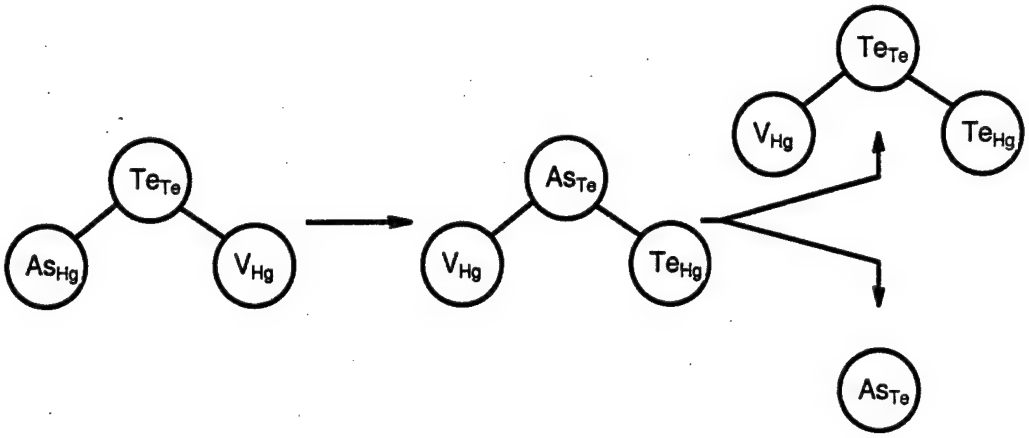

FIGURE 1. Pathway for transfer of arsenic from the cation to the anion sublattice

4.0 CONCLUSIONS

We have identified arsenic on the cation sublattice bound to a cation vacancy as the dominant means by which arsenic is incorporated into $Hg_{0.7}Cd_{0.3}Te$ grown by MBE. The switching of arsenic atoms from the cation sublattice to the anion sublattice is identified as the key step in activating arsenic atoms as acceptors. For the transfer of the arsenic from the cation to the anion sublattice to take place, a sufficient reservoir of cation vacancies must be present and care must be taken in developing an activation strategy so as not to annihilate the mercury vacancies before the transfer is complete. Sufficient thermal energy must also be available to increase the rates of transfer of arsenic between the cation and anion sublattice.

APPENDIX F

M. A. Berding, A. Sher, and M. van Schilfgaarde, "Lithium, sodium, and copper in $Hg_{0.78}Cd_{0.22}Te$ and CdTe-based substrates," *J. Electron. Mater.*, 1997

Lithium, sodium, and copper in $Hg_{0.78}Cd_{0.22}Te$ and CdTe-based substrates

M. A. Berding,* A. Sher, and M. van Schilfgaarde
SRI International, Menlo Park, California
(November 14, 1997)
(submitted for publication in Journal of Electronic Materials)

We present a theoretical examination of the behavior of lithium, sodium, and copper in $Hg_{0.78}Cd_{0.22}Te$ and in CdTe. In both HgCdTe and CdTe, all three impurities are determined to incorporate predominantly on the cation sublattice for most pressures and temperatures, where all the impurities have acceptor levels. All three impurities have secondary incorporation as interstitials, where they all behave as donors. Under conditions present in low-temperature, mercury-saturated anneals, lithium and sodium are mobilized because of the relatively high interstitial fraction, lower solubility, and an exothermic impurity kick-out reaction when the material is subjected to an injection of mercury interstitials. The relatively high interstitials predicted for these impurities is also likely to attribute to their large diffusion coefficients. Strain effects on the impurity incorporation are small and do not provide a strong driving force for these impurities to segregate. By examining the relative behavior of the impurities in CdTe and HgCdTe, we have derived prescriptions for maximizing gettering the impurities from CdTe-based substrates using a sacrificial HgCdTe epilayer, and for minimizing gettering from the substrates during epilayer growth.
KEY WORDS: HgCdTe, lithium, sodium, copper, doping, defects

INTRODUCTION

Lithium, sodium, and copper are all impurities which in most HgCdTe-based device structures are considered undesirable, but that are often observed to be present. Copper is a known fast diffuser in HgCdTe, and although in some cases it is introduced intentionally as a p-type dopant, its high diffusion coefficient is a liability in subsequent processing steps. It is known that copper present in $Cd_{1-x}Zn_xTe$ substrates (with nominally x=0.04) out-diffuses into HgCdTe epilayers during growth and can lead to undesirable effects.[1,2] Copper has also been observed to getter in tellurium inclusions present in substrates.[2] Less work has been done on the properties of lithium and less still on the properties of sodium in HgCdTe, but both are typically characterized as fast diffusers.[3] Lithium gettering to regions of damage and high vacancy concentration has also been observed.[4]

In previous work[5] we examined the properties of copper in x=0.22 HgCdTe and found that although copper atoms reside primarily on the cation sublattice, a significant fraction was incorporated interstitially. In this paper we discuss our recent work on the fundamental properties of copper, lithium, and sodium in HgCdTe and CdTe. We will also discuss the relative interaction of copper with the CdTe-base substrates and $Hg_{0.78}Cd_{0.22}Te$ epilayers and suggest strategies for encouraging or discouraging out-diffusion of the impurities from substrates.

APPROACH

The calculation of thermodynamic behavior of impurities in HgCdTe can be divided into two major parts: (1) the calculation of energies of the impurities in various possible configurations in the lattice; and (2) the statistical theory from which the concentrations of the impurities in the various configurations can be predicted.

In this paper, energies for the impurities lithium, sodium and copper (X) in a number of configurations in the lattice were considered (which we refer to collectively as "impurity defects"):

- X_{Hg}, the impurity substituting on the cation sublattice
- X_{Te}, the impurity substituting on the anion sublattice
- X_I, the impurity incorporating interstitially at both tetrahedral interstitial sites.

In addition to the arsenic defects, various native point defects were included:

*Author to whom all correspondences should be addressed: marcy@plato.sri.com

- V_{Hg}, the cation vacancy
- Hg_I, the cation interstitial
- Te_{Hg}, the tellurium antisite
- V_{Hg}–Te_{Hg}, the tellurium antisite, cation vacancy pair.[6]

Energies for the native point and impurity defects were calculated using the full-potential version of the linearized muffin-tin orbital (FP-LMTO) method[7] within the local density approximation (LDA) of von Barth and Hedin.[8] For each defect studied, a periodic array of that defect in the lattice is constructed. In principle, one would like to choose the ratio of the defect to the host atoms to be comparable to realistic concentrations. In practice, though, one is restricted to much higher ratios due to computational limitations. In this work we used supercells containing sixteen zinc-blende unit cells, with each supercell containing one defect. For the native point defect, LDA calculations were done for both HgTe and CdTe hosts. For the x=0.22 material, the formation energies in pure HgTe were used. The 4% zinc typically incorporated into CdTe for lattice matching to HgCdTe was also ignored in the present calculation. To ensure a good fit to the charge density and potential in the interstitial region of the relatively open zinc-blende structure, empty spheres have been included and orbitals added to the basis by centering them on the empty spheres. The charge density was expanded to l=5. The empty 5d-orbitals of the cations were included explicitly in the basis; the filled 4p-orbitals were included in a second panel.[9] A minimal "linked" basis set was used to relax up to the second neighbor shell of atoms about the defect.[9] The calculation was repeated with a larger, "triple-kappa" basis at this relaxed geometry, and using 14 k-points in the Brillioun zone.

As discussed previously,[10] gradient corrections to the LDA were found to be important when the vapor pressure of a monomer is used to establish a reference chemical potential of the system. Because we wish to use the mercury vapor pressure in determining the thermodynamic state of the system, we have included gradient corrections of the Langreth-Mehl-Hu type[11] in the present work. The gradient correction is believed to correct mostly for LDA errors in the free atom energies. Therefore, in lieu of completing a gradient correction calculation for each of the defects, we have identified a specific gradient correction term for each atom, which is added to the LDA energies of each of the supercells. Details of the calculation of the ionization states for each of the defects can be found in Ref. 12. Vibrational free energies for the defects were also calculated and included in the analysis, as discussed in Ref. 10.

The statistical model we use is based on the generalized quasichemical (QCA) formalism developed by Sher et al.,[13] and which has been extended also to include arbitrary size clusters, and to include equilibration of the electronic subsystem simultaneously with the atomic system. In our extended QCA, the real space lattice is divided into clusters. An energy, a set of ionization states,[14] and a set of ionization-dependent degeneracies is identified with each cluster. The chemical identity (that is, the number of each atom type) of each cluster is also specified. The free energy of the system can be expressed in terms of the cluster-specific free energies, the configuration entropy, and the free energy in the electronic excitations. In the QCA, the equilibrium set of clusters is determined by minimizing the free energy, subject to a set of constraint equations. Details of the extended QCA can be found in Ref. 12.

The free energy of the electronic excitations was calculated using Fermi-Dirac statistics. Because the LDA is for zero temperature and because the LDA systematically underestimates the band gap of semiconductors, we use experimental expressions for the temperature- and x-dependent band gap.[15] A density-of-states hole effective mass of 0.43 was used. The conduction band effective density of state was chosen to fit to the experimentally observed intrinsic carrier concentrations.[16,?] For CdTe, the conduction and valence band density of states were calculated assuming parabolic bands, with m_h^*=0.8 and m_e^*=0.09. For all calculations, the mercury pressure along the bounds of the existence region were taken from expressions given in Astles[17] for HgCdTe, and from Zanio[18] for CdTe.

PROPERTIES OF LITHIUM, SODIUM, AND COPPER IN HgCdTe

All three impurities are found to behave as acceptors when they reside on the cation sublattice, although the exact location of the levels in the gap are difficult to determine due to the LDA error in predicting the band gap and dispersion due to superlattice effects. If the acceptor levels E_a are referenced to the top of the valence band, we find

$$E_a^{Cu} > E_a^{Na} > E_a^{Li}; \tag{1}$$

that is, copper has the deepest and lithium the most shallow acceptor level. Donor levels are found for all of the impurities when they occupy interstitial positions, and the donor levels for all three are resonant deep in the conduction band for x=0.22 material. Negligible incorporation of all three impurities was found on the anion sublattice for all temperatures and mercury partial pressures.

We have examined the incorporation of copper, lithium, and sodium in the lattice throughout the existence region and find that at most temperatures and pressures they all incorporate predominantly on the cation sublattice where

they behave as acceptors. In Fig. 1 we have plotted the native point defects and the concentrations of the impurities at substitutional and interstitial sites as a function of mercury partial pressures throughout the existence region for 470 °C, corresponding roughly to the growth temperature for liquid phase epitaxy (LPE) of this material. Calculations were done assuming a fixed impurity concentration of 10^{14} cm^{-3}. The interstitial densities are highest for sodium, and lowest for copper. In Fig. 1 we can consider the lower and upper pressure bounds as representing the equilibration conditions of LPE material as-grown from the tellurium and mercury melts, respectively. The relative fraction of interstitials is found to increase as the mercury partial pressure increases, as expected. The ratio of substitutional to interstitial impurities was found to be nearly independent of the impurity density.

As the temperature is lowered, holding the mercury partial pressure constant, the lithium and sodium interstitial concentrations relative to the substitutional concentration increases. This is also true if the temperature is lowered along the mercury-rich side of the existence region, as is illustrated for sodium in Fig. 2. From Fig. 2 we see that for conditions corresponding to the low-temperature, mercury-saturated annealing conditions typically used to reduce the as-grown mercury vacancy concentrations, the sodium interstitial and substitutional densities are comparable. The same is found for lithium. Additionally, we find that the reaction

$$\mathrm{Hg}_I + X_{\mathrm{Hg}} \rightarrow X_I + \mathrm{Hg}_{\mathrm{Hg}} \tag{2}$$

is exothermic, with a reaction energy in excess of 1 eV for both lithium and sodium.

The preference for the interstitial site at lower temperatures and the exothermic reaction energy of Eq. 2 has some interesting consequences for lithium and sodium for the conditions present during the low-temperature, mercury-saturated anneals. As the material is annealed, mercury from the vapor diffuses into the material via mercury interstitials. These mercury interstitials annihilate cation vacancies, the desired effect. The mercury interstitials also result in a net forward reaction of Eq. 2 for a number of reasons. First, the interstitial fraction is higher for the annealing conditions than for the conditions present during high temperature growth by LPE (from Fig. 1) or those present during MBE, which, although they occur at low temperatures, are believed to take place under tellurium-rich conditions where the interstitial fraction is also low. Because the reaction in Eq. 2 is exothermic, the generation of impurity interstitials should happen rapidly. Additionally, for a given concentration of lithium or sodium in the lattice at a given temperature, the chemical potential increases as the mercury partial pressure increases, as is illustrated in Fig. 3, resulting in a driving force for impurities to diffuse from mercury-rich regions into mercury-deficient regions. Thus, as HgCdTe is subjected to a low-temperature mercury-saturated anneal, lithium and sodium will be quickly mobilized by going to predominantly interstitial positions, and then pushed ahead of the mercury diffusion front by their higher solubility in the unannealed regions. This will have a desired consequence of sweeping impurities out of the active material toward the substrate.

PROPERTIES OF LITHIUM, SODIUM, AND COPPER IN CdTe

The properties of the impurities in CdTe have also been calculated. Although ~4% zinc is typically incorporated into CdTe substrates to provide a lattice matching substrate for HgCdTe epitaxial growth, we have ignored its presence in these calculations. Because the amount of zinc is small, we expect that its impact on the energies used to determine the relative impurity incorporation on the substitutional and interstitial sublattice to be small and outside the accuracy of our calculations. The native defect equilibrium in CdTe was also calculated and will be discussed elsewhere.

The basic properties of the impurities in CdTe are similar to those found in HgCdTe: incorporation on the cation sublattice dominates for most temperatures and pressures; on the cation sublattice they all produce acceptor levels near to the valence band edge, with the same ordering indicated in Eq. 1; interstitials represent the second most important incorporation site; and incorporation on the anion sublattice is negligible.

For conditions present during Bridgeman growth (1100 °C, $P_{\mathrm{Hg}} \simeq 1$ atm), we find that the primary incorporation is on the cation sublattice, with about ~10% interstitials for lithium and sodium and < 1% interstitials for copper. The primary native point defect is the cation vacancy, with a concentration of $\sim 3 \times 10^{17}$ cm^{-3}.

In Fig. 4 we have plotted the native point defects and the concentrations of the impurities at substitutional and interstitial sites as a function of mercury partial pressures throughout the existence region for 470 °C, corresponding roughly to the growth temperature for LPE of HgCdTe. The CdTe-based substrates are held at this temperature during epilayer growth, and therefore it represents an important equilibration condition. Calculations were done assuming a fixed impurity concentration of 10^{14} cm^{-3}, and calculations for each impurity were done separately.

IMPURITY INTERACTIONS BETWEEN SUBSTRATES AND EPILAYERS

When examining the impurity redistribution that will occur when a HgCdTe epilayer is grown on a CdTe substrate, we cannot refer to a true equilibrium condition because the heterojunctions themselves represent a nonequilibrium condition. Here we shall examine the case in which the impurities are permitted to equilibrate in the constrained system, where the mercury and cadmium are not allowed to inter-diffuse. Although the assumption of no inter-diffusion is not justified at the relatively high temperatures of LPE growth, the following discussion will provide some guidelines for the driving forces on the impurities by considering the relative properties of the impurities far from an interface. The issue of the equilibrium state of the native point defects in the CdTe substrates during epitaxial growth of the $Hg_{0.78}Cd_{0.22}Te$ base layer is more difficult, because only a small amount of inter-diffusion is necessary to modify the point defect equilibrium, small enough that compositional changes resulting from the inter-diffusion can be ignored. A similar issue arises when an x=0.3 cap layer is grown on an x=0.22 base layer of $Hg_{1-x}Cd_xTe$, especially if the base layer is grown from the tellurium melt (easier to handle because of the lower vapor pressures) and the cap layer is grown from the mercury melt (necessary if active p-type group V impurities are desired). Here we shall restrict our discussion to the behavior of impurities between the substrate and the epilayer.

In the following discussion we will refer to Fig. 3, which is a plot of the chemical potential at 470 °C for each of the impurities in $Hg_{0.78}Cd_{0.22}Te$ and CdTe, for a fixed impurity concentration of 10^{14}. The calculation for each material was done separately. Although there is an arbitrary zero for the impurity chemical potentials, for a given impurity, only the relative values of the chemical potential between HgCdTe and CdTe are meaningful. Because it is an element common to both materials, the cadmium partial pressure was chosen to characterize the position of the material in the existence region. The bounds of the existence region for $Hg_{0.78}Cd_{0.22}Te$ and CdTe are indicated at the top of Fig. 3. The change in slope for the impurity chemical potential in CdTe corresponds to the position below which the cation vacancy concentration exceeds the impurity concentration and above which the impurity concentration exceeds the vacancy concentration, as can be seen from Fig. 4.

First we consider HgCdTe growth on CdTe in which the native defects have been frozen in from the Bridgeman growth. As discussed above, under Bridgeman growth conditions, there are $\sim 3 \times 10^{17}$ cm^{-3} cation vacancies. As the material is cooled from the Bridgeman growth temperature to the epilayer growth temperature (assuming a nominal LPE growth temperature of 470 °C), interstitial impurities will drop into substitutional sites provided by the vacancies, until a new ratio of substitutionals-to-interstitials is established. If we restrict our discussion to low concentrations of the impurities, as might be present from unintentional sources, this rearrangement of impurities within the bulk of the material will not significantly alter the cation vacancy population. For the $\sim 3 \times 10^{17}$ cm^{-3} cation vacancies frozen in, the conditions will resemble those of an effective cadmium partial pressure of $\sim 5 \times 10^{11}$ atm at 470 °C, obtained by extrapolating outside of the existence region in Fig. 4; the corresponding effective chemical potential of the impurity for Bridgeman material quench-cooled to the LPE growth temperature can be obtained from Fig. 3. If this material is subjected to HgCdTe LPE growth conditions, with the impurity concentration the same in the epilayer as in the substrate, the chemical potential of the impurity in the CdTe will be lower than in the epilayer, representing a driving force for the impurity to getter out of the epilayer into the substrate, a desirable condition for epilayer growth.

Fig. 3 also suggests a strategy for cleaning substrates. If the CdTe material is subjected to a cadmium-rich anneal prior to the epilayer growth, the cation vacancy concentration will be reduced and the impurity chemical potential increased. Consider a preanneal at 470 °C under cadmium-saturated conditions ($P_{Cd} = 10^{-2}$ atm). If this material is subjected to LPE growth of HgCdTe with comparable impurity density, there will be a strong driving force for the impurity to leave the region of high chemical potential (in the CdTe) and enter a region of low chemical potential (the HgCdTe). The lower the temperature for the cadmium-saturated preannealing of the CdTe, the larger the driving force for the gettering. Optimal impurity gettering will also occur if the HgCdTe is grown tellurium rich. This sacrificial HgCdTe layer could then be removed. A version of this strategy has been reported previously by Harris.[1]

A strategy for minimizing impurity gettering from the substrates into the epilayer is also suggested by Fig. 3. If the CdTe material is subjected to a tellurium-saturated anneal prior to epilayer growth, the vacancy density will be maximized and the impurity chemical potential in the substrate will be driven down, reducing the driving force for out-diffusion into the HgCdTe. The more cation vacancies introduced into the CdTe during the preanneal, the lower the impurity chemical potential in the substrate will be during epilayer growth, and the larger the gettering into the substrate (or the smaller the gettering into the epilayer) will be.

The above strategies are based on the impurity density in the substrates prior to growth being the same as in the growing HgCdTe epilayer. If the impurity densities in the two materials are substantially different, the above arguments must be modified to account for a concentration gradient.

We have also examined the response of the impurities to strain in the lattice, in part to see if the occasionally observed pile-up of these impurities at interfaces can be explained by a strain release mechanism. Our calculations show that the strain associated with lithium, sodium, and copper impurities substituting both on the cation sublattice and interstitially is small, and could result in no more than a 10% concentration enhancement of the impurity at an otherwise ideal interface. As we showed above, though, lithium and sodium will be mobilized during the low-

temperature, mercury-saturated anneal, and will be pushed ahead of the in-diffusing flux of mercury interstitials. Thus, these impurities will be swept out of the HgCdTe toward the epilayer–substrate interface, where they might be pinned by dislocations (both by decorating the core and by forming a Cotrell atmosphere), and other extended defects.

SUMMARY AND CONCLUSIONS

We have examined the properties of copper, lithium and sodium in $Hg_{0.78}Cd_{0.22}Te$ and in CdTe and find that they all substitute primarily on the cation sublattice where they behave as acceptors, and all have donor-like interstitials which are also present in substantial quantities. Under mercury-saturated low-temperature annealing conditions we have shown that lithium and sodium are mobilized and driven out of the annealed regions toward the substrate. No microscopic mechanism for keeping impurities at the epilayer–substrate interface is found, although the impurities may be trapped at interfaces by extended defects such as misfit dislocations. We have proposed a method for cleaning CdTe substrates by preannealing them under cadmium-saturated conditions at a temperature as low as possible, followed by the LPE growth of a sacrificial HgCdTe epilayer, preferably from the tellurium-rich melt. For minimizing gettering of impurities from the CdTe substrates into the HgCdTe epilayers, the substrates should be annealed under conditions designed to introduce as many cation vacancies as possible – that is, tellurium-rich conditions at elevated temperatures. Substrates grown by Bridgeman as-grown may closely mimic these conditions.

ACKNOWLEDGMENTS

This work was supported by the U.S. Air Force Wright Laboratories through a subcontract with Universal Technology Corporation, subcontract no. 97-S402-22-13-C1, and by DARPA through AFOSR contract no. F49620-95-C-0004. We also wish to acknowledge discussions with K. Harris at II-VI Corporation, and H. Robinson at SRI Interational.

---

[1] K. Harris, II-VI Corporation, private communication.
[2] J. P. Tower, S. P. Tobin, P. W. Norton, A. B. Bollong, A. Socha, J. H. Tregilgas, C. K. Ard, and J. F. Arlinghaus, *J. Electron. Mater.* **25**, 1183 (1996).
[3] P. Capper, in *Properties of Narrow Gap Cadmium–Based Compounds*, EMIS Datareviews Series No. 10, ed. P. Capper, (INSPEC, 1994), p. 158 and p.163, and references therein.
[4] L. O. Bubulac, W. E. Tennant, R. A. Riedel, J. Bajaj, and D. D. Edwall, *J. Vac. Sci. Technol. A* **1**, 1646 (1983).
[5] M. A. Berding, A. Sher, and M. van Schilfgaarde, *J. Electron. Mater.* **26**, 624 (1997).
[6] The tellurium vacancy, tellurium interstitial, and the mercury antisite have been previously identified as minority defects for the purpose of establishment of the majority defect equilibrium, and have not been included in the present analysis.
[7] O. K. Andersen, O. Jepsen, and D. Glotzel, *Highlights of Condensed Matter Theory*, ed. F. Bassani et al. (Amsterdam, The Netherlands: North Holland, 1985), p. 59.
[8] U. von Barth and L Hedin, *J. Phys.C* **5**, 1629 (1972).
[9] M. van Schilfgaarde, unpublished.
[10] M. A. Berding, A. Sher, and M. van Schilfgaarde, *Phys. Rev. B* **50**, 1519 (1994).
[11] D. Langreth and D. Mehl, *Phys. Rev. B* **28**, 1809 (1983).
[12] M. A. Berding, unpublished.
[13] A. Sher, M. van Schilfgaarde, A.-B. Chen, and W. Chen, *Phys. Rev. B* **36**, 4279 (1987).
[14] We have used a one-electron picture of the ionization states, although the formalism is capable of dealing with negative-U centers.
[15] G. L. Hansen, J. L. Schmit, and T. N. Casselman, *J. Appl. Phys.* **53**, 7099 (1982).
[16] The conduction band was fit to a linear dispersion to give agreement with experimental intrinsic carrier concentrations. The conduction bands have a more nearly hyperbolic dispersion near the band edge, but we found that for the purpose of fitting the carrier concentrations, the linear dispersion assumption was adequate.
[17] M. G. Astles, in *Properties of Narrow Gap Cadmium-Based Compounds*, EMIS Datareviews Series No. 10, ed. P. Capper, (INSPEC, 1994), p. 13, and references therein.
[18] K. Zanio, *Semiconductors and Semimetals*, Vol. 13, edited by R. K. Willardson and A. C. Beer (Academic Press, New York,

1978).

FIG. 1. Native point defect and impurity densities in $Hg_{0.78}Cd_{0.22}Te$ at 470 °C. Calculations were done for one impurity at a time, with the impurity density held constant at 10^{14} cm^{-3}.

FIG. 2. Native point defect and sodium densities in $Hg_{0.78}Cd_{0.22}Te$ as a function of temperature along the mercury-saturated side of the existence region. Calculations were for an impurity density held constant at 10^{15} cm^{-3}.

FIG. 3. The relative chemical potential of lithium, sodium, and copper in $Hg_{0.78}Cd_{0.22}Te$ and CdTe as a function of cadmium partial pressure. The bounds of the existence region for each of the materials also are indicated. Because the alloy concentration of HgCdTe is kept constant, the cadmium-rich (-poor) bounds map into the mercury-rich (-poor) bounds of the existence region. The dotted line for CdTe corresponds to regions outside of the CdTe existence region.

FIG. 4. Native point defect and impurity densities in CdTe at 470 °C. Calculations were done for one impurity at a time, with the impurity density held constant at 10^{14} cm^{-3}.

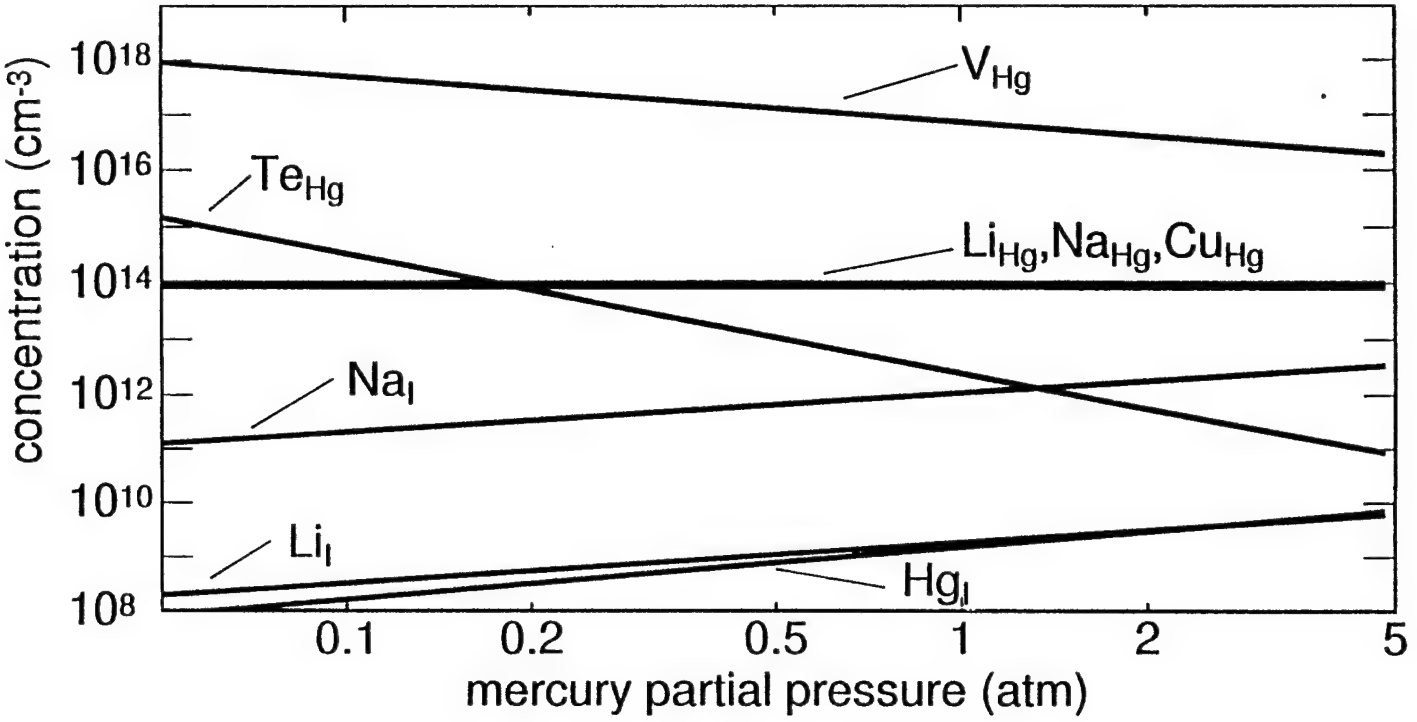

BERDING
FIGURE 1

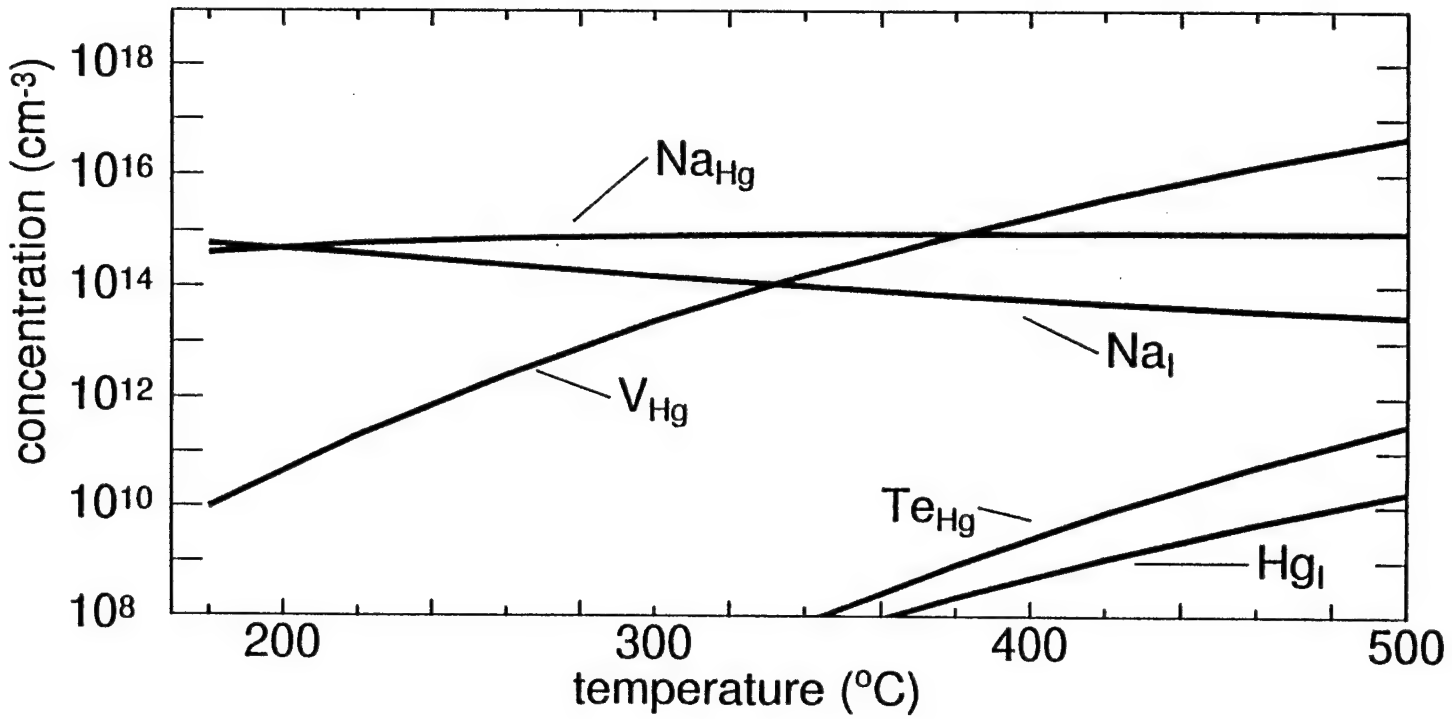

BERDING
FIGURE 2

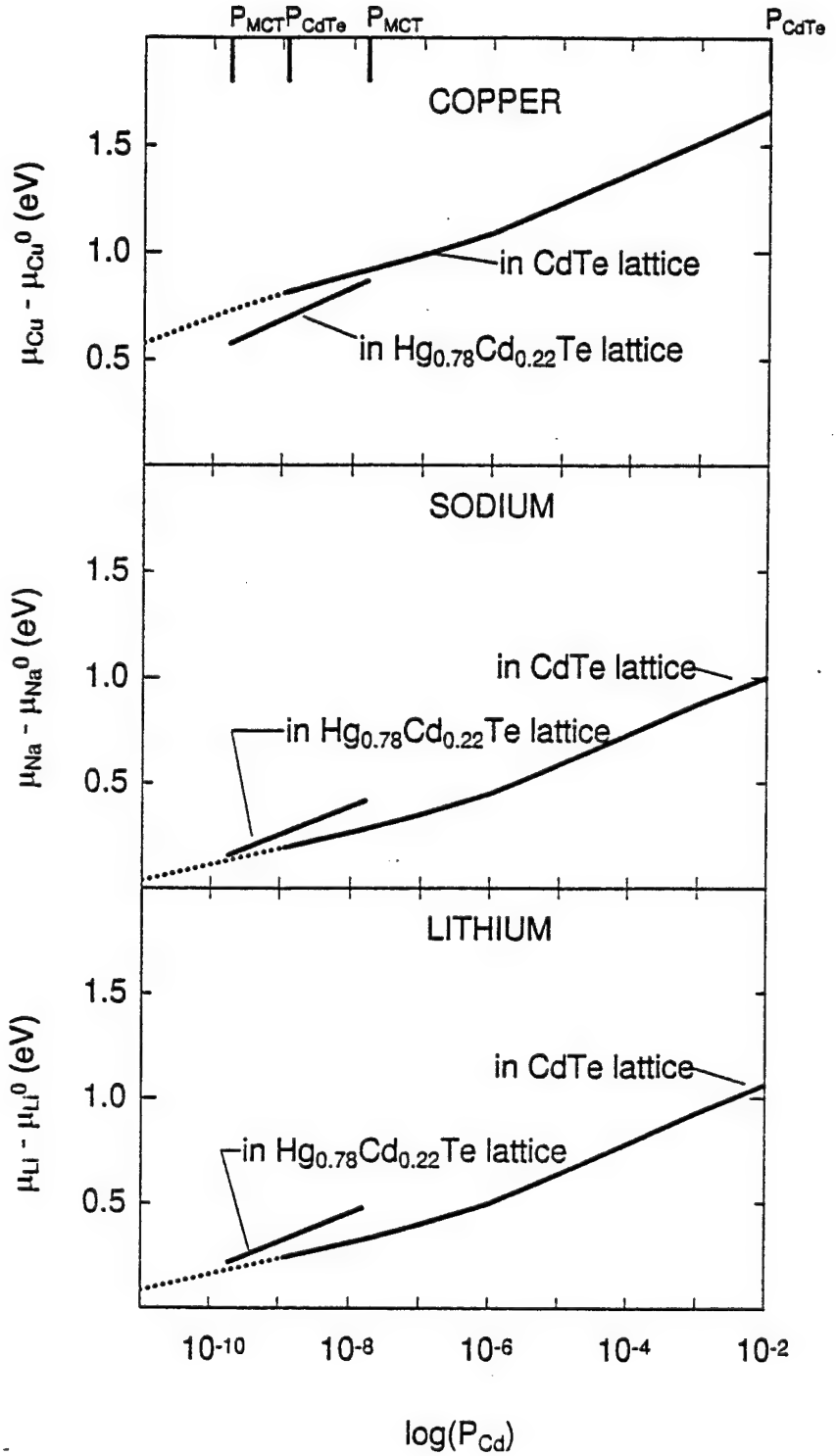

BERDING
FIGURE 3

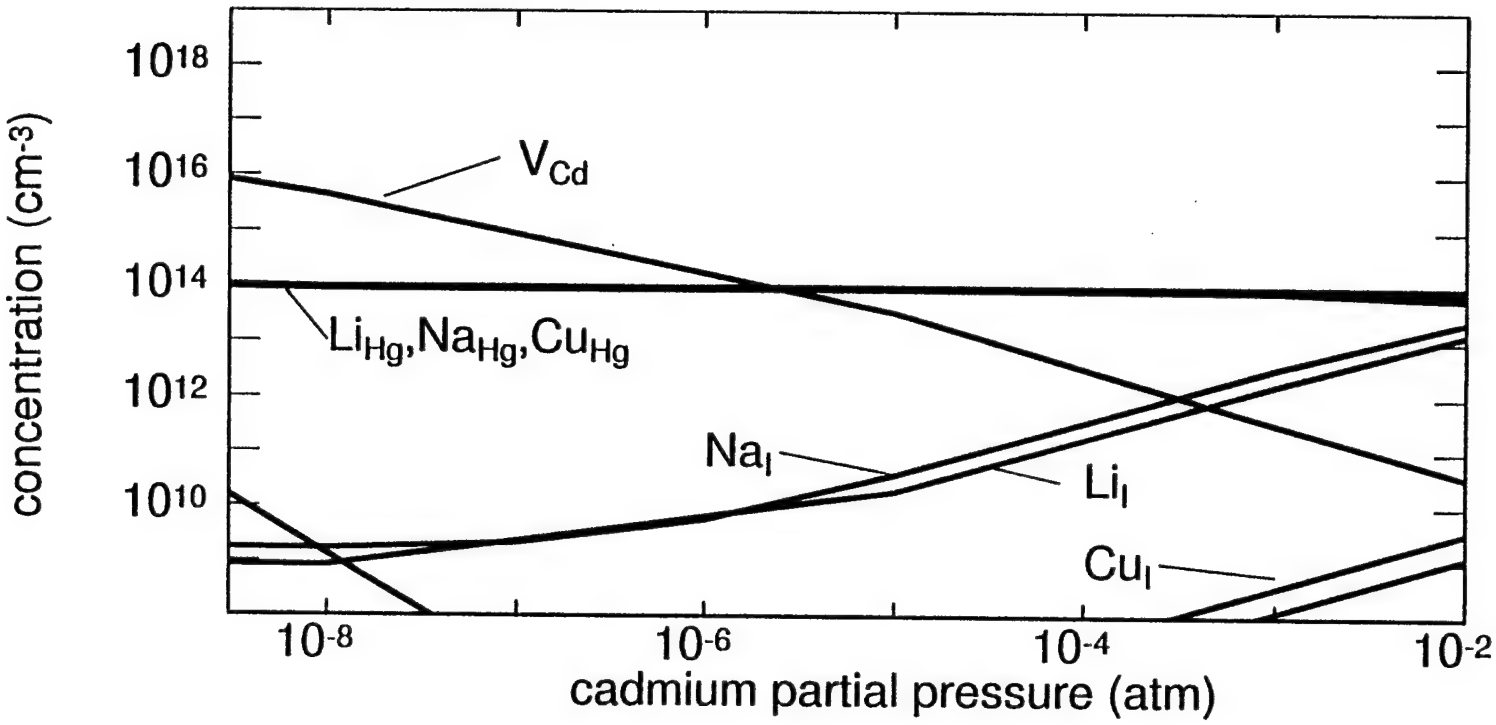

BERDING
FIGURE 4

APPENDIX G

M. A. Berding, A. Sher, and M. van Schilfgaarde, "Modeling of arsenic activation in HgCdTe," *J. Electron. Mater.*, 1997

Modeling of arsenic activation in HgCdTe

M. A. Berding,* A. Sher, and M. van Schilfgaarde
SRI International, Menlo Park, California

A. C. Chen and J. Arias
Rockwell International Corporation, Thousand Oaks, California
(November 18, 1997)
(submitted for publication in Journal of Electronic Materials)

We present a theoretical examination of the behavior of arsenic atoms in $Hg_{1-x}Cd_xTe$ for $x = 0.3$, focusing on the thermodynamic conditions that most closely mimic molecular beam epitaxial growth and subsequent annealing steps. We show that, for molecular beam epitaxial growth where tellurium-saturated conditions apply, arsenic incorporates onto the cation sublattice and becomes inactive. A significant fraction of these arsenic atoms are bound to mercury vacancies. We also propose a model of the activation, which involves transfer of the arsenic from the cation to the anion sublattice. The model suggests that activation anneals must be done at high enough temperatures to surmount an activation barrier, and that the phase field from tellurium- to mercury-rich conditions should be traversed slowly enough so that the cation vacancies are not filled before the site transfer can be completed.

KEY WORDS: HgCdTe, arsenic, doping, defects

INTRODUCTION

Growth of $Hg_{1-x}Cd_xTe$ by molecular beam epitaxy (MBE) is being established as an important growth technique for long-wave infrared (LWIR) focal plane arrays, and has the advantage over competing growth methods in that it is a low-temperature process.[1] In the p-on-n double layer heterojunction device, a p-type cap layer with $x \approx 0.3$ is grown on an n-type LWIR base layer. The cap layer is typically doped with arsenic because of arsenic's relatively low diffusion coefficient. Following a standard low-temperature mercury-saturated anneal to fill the high concentration of as-grown cation vacancies, the material is observed to be n-type. Activation anneals at higher temperature are used to render the cap layer p-type.[2,3] If activation anneals are performed at temperatures much above the growth temperature or for very long times, the advantages of the low-growth temperature of MBE are reduced.

A number of efforts have focused on the behavior of group V impurities in HgCdTe in growth by bulk methods,[4] liquid phase epitaxy,[5] and MBE.[2,6] The amphoteric behavior for arsenic has been seen in materials grown by all of these approaches,[7] with incorporation as a p-type dopant under Hg-rich conditions, and as an n-type dopant or inactive under Te-rich conditions. The arsenic can be switched from an n- to p-type dopant through post-growth annealing.[8]

In this paper we present the results of a theoretical examination of the behavior of arsenic atoms in $x = 0.3$ $Hg_{1-x}Cd_xTe$. We focus on the thermodynamic conditions relevant to MBE growth and subsequent annealing steps. The method we use is similar to that discussed previously in our studies of native point defects[9] and p-type dopants[10] in HgCdTe.

APPROACH

The calculation of thermodynamic behavior of arsenic in HgCdTe can be divided into two major parts: (1) the calculation of energies of arsenic in various possible configurations in the lattice; and (2) the statistical theory from which the concentrations of arsenic in the various configurations can be predicted.

In this paper, energies for arsenic in a number of configurations in the lattice are considered (which we refer to collectively as "arsenic defects"):

- As_{Hg}, arsenic substituting on the cation sublattice;

*Author to whom all correspondences should be addressed: marcy@plato.sri.com; (650)859-4267; (650)859-5303(Fax)

- As_{Te}, arsenic substituting on the anion sublattice;
- As_{Hg}–As_{Te}, near-neighbor pair of arsenic both on the cation and anion sublattice;
- As_{Hg}–V_{Hg}, arsenic substituting on the cation sublattice bound to a cation vacancy;
- sites, As_I, arsenic incorporating interstitially at both tetrahedral interstitial;
- As_I–As_{Te}, an arsenic interstitial bound to an arsenic on the anion site;
- As_I–As_{Hg}, an arsenic interstitial bound to an arsenic on the cation site;
- As_{Te}–Te_{Hg}, arsenic substituting on the anion sublattice and bound to an antisite; and
- As_{Te}–Hg_I, arsenic substituting on the anion sublattice and bound to a mercury vacancy.

In addition to the arsenic defects, various native point defects were included:

- V_{Hg}, the cation vacancy;
- Hg_I, the cation interstitial;
- Te_{Hg}, the tellurium antisite; and
- V_{Hg}–Te_{Hg}, the tellurium antisite, cation vacancy pair.[11]

Energies for the native point and arsenic defects were calculated using the full-potential version of the linearized muffin-tin orbital (FP-LMTO) method[12] within the local density approximation (LDA) of von Barth and Hedin.[13] For each defect studied, a periodic array of that defect in the lattice is constructed. In principle, one would like to choose the ratio of the defect to the host atoms to be comparable to realistic concentrations. In practice, though, one is restricted to much higher ratios due to computational limitations. In this work we used supercells containing sixteen zinc-blende unit cells, with each supercell containing one defect. For the native point defect, LDA calculations were done for both HgTe and CdTe hosts, and the values at intermediate compositions were determined by a linear interpolation. For arsenic on the tellurium sublattice, calculations were done with from one to four near-neighbor cadmium. To ensure a good fit to the charge density and potential in the interstitial region of the relatively open zinc-blende structure, empty spheres have been included and orbitals added to the basis by centering them on the empty spheres. The charge density was expanded to l=5. The empty 5d-orbitals of the cations were included explicitly in the basis; the filled 4p-orbitals were included in a second panel.[14] A minimal "linked" basis set was used to relax up to the second neighbor shell of atoms about the defect.[14] The calculation was repeated with a larger, "triple-kappa" basis at this relaxed geometry, and using 14 k-points in the Brillioun zone

As discussed previously,[9] gradient corrections to the LDA were found to be important when the vapor pressure of a monomer is used to establish a reference chemical potential of the system. Because we wish to use the mercury vapor pressure in determining the thermodynamic state of the system, we have included gradient corrections of the Langreth-Mehl-Hu type[15] in the present work. The gradient correction is believed to correct mostly for LDA errors in the free atom energies. Therefore, in lieu of completing a gradient correction calculation for each of the defects, we have identified a specific gradient correction term for each atom, which is added to the LDA energies of each of supercells. Details of the calculation of the ionization states for each of the defects can be found in Ref. 16. Vibrational free energies for the defects were also calculated and included in the analysis, as discussed in Ref. 9.

The statistical model we use is based on the generalized quasichemical (QCA) formalism developed by Sher et al.,[17] and which has been extended also to include arbitrary size clusters, and to include equilibration of the electronic subsystem simultaneously with the atomic system. In our extended QCA, the real space lattice is divided into clusters. An energy, a set of ionization states,[18] and a set of ionization-dependent degeneracies is identified with each cluster. The chemical identity (that is, the number of each atom type) of each cluster is also specified. The free energy of the system can be expressed in terms of the cluster-specific free energies, the configuration entropy, and the free energy in the electronic excitations. In the QCA, the equilibrium set of clusters is determined by minimizing the free energy, subject to a set of constraint equations. Details of the extended QCA can be found in Ref. 16.

The free energy of the electronic excitations was calculated using full Fermi-Dirac statistics. Because the LDA is for zero temperature and because the LDA systematically underestimates the band gap of semiconductors, we use experimental expressions for the temperature- and x-dependent band gap.[19] A density of states hole effective mass of 0.43 was used. The conduction band effective density of state was chosen to fit to the experimentally observed intrinsic carrier concentrations.[20,21]

In this work we have not attempted to determine the absolute solubility of arsenic in HgCdTe. Rather we chose to specify the total arsenic concentration in the material for each calculation. We shall also specify the cadmium concentration to be $x = 0.3$ for all calculations in this paper. Two additional constraints on the system were set by specifying the temperature and the mercury partial pressure.

Although annealing of HgCdTe, discussed below, can most likely be viewed as an equilibrium process, MBE growth itself is a non-equilibrium process, and there is some question about the use of thermodynamics in determining the properties of the as-grown material. Because MBE of HgCdTe is believed to occur under tellurium-saturated conditions, we shall assume that the defect structure locked into the material during the relatively low-temperature MBE growth corresponds to those in tellurium-saturated material at the growth temperature.

PROPERTIES OF ARSENIC IN AS-GROWN MBE CAP LAYERS

As discussed in Ref. 3, a growth temperature of 175°C is used by Rockwell to grow arsenic-doped layers. This temperature is lower than the optimal growth temperature of 190°C, and was found to be necessary to increase the arsenic incorporation efficiency. The conditions for MBE growth are modeled by equilibrating all of the defects at the growth temperature of 175°C under tellurium-saturated conditions, corresponding to $P_{\mathrm{Hg}} = 10^{-5}$ atm.[22] Although MBE is not an equilibrium process per se, if the diffusion rates on the surface and within the first few layers of the growing surface are fast enough, it is reasonable to assume that near-equilibrium defect distributions will be obtained.

In Fig. 1 the defect concentrations are plotted as a function of the total arsenic in the lattice for material equilibrated at 175°C under tellurium-saturated conditions. Under these conditions, our calculations predict that much less than 1% of the arsenic will be incorporated on the tellurium sublattice where it behaves as a p-type dopant. For the arsenic concentrations considered, between 30 and 50% of the arsenic is predicted to be incorporated on the cation sublattice as part of a neutral complex where it is bound to a cation vacancy ($\mathrm{As_{Hg}}$–V_{Hg}). The remainder of the arsenic is incorporated on the cation sublattice as isolated defects, $\mathrm{As_{Hg}}$, unbound to vacancies, where the arsenic behaves as a donor. The calculations predict that material will be cation vacancy doped p-type at low arsenic concentrations and n-type due to arsenic incorporation on the cation sublattice for higher arsenic concentrations. The concentration of arsenic interstitials is less than 10^{10} cm^{-3}.

PROPERTIES OF ARSENIC IN ANNEALED CAP LAYERS

Next we turn to the properties of $x = 0.3$ material subjected to a 220°C anneal. In Fig. 2 we have plotted the defect concentrations as a function of the mercury partial pressures across the existence region for 220°C, assuming a total arsenic concentration in the lattice of 10^{16} cm^{-3}. Under mercury-saturated conditions at low temperature, we predict that *in equilibrium* the arsenic will reside predominantly on the tellurium sublattice, with over 99% activation for all arsenic concetrations considered.

Starting from material grown by MBE (Fig. 1), for equilibrium to be reached for the low-temperature, mercury-saturated anneal (corresponding to the righthand side of Fig. 2) arsenic must transfer from the cation to the anion sublattice. The focus of the rest of this paper will be on how this activation via site transfer takes place and what is the optimal path (in time, temperature, and mercury partial pressure) for reaching this equilibrium state for a sample prepared by MBE. We begin by discussing a model for the arsenic activation.

MODEL OF ARSENIC TRANSFER FROM CATION TO ANION SUBLATTICE

We propose a mechanism for transfer of an arsenic from the cation to anion sublattice (the essential step in the activation process) as follows, and as shown schematically in Fig.3. The starting defect for the transfer is the arsenic on a cation site bound to a mercury vacancy. From Fig. 1 we see that this defect complex will be present in large densities in as-grown material. In the first step of the activation process, the intervening tellurium will transfer into the cation vacancy site, creating a tellurium antisite, with the arsenic following and transferring to the vacated tellurium site and leaving behind a cation vacancy. In the final step, the cation vacancy–tellurium antisite pair, which was previously shown to form a bound pair,[23] will diffuse away from the arsenic now residing on the tellurium sublattice. As a result of the transfer process, the density of the vacancy–antisite pairs will be supersaturated, and they must diffuse to a surface where they can be annihilated.

The model of the activation has a number of attractive features. The activation model involves only a short-range bulk process. It does not require the creation or destruction of a unit cell, other than through the eventual equilibration of the neutral vacancy–antisite pair which is generated in the site transfer process. The model also involves only the major defects in the lattice. Unfortunately, as a result of the arsenic site transfer, the system is supersaturated with tellurium; the vacancy–antisite pairs can annihilate either at a free surface, or they can form tellurium precipitates in the bulk. Because the vacancy–antisite pair is neutral, even if it is not fully equilibrated and

nonequilibrium concentrations remain in the material following the activation, it will not be electrically active and will not affect the carrier concentrations. Due to its strain (the tellurium antisite results in a compressive strain in the surrounding lattice) and charge dipole, the vacancy–antisite pair will provide an additional scattering center, and if present, may adversely affect mobilities.

ACTIVATION ANNEALING STRATEGIES

Now we consider the mechanisms occuring when MBE-grown material is subjected to a low-temperature mercury-saturated anneal directly following growth. As the temperature is raised to $\sim$ 220°C under mercury-saturated conditions, two processes will occur simultaneously: (1) cation vacancies are filled, establishing new equilibrium concentrations; and (2) arsenic is transfered from the cation to the anion sublattice, approaching a new equilibrium with arsenic on the two sublattices. According to our proposed model, for the second process to proceed, cation vacancies must be present, so that for optimum transfer one wants the second process to occur more rapidly than the first. We predict that if the phase field is traversed too rapidly—which can occur by going directly to mercury-saturated conditions following MBE growth—the mobile mercury interstitials fill the cation vacancies more quickly than the site transfer can occur. Because vacancies are necessary for the site transfer to proceed, the arsenic becomes locked onto the cation sublattice, where it behaves as a donor. This is consistent with the finding that MBE material subjected to a mercury-saturated anneal directly following growth is n-type. We have calculated the 77 K carrier concentration for material that has been equilibrated under MBE growth conditions, and then subjected to a mercury-saturated anneal at 220°C, but suppressed the transfer of arsenic to the anion sublattice to mimic this phenomenon. We find that the material is n-type with a carrier concentration equal to the total arsenic concentration. The experiments find that n-type carrier concentration is closer to 10% of the total arsenic concentration. The discrepancy between theory and experiment can be attributed to uncertainties in the theory—for example, the exact location of the donor level associated with As_{Hg} and its temperature dependence, or our prediction of the pressure at which the crossover between arsenic occupying the cation and anion sublattice occurs—or the partial activation of the arsenic, with some of it transfering to the anion sublattice under the annealing conditions.

Next we consider equilibration along several different annealing paths, as shown in Figs. 4 and 5, both for material containing a total arsenic concentration of 10^{18} cm^{-3}. In Fig. 4, the material starts from MBE growth conditions at 175°C, is heated to 220°C under tellurium-saturated conditions, and is then subjected to increasing mercury partial pressures while the temperature is held at 220°C. In Fig. 5, starting from MBE material growth conditions at 175°C, the material is heated to 350°C under tellurium-saturated conditions, and is then subjected to increasing mercury partial pressures while the temperature is held at 350°C; then the temperature is reduced to 220°C under mercury-saturated conditions. For both paths, the crucial steps take place in the region where the As_{Hg} population is sharply decreasing and the As_{Te} population is sharply increasing. There are advantages to traversing the phase field at higher temperatures. First, there is more thermal energy to surmount the activation barrier between the initial and final configurations in Fig. 3, which we calculate to be greater than 1 eV. Secondly, at the higher temperatures more vacancies and As_{Hg}–V_{Hg} pairs are present both at the crossover where the As_{Hg} and As_{Te} concentrations are equal, and even under the mercury-saturated conditions, so that under nonequilibrium conditions there will more likely be a supply of cation vacancies to affect the site transfer.

SUMMARY AND CONCLUSIONS

We find the amphoteric behavior of arsenic in $Hg_{0.7}Cd_{0.3}Te$ can be explained by arsenic incorporation on the cation sublattice under the tellurium-saturated MBE growth conditions. We predict that arsenic interstitial densities are negligible and the activation model that we propose does not depend on arsenic interstitials being present in the lattice. This differs from previous models of the amphoteric behavior and activation.[7,8] Our model for the activation process involves only the primary defects in the lattice. The net product of the activation process is the generation of a tellurium antisite in the form of a tellurium antisite–vacancy pair; and as a consequence of the activation process, the density of this defect pair is initially supersaturated. Although the pair is neutral, if the vacancy–antisite pairs do not all equilibrate in post-growth processing, it may serve as a scattering and/or recombination center and thereby degrade the device properties. This is because the antisite produces strain in the lattice (the antisite is too big, producing tensile stress about it) and additionally will have a charge dipole associated with it. This supersaturated density of vacancy-antisite pairs may also condense to form micro-precipitates.

Effective activation anneals will involve elevated temperatures so that sufficient thermal energy is available to surmount the activation barrier for site transfer, and also so that sufficient vacancies are available to catalyze the

reaction. More important is the need to traverse the phase field from tellurium- to mercury-saturated conditions slowly, particularly in the pressure regime where the dominant arsenic incorporation changes from the cation to the anion sublattice, so that the transfer process outlined in Fig. 3 can take place before the mercury vacancies are depleted.

ACKNOWLEDGMENTS

This work was supported by the U.S. Air Force Wright Laboratories through a subcontract with Universal Technology Corporation, subcontract No. 97-S402-22-13-C1, and by DARPA through AFOSR contract No. F49620-95-C-0004.

---

[1] See for example, J. M. Arias, *Properties of Narrow Gap Cadmium-Based Compounds*, EMIS Datareviews Series No. 10, Ed. P. Capper, (INSPEC, 994), p.30.
[2] S. Sivananthan, P. S. Wijewarnauriya, F. Awariden, H.R. Vydyanath, M. Zandian, D. D. Edwall, and J. M. Arias, *J. Electron. Mater.* **26**, 621 (1997).
[3] A. C. Chen, M. Zandian, D. D. Edwall, J. M. Arias, P. S. Wijewarnasuriya, S. Sivananthan, M. Berding, and A. Sher, this conference.
[4] H. R. Vydyanath, R. C. Abbott, and D. A. Nelson, *J. Appl. Phys.* **54**, 1323 (1983).
[5] H. R. Vydyanath, J. A. Ellsworth, and C. M. Devaney, *J. Electron. Mater.* **16**, 13 (1987).
[6] See, for example, P. S. Wijewarnasuriya, S. S. Yoo, J. P. Faurie, and S. Sivananthan, *J. Electron. Mater.* **25**, 1300 (1996).
[7] H. R. Vydyanath, *Semicond. Sci. Technol.* **5**, S213 (1990).
[8] H. R. Vydyanath, L. S. Lichtmann, S. Sivanathan, P. S. Wijewarnasuriya, and J. P. Faurie *Semicond. Sci. Technol.* **24**, 625 (1995)
[9] M. A. Berding, A. Sher, and M. van Schilfgaarde, *Phys. Rev. B* **50**, 1519 (1994).
[10] M. A. Berding, A. Sher, and M. van Schilfgaarde, *J. Electron. Mater.* **26**, 624 (1997).
[11] The tellurium vacancy, tellurium interstitial, and the mercury antisite have been previously identified as minority defects for the purpose of establishment of the majority defect equilibrium, and have not been included in the present analysis.
[12] O. K. Andersen, O. Jepsen, and D. Glotzel, *Highlights of Condensed Matter Theory*, ed. F. Bassani et al. (Amsterdam, The Netherlands: North Holland, 1985), p. 59.
[13] U. von Barth and L Hedin, *J. Phys.C* **5**, 1629 (1972).
[14] Mark van Schilfgaarde, unpublished.
[15] D. Langreth and D. Mehl, *Phys. Rev. B* **28**,1809 (1983).
[16] M. A. Berding (unpublished)
[17] A. Sher, M. van Schilfgaarde, A.-B. Chen, and W. Chen, *Phys. Rev. B* **36**, 4279 (1987).
[18] We have used a one-electron picture of the ionization states, although the formalism is capable of dealing with negative-U centers.
[19] G. L .Hansen, J. L. Schmit, and T. N. Casselman, *J. Appl. Phys.* **53**, 7099 (1982).
[20] P. Capper, in *Properties of Narrow Gap Cadmium-Based Compounds*, EMIS Datareviews Series No. 10, ed. P. Capper, (INSPEC, 1994), p. 212.
[21] The conduction band was fit to a linear dispersion to give agreement with experimental intrinsic carrier concentrations. The conduction bands have a more nearly hyperbolic dispersion near the band edge, but we found that for the purpose of fitting the the carrier concentrations, the linear dispersion assumption was adequate.
[22] Expressions for the edge of the existence region for $Hg_{1-x}Cd_xTe$ were taken from J. C. Brice, *Prog. Cryst. Growth Charact.* **13**, 39 (1986).
[23] M. A. Berding, A. Sher, and M. van Schilfgaarde, *J. Electron. Mater.* **24**, 1127 (1995).

FIG. 1. Calculated defect densities in material equilibrated at 175°C under tellurium-saturated conditions. Concentrations shown include neutral and all ionized states.

FIG. 2. Calculated defect densities as a function of mercury partial pressure for material equilibrated at 220°. The total arsenic concentration was held fixed at 10^{16} cm^{-3}.

FIG. 3. Proposed model of the arsenic activation path, involving the transfer of the arsenic from the cation to the anion sublattice.

FIG. 4. Possible annealing path for $Hg_{0.7}Cd_{0.3}Te$ containing 10^{18} arsenic atoms. Path proceeds from left to right.

FIG. 5. Another possible annealing path (proceeding from left to right). Although both this figure and Fig. 4 have the same begining and ending points for the mercury partial pressure and temperature, this path is considered preferable, as discussed in the text.

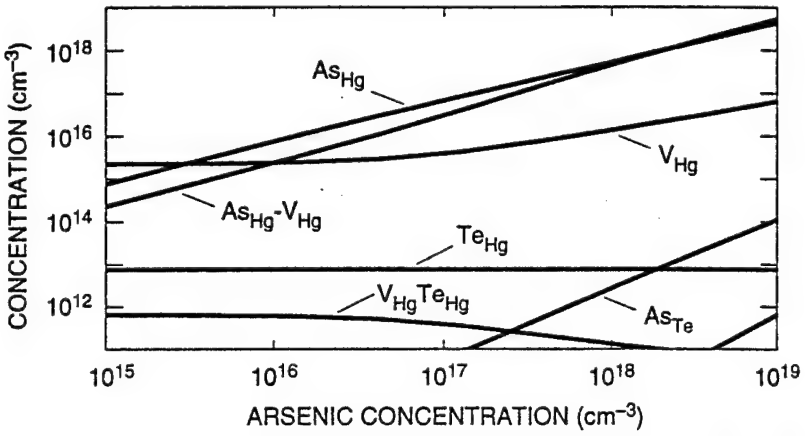

Figure 1
Author: Berding

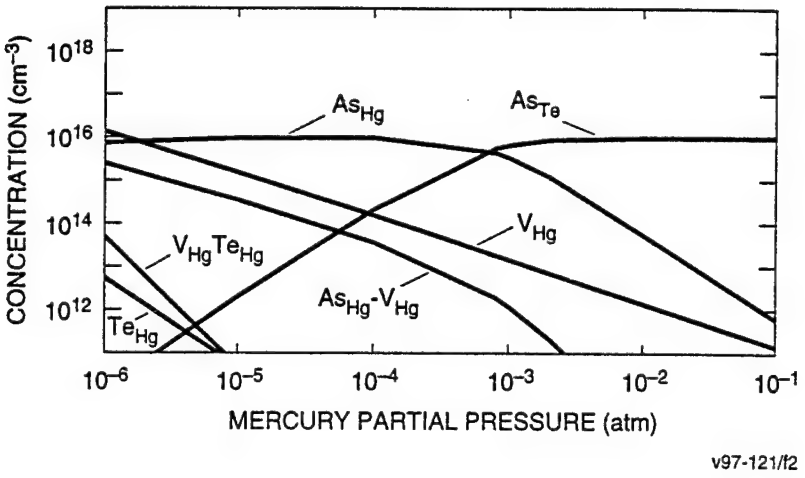

Figure 2
Author: Berding

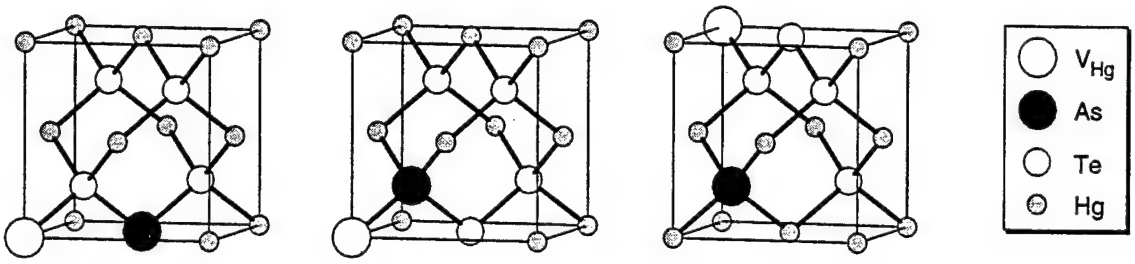

Figure 3
Author: Berding

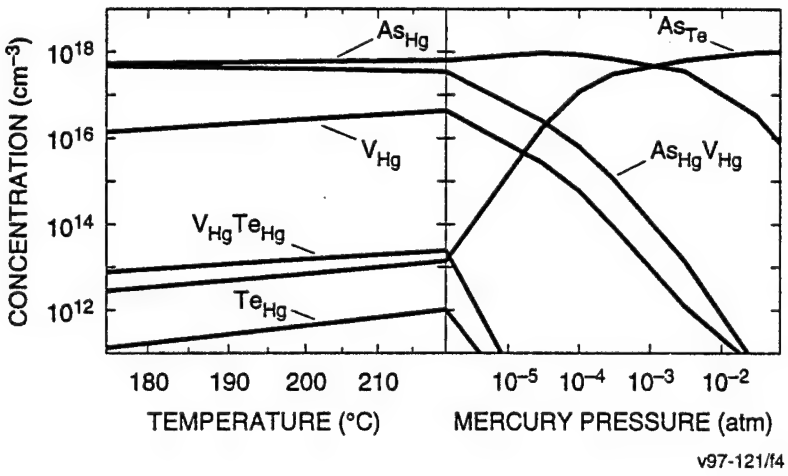

Figure 4
Author: Berding

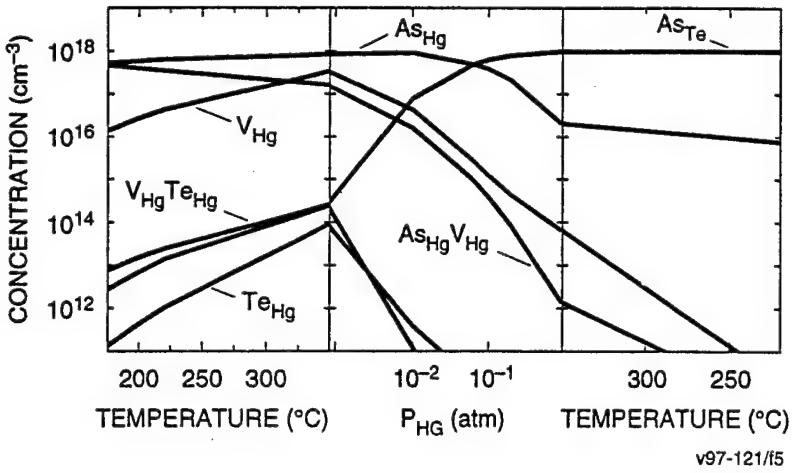

Figure 5
Author: Berding

APPENDIX H

M. A. Berding and A. Sher, "Dopants in HgCdTe," *J. Electron. Mater.*, 1997

DOPANTS IN HgCdTe

M.A. BERDING, A. SHER
Applied Physical Sciences Laboratory, SRI International, 333 Ravenswood Ave., Menlo Park, CA 94025, marcy@plato.sri.com

ABSTRACT

In this paper we discuss our *ab initio* calculations of native point defect and impurity densities in HgCdTe. Our calculations have explained the experimental finding in general, and in particular have explained the in-active incorporation of the group VII elements under mercury-deficient conditions; have shown that the group I elements have a large fraction of interstitial incorporation, thereby explaining their fast diffusion; and have described a microscopic mechanism for the amphoteric behavior of the group V elements. We discuss the trends found among the compounds in terms of the underlying bond strengths to understand why the various elements behave the way they do.

INTRODUCTION

$Hg_{1-x}Cd_xTe$ is a continuously soluble, pseudobinary alloy, with a band gap ranging from -0.3 eV for HgTe (x=0) to 1.6 eV for CdTe (x=1) [1]. The primary application of HgCdTe is for detectors in the long-wave infrared region of the spectrum. Unfortunately, the HgTe bond is weak, and consequently native point defect densities are high, with the primary defect being the cation vacancy [2].

A typical device structure in use today is a p-on-n double layer heterojunction, in which the infrared radiation incident through the substrate is absorbed in a lightly doped n-type base layer with x=0.22 and is confined in the junction region by a more heavily doped p-type cap layer with x=0.3. The material is typically grown on lattice-matched $Cd_{0.96}Zn_{0.04}Te$ substrates by liquid phase epitaxy (LPE) [3,4], molecular beam epitaxy (MBE) [5], or metal-organic chemical vapor deposition [6]. Although the n-type doping of the base layer with indium is pretty well controlled for both LPE [7,8] and MBE [9] growth, gas phase reactions of the tellurium and indium precursors has led to a renewed interest in the group VIIA elements for n-type doping [10]. Although cation vacancy densities can be high enough to be useful as the p-type dopant, the relatively high diffusivity of the vacancy and the short minority carrier lifetimes in vacancy-doped material have made vacancy doping undesirable. The group IA and IB elements behave as acceptors, but their use as p-type dopants is considered undesirable for most applications because of their relatively high diffusivity [11], which may lead to unstable doping profiles during subsequent processing. The group VA elements on the other hand are slow diffusers [12], in particular under mercury-rich conditions, but unfortunately are amphoteric [13], necessitating growth under mercury-rich conditions or post-growth activation anneals to produce p-type behavior [14].

APPROACH

The calculations of thermodynamic behavior of impurities and native defects in HgCdTe can be divided into two major parts: the first consists of the statistical theory from which the concentrations of the defects in various positions in the lattice are predicted; the second consists of all of the parameters that enter into the statistical theory.

The statistical theory we use is based on an extended quasichemical formalism which includes an arbitrary cluster size and overlap, and which includes the equilibration of the electronic subsystem simultaneously with the atomic system. In the theory, the real space lattice is divided into clusters. Here we choose clusters consisting of four lattice sites (two cation and two anion) and four tetrahedral interstitial sites. This is the minimum size cluster for calculating the defect complexes considered in this paper. An energy, a set of ionization states, a set of ionization-dependent degeneracies, and a chemical identity is associated with each cluster. The free energy of the system can be expressed in terms of the cluster-specific

free energies, the configurational entropy, and the free energy of the electronic excitations. The equilibrium set of clusters is determined by minimizing the free energy, subject to a set of constraint equations. Preliminary details of the theory can be found in ref. [15].

One of the inputs to the statistical theory is the set of neutral cluster energies; these energies are calculated using the full-potential linear muffin-tin orbital method (FP-LMTO) within the local density approximation (LDA) [16]. Gradient corrections [17] to the LDA were added so that the vapor phase of mercury could be used in the calculations to establish the state of the material within the existence region [15]. Defect energies were calculated in the FP-LMTO using 32-lattice-site supercells, and 4-lattice-site cluster energies for the statistical theory were extracted by subtracting off the energy of a 28-lattice-site cell with no defect. Ionization energies were also calculated in the LDA and are cast in terms of one-electron excitations. No negative-U states were found. Vibrational excitations were also calculated, as described in ref. [15]. Electronic excitations are calculated using Fermi-Dirac statistics. The temperature- and x-dependent band gap were taken from experiment [18]. The density of states hole effective mass of 0.43 was used, and the conduction band density of states was fit to the intrinsic carrier concentrations using a linear dispersion for the band shape.

NATIVE POINT DEFECTS

We have previously reported on the properties of the native point defects in $Hg_{0.8}Cd_{0.2}Te$ [15]. More recent calculations have been performed that included larger supercells, calculation of the localized levels within the FP-LMTO, and consideration of various defect complexes. Our recent findings are in general agreement with results reported in ref. [15], and with experiment, and are summarized here.

For equilibration at all temperatures and pressures, we find that the cation vacancy is the dominant defect, in agreement with experiment [2], although our calculations indicate that the vacancy is singly ionized in x=0.2 material, rather than doubly ionized as deduced from electrical measurements in ref. [2]. Although it never dominates the carrier concentration, the anion antisite density is significant at low mercury partial pressures. The tellurium antisite is a donor, and the cation vacancy-tellurium antisite pair is a strongly bound complex (~1 eV), with a relatively high density at low mercury partial pressures. This complex is important both for the diffusion of the tellurium antisite and as a precursor to precipitation. If the cation vacancies are annihilated in a typical low-temperature mercury-saturated anneal before the tellurium antisites can equilibrate, nonequilibrium densities of the antisites may be frozen into the material, and may account for an uncontrolled recombination center. The defect densities at 500 °C as a function of mercury partial pressure throughout the existence region are shown in Fig. 1. As shown in Fig. 2, we predict that the material is anion-rich throughout the existence region.

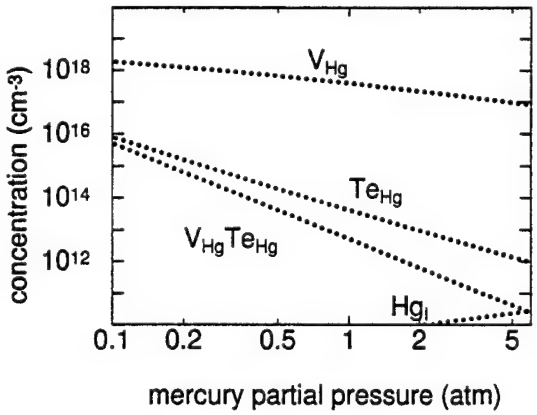

FIGURE 1: Native point defect densities as a function of mercury partial pressure throughout the existence region, at 500 °C.

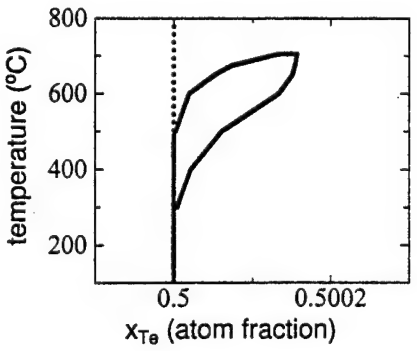

FIGURE 2: The equilibrium deviation from stoichiometry in $Hg_{0.8}Cd_{0.2}Te$.

N-TYPE DOPANTS

Group III Elements

Indium is the element most often used for n-type doping in both LPE [7,8] and MBE [9] growth, and is generally considered to be "well behaved." Our calculations reflect these findings. We predict that the indium incorporates nearly 100% on the cation sublattice where it behaves as a shallow donor. There is a significant binding of an indium substituting on the cation sublattice to a cation vacancy, and these complexes are present in the material, but account for less than 1% of the indium incorporation for all temperatures. The indium interstitial fraction is extremely small, and therefore the vacancies-indium complexes are probably the means by which indium diffuses. In material doped with 10^{15} cm^{-3} indium and subjected to a typical 250 °C, mercury-saturated anneal, the indium-vacancy complex density is only $\sim 10^{7}$ cm^{-3}, accounting for the observed stability of indium-doped devices.

Group VII Elements

Like indium, iodine has a low interstitial fraction and low incorporation fraction on the "wrong" sublattice, and in this sense iodine is a well-behaved n-type donor. Iodine substituting on the anion sublattice behaves as a donor and binds to the cation acceptor vacancy, resulting in a neutral complex. For high iodine densities and mercury-deficient conditions, this complex accounts for the majority of the iodine incorporation. In Fig. 3 we have plotted the iodine incorporation and native point defects for a fixed iodine concentration of 3×10^{19} cm^{-3}, as a function of the mercury partial pressure at 500 °C. We have also calculated the carrier concentrations at 77 K assuming the high-temperature defect structure is quenched into the crystal, and we compare this to some experimental results on bulk grown and annealed samples [19]. One can see that the theory is in very good agreement with experiment, showing a p-to-n type conversion as the mercury partial pressure is increased, with the p-type behavior at low pressures due to cation vacancies and the n-type behavior at higher mercury partial pressure due to the iodine. The discrepancy with experiment can be accounted for by a small shift in our predicted position in the existence region.

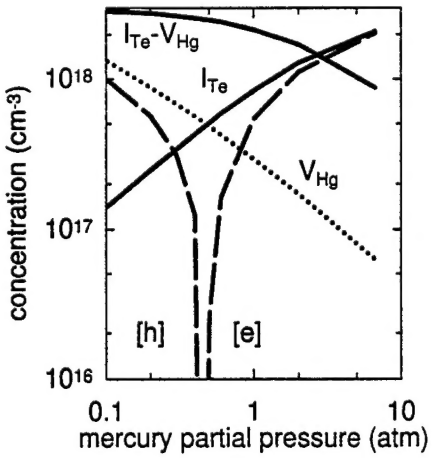

FIGURE 3: Iodine incorporation as a function of mercury partial pressure at 500 °C, compared to experimental results [19] for [h] (open circles) and [e] (closed circles).

P-TYPE DOPANTS

Group Ia and Ib Elements

Lithium and sodium are known fast diffusers [11] and are typically classified as "bothersome" impurities. In Fig. 4 we have plotted the lithium, sodium, and native point defect densities as a function of mercury partial pressure throughout the existence region at 250 °C, a typical temperature used for a mercury-saturated anneal to remove cation vacancies. Both lithium and sodium repel cation acceptor vacancies, and therefore have a negligible pairing with vacancies. The interstitial concentration is quite high under mercury-rich conditions, especially for sodium, and we expect both lithium and sodium to be interstitial diffusers. Furthermore, the interstitial fraction increases as the temperature decreases, and thus we expect these impurities to be very mobile under conditions of low-temperature, cation-rich anneals. Copper, silver, and gold all incorporate primarily on the cation sublattice, show negligible antisite incorporation and pair densities, and have a small interstitial density that increases in going from copper to silver to gold [20].

Group V Elements

We will discuss arsenic as the prototypical group V dopant; qualitatively similar behavior for phosphorus and antimony was found in our previous work [20]. Arsenic has been known to behave amphoterically in HgCdTe, with the desired p-type behavior under mercury-rich conditions, and n-type behavior under tellurium-rich conditions [13]. Our calculations predict this amphoteric behavior, as illustrated in Fig. 5. We find negligible incorporation of arsenic at interstitial sites, but do find incorporation on the cation sublattice that dominates the arsenic incorporation at low mercury partial pressures. The arsenic on the cation sublattice behaves as a donor, thus explaining the observed n-type behavior of arsenic-doping in mercury-deficient materials. Some of the arsenic on the cation sublattice are bound to cation vacancies, creating neutral complexes. These complexes are most likely the means by which arsenic diffuses in this material.

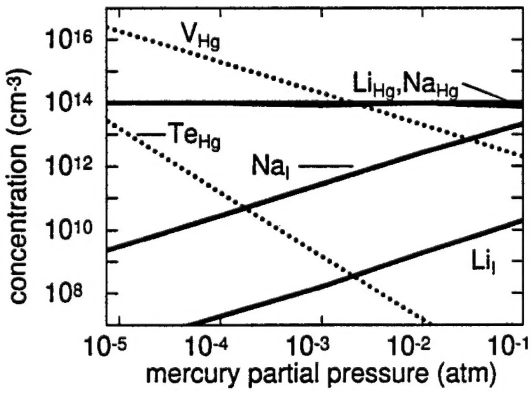

FIGURE 4: The lithium, sodium, and native point defect densities throughout the existence region at 250 °C for fixed impurity concentration of 10^{14} cm^{-3}.

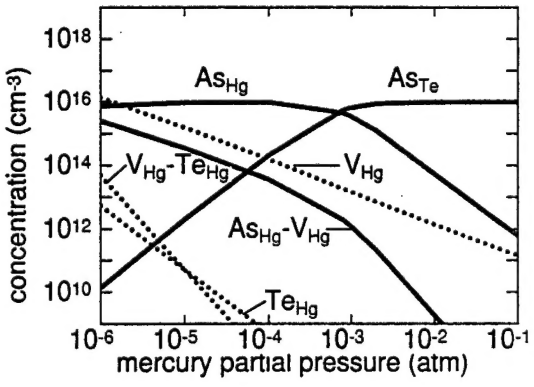

FIGURE 5: The arsenic and native point defect densities throughout the existence region at 220 °C for fixed arsenic concentration of 10^{16} cm^{-3}.

DISCUSSION

Only the group V elements have a significant incorporation on the "wrong," or antisite, sublattice, although the group VI antisite is predicted to be present, but never dominant. The formation of the group V and VI antisites can be attributed to the weakness of bonds that mercury makes with the group V elements and tellurium, and the relative strength of the group V-Te and the Te-Te bonds. Unlike the group V and VI elements, the group VII element iodine does not show significant incorporation on the cation sublattice. As more electrons are added to the valency in going from the V to the VI to the VII elements, the chemical difference with the group II element for which they are substituting become more significant – for example, the iodine has seven valence electrons compared to two for mercury – thus disfavoring incorporation on the cation sublattice in the tetrahedral environment. Furthermore, stable metal-iodine compounds such as HgI_2 are stable, whereas pure tellurium metal and arsenic-telluride compounds like to form, demonstrating the different chemistry of these elements.

We find no significant incorporation of the group I, II, or III elements on the anion sublattice. This can be attributed in part to the relative weakness of the bonds mercury and cadmium make with these elements, compared to those they make with tellurium. For the group I elements, the chemical differences with the tellurium are significant (one valence electron compared with six for tellurium), which also accounts for the lack of substitution of these elements on the anion sublattice. Hg-Hg bonds are very weak, as is evident from the low melting temperature of mercury. The strength of bonds that the group III elements make with tellurium is evidenced by the presence of well-xsybound phases, such as In_2Te_3. No significant incorporation of the group VII elements on the cation sublattice is found, attributable to lack of strong I-Te bonding, and relatively strong Hg-I bonds, as evident from the presence of a HgI_2 phase.

All of the impurities that incorporate into HgCdTe as donors (which includes the group III and VII elements, and tellurium and the group V elements incorporating on the cation sublattice) have a significant binding energy to the cation vacancy (greater than 1 eV). For indium and iodine which are introduced as intentional n-type dopants, this pairing is undesirable, although for the low doping densities used and under mercury-saturated conditions at low temperature the pair densities will be negligible and nearly 100% activation of the n-type dopants will be realized.

The group I elements have been shown to have the highest percent of interstitial substitution. This is in part due to the fact that these elements do not readily make sp^3 hybrids for bonding in the tetrahedral environment and therefore interstitial incorporation can compete effectively. The group III and V elements readily make sp^3 hybrids, so although the bond energies they make at substitutional sties may be small, they can still compete effectively against interstitial incorporation. Based on these arguments, one would expect iodine to have a significant interstitial incorporation, which we do not find in the present calculations.

Although the determination of the dominant diffusion mechanism for the impurities in HgCdTe involves more than an examination of the various defect densities, the defect densities can suggest the mechanism that dominates. With this caveat in mind, we will see how our results give a hint about how the various impurities will diffuse in the material.

We expect the group I elements to be interstitial diffusers. They all have relatively large interstitial fractions, and as acceptors, have very low pair densities with the cation vacancies. For lithium and sodium, we have shown that the interstitial fraction is highest for low-temperature, mercury-saturated conditions [21], accounting to the high mobility of these impurities under typical annealing conditions.

The group III element indium is expected to diffuse via cation vacancies, due to the large fraction of vacancy-indium pairs, and the negligible fraction of indium interstitials. Because the diffusion correlates with the presence of the cation vacancies, indium should be relatively stable after the vacancies are filled in a typical low-temperature, mercury-saturated anneal. The diffusion of group V and VII elements, along with the group VI tellurium self diffusion, are more complicated because of the exceedingly low anion vacancy and anion interstitial densities [15]. The group V and VI elements may diffuse by their antisites via

the cation vacancy, which show a significant binding. We have demonstrated a correlation of the pressure dependence of the diffusion with the concentration of the arsenic antisite-cation vacancy pairs [21]. No specific means for iodine diffusion is suggested by our work.

CONCLUSIONS

We have given an overview of the behavior of a wide array of elements in HgCdTe, and have shown that theory is quite capable of predicting their fundamental properties. Accurately identifying the position of the material within the existence region in the theory is essential to correlating the theory with the experimental findings.

ACKNOWLEDGMENTS

This work was supported by the U.S. Air Force Wright Laboratories through a subcontract with Universal Technology Corporation, subcontract no. 97-S402-22-13-C1, and by DARPA through AFOSR contract no. F49620-95-C-0004. The work benefited from discussions with Mark van Schilfgaarde at SRI International.

REFERENCES

1. D. Long and J. L. Schmit, in Semimetals and Semimetals, Vol. 5, Edited by R. K. Willardson and A. C. Beer, Academic Press, NY, 1970, p. 175.
2. H. R. Vydyanath, J. Electrochem. Soc. **128**, p. 2609 (1981).
3. B. Pelliciari, Prog. Crystal Growth and Charact. **29**, p. 1 (1994).
4. M. H. Kalisher, P. E. Herning, and T. Tung, Prog. Crystal Growth and Charact. **29**, p. 41 (1994).
5. See for example, J. M. Arias, Properties of Narrow Gap Cadmium-Based Compounds, EMIS Datareviews Series No. 10, Edited by P. Capper, INSPEC, 1994, p. 30.
6. See for example, A. J. C. Irvine, ibid., p. 24.
7. T. Tung, M. H. Kalisher, A. P. Stevens, and P. E. Herning, Mater. Res. Soc. Symp. **90**, p. 321 (1987).
8. L. Colombo, G. H. Westphal, P. K. Liao, M. C. Chen, and H. F. Schaake, Proc. SPIE (USA) 1683, p. 33 (1992).
9. P. S. Wijewarnasuriya, M. D. Lange, S. Sivanathan, and J. P. Faurie, J. Electron. Mater. **24**, p. 5 (1995).
10. P. Mitra....
11. P. Capper, in Properties of Narrow Gap Cadmium-Based Compounds, EMIS Datareviews Series No. 10, Edited by P. Capper, INSPEC, 1994, p. 158 and p. 163, and references within.
12. D. Chandra, M. W. Goodwin, M. C. Chen, and J. A. Dodge, J. Electron. Mater. **22**, p. 1033 (1993).
13. H. R. Vydyanath, Semicond. Sci. Technol. **5**, p. S213 (1990).
14. H. R. Vydyanath, L. S. Lichtmann, S. Sivanathan, P. S. Wijewarnasuriya and J. P. Faurie, J. Electron. Mater. **24**, p. 625 (1995).
15. M. A. Berding, M. van Schilfgaarde, and A. Sher, Phys. Rev. B. **50**, p. 1590 (1994).
16. O. K. Andersen, O. Jepsen, and D. Glotzel, Highlights of Condensed Matter Theory, Edited by F. Bassani et al. Amsterdam, The Netherlands: North Holland, 1985, p. 59.
17. Langreth and D. Mehl, Phys. Rev. B **28**, p. 809 (1983).
18. G. L. Hansen, J. L. Schmit, and T. N. Casselman, J. Appl. Phys. **53**, p. 7099 (1982).
19. H. R. Vydyanath and F. A. Kröger, J. Electron. Mater. **11**, p. 111 (1982).
20. M. A. Berding, M. van Schilfgaarde, and A. Sher, J. Electron. Mater. **26**, p. 625 (1997).
21. M. A. Berding, presented at The 1997 U. S. Workshop on the Physics and Chemistry of II-VI Materials, October 21-23, 1997, Santa Barbara, CA.